WARWICK
THE UNIVERSITY OF WARWICK

Exploring magnetic correlation lengths in frustrated systems via single-crystal neutron diffraction

Oleg Petrenko
University of Warwick
UK

Outline

- Rare-earth disilicates magnets $RE_2Si_2O_7$ (RE = Er, Ho, Tm)

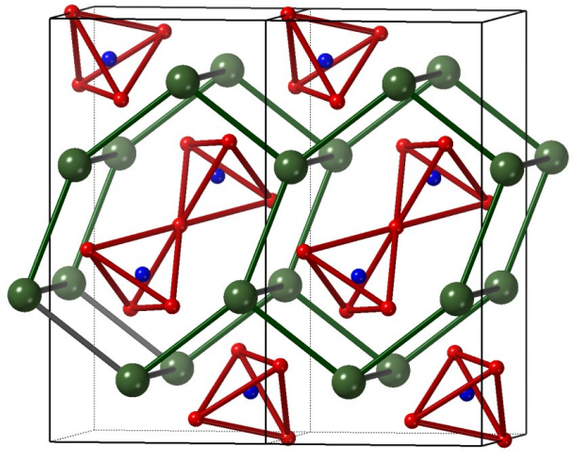

- Honeycomb/zig-zag antiferromagnets $SrRE_2O_4$ (RE = Er, Gd, Ho, Dy, Nd, Tb)

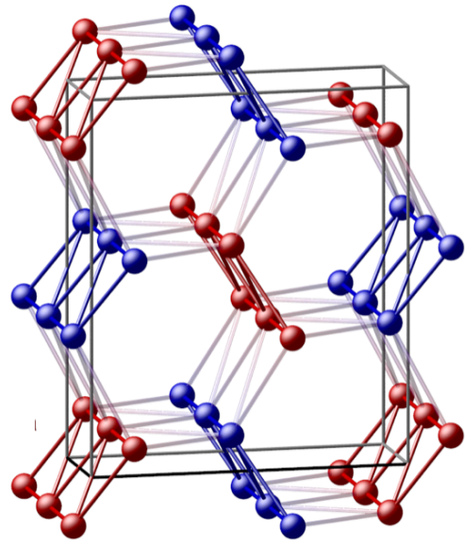

- Shastry-Sutherland lattice REB_4 tetraborides (RE = Ho, Tm, Er, Nd)

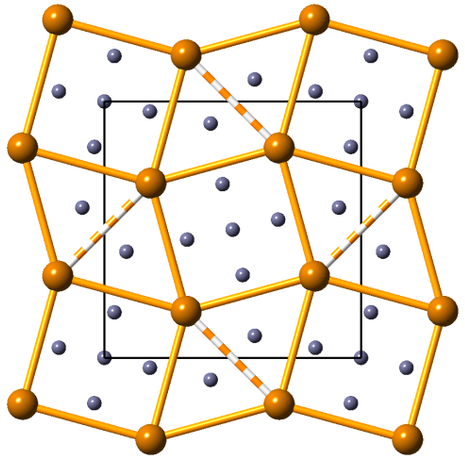

Acknowledgements

$RE_2Si_2O_7$

M. Islam, M. Ciomaga Hatnean (Warwick & PSI)
N. d'Ambrumenil, G. Balakrishnan (Warwick)
D.D. Khalyavin, P. Manuel, F. Orlandi (ISIS)
J. Ollivier, B. Ouladdiaf (ILL)

$SrRE_2O_4$

O. Young, S.X.M. Riberolles, G. Balakrishnan (Warwick)
P. Manuel, D.D. Khalyavin (ISIS)
N. Qureshi, O. Fabelo, B. Ouladdiaf, A.R. Wildes (ILL)

REB_4

D. Brunt, G. Balakrishnan, D.A. Mayoh, M.R. Lees (Warwick)
D.D. Khalyavin, P. Manuel, F. Orlandi (ISIS)
R.D. Johnson (UCL)
N. Qureshi, B. Ouladdiaf, A.R. Wildes (ILL)

$RE_2Si_2O_7$

Rare-earth disilicates

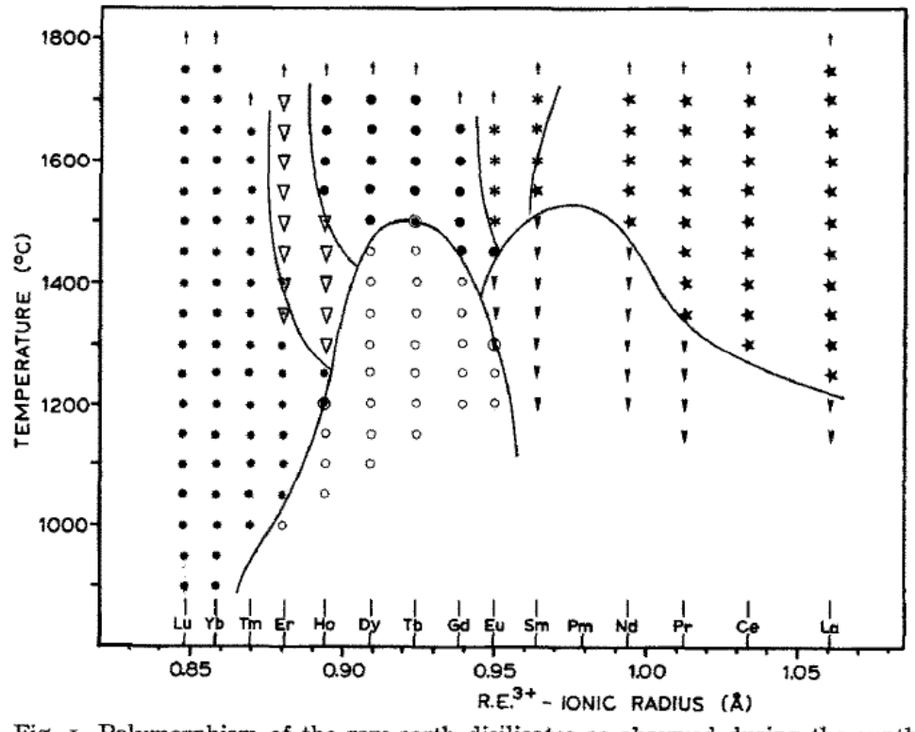

Fig. 1. Polymorphism of the rare-earth disilicates as observed during the synthesis at normal pressure. Seven different structure types, A ▼, B ○, C✱, D ▽, E ●, F★, G★, were identified by X-ray work. Arrow on top of each column indicates melting point of the compound.

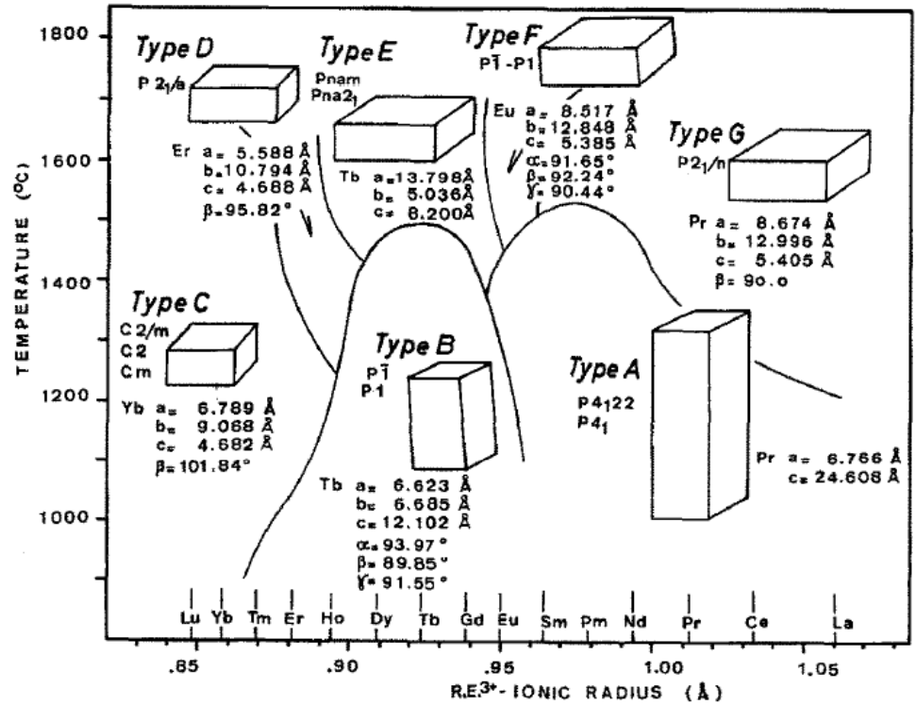

Fig. 2. Graphical presentation of the unit-cell geometry of the 7 observed structure types, A–G, each represented by data of one disilicate compound from TABLE I. (Type A ▼, B ○, C✱, D ▽, E ●, F★, and G★.)

J. Less-Common Metals, 21 (1970) 1–14

$RE_2Si_2O_7$

M. Ciomaga Hatnean et al,
Cryst. Growth Des. 2020, 20, 6636−6648

Single crystal sample are available for:

$Er_2Si_2O_7$ D-type
$P2_1/b$ space group

$Tm_2Si_2O_7$ C-type
C2/m space group

$Ho_2Si_2O_7$ E-type
$Pna2_1$ space group

Rare-earth disilicates

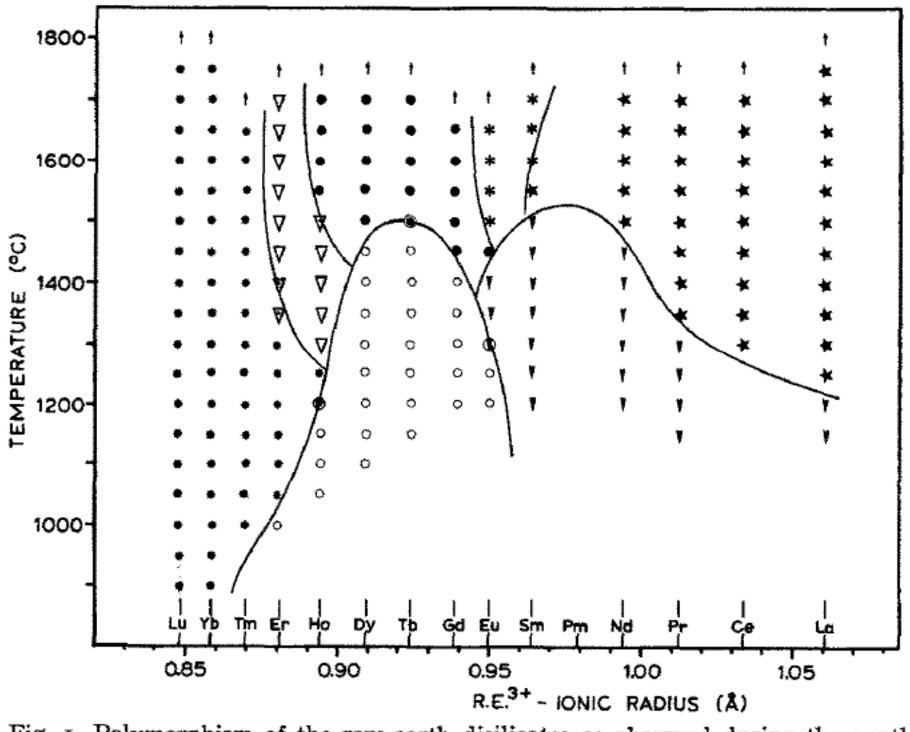

Fig. 1. Polymorphism of the rare-earth disilicates as observed during the synthesis at normal pressure. Seven different structure types, *A* ▼, *B* ○, *C*✱, *D* ▽, *E* ●, *F*⋆, *G*★, were identified by X-ray work. Arrow on top of each column indicates melting point of the compound.

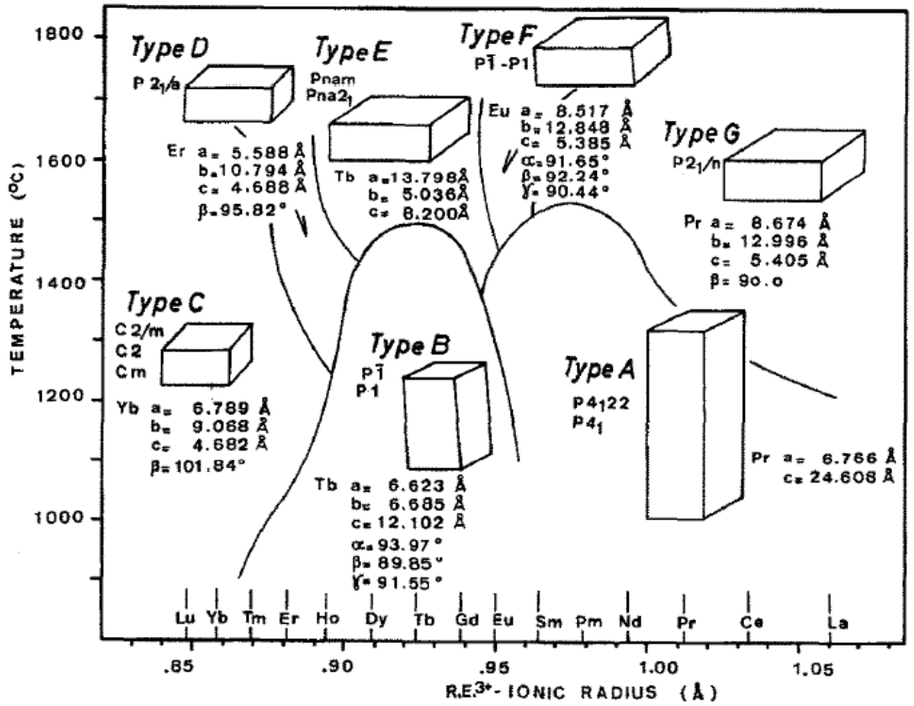

Fig. 2. Graphical presentation of the unit-cell geometry of the 7 observed structure types, *A*–*G*, each represented by data of one disilicate compound from TABLE I. (Type *A* ▼, *B* ○, *C*✱, *D* ▽, *E* ●, *F*⋆, and *G*★.)

J. Less-Common Metals, 21 (1970) 1–14

$Er_2Si_2O_7$

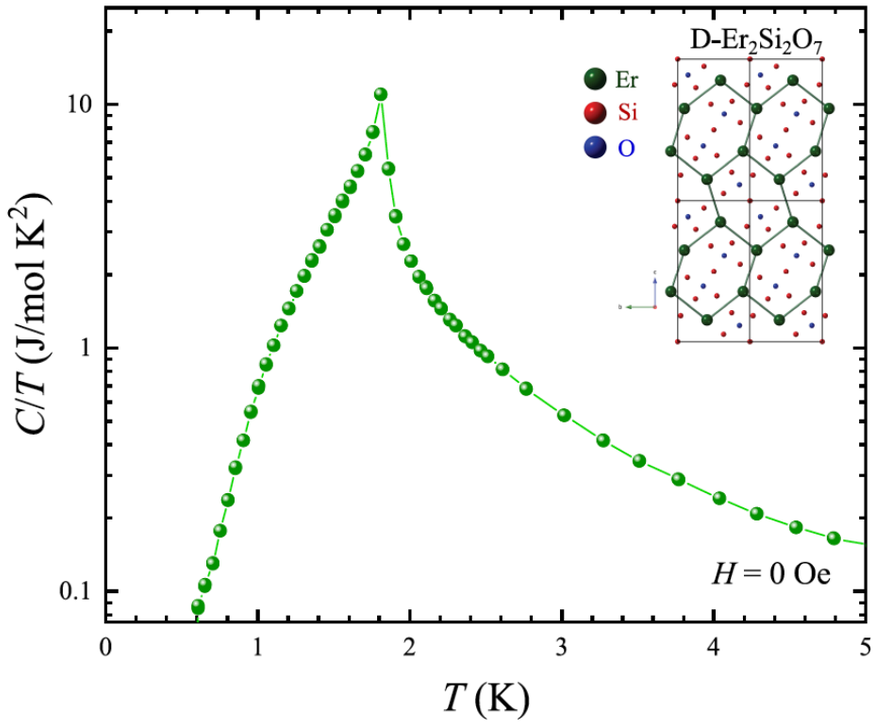

D-type $Er_2Si_2O_7$

monoclinic space group $P2_1/b$

a=4.69 Å, b=5.56 Å, c=10.79 Å, γ= 96°

T_N=1.85 K

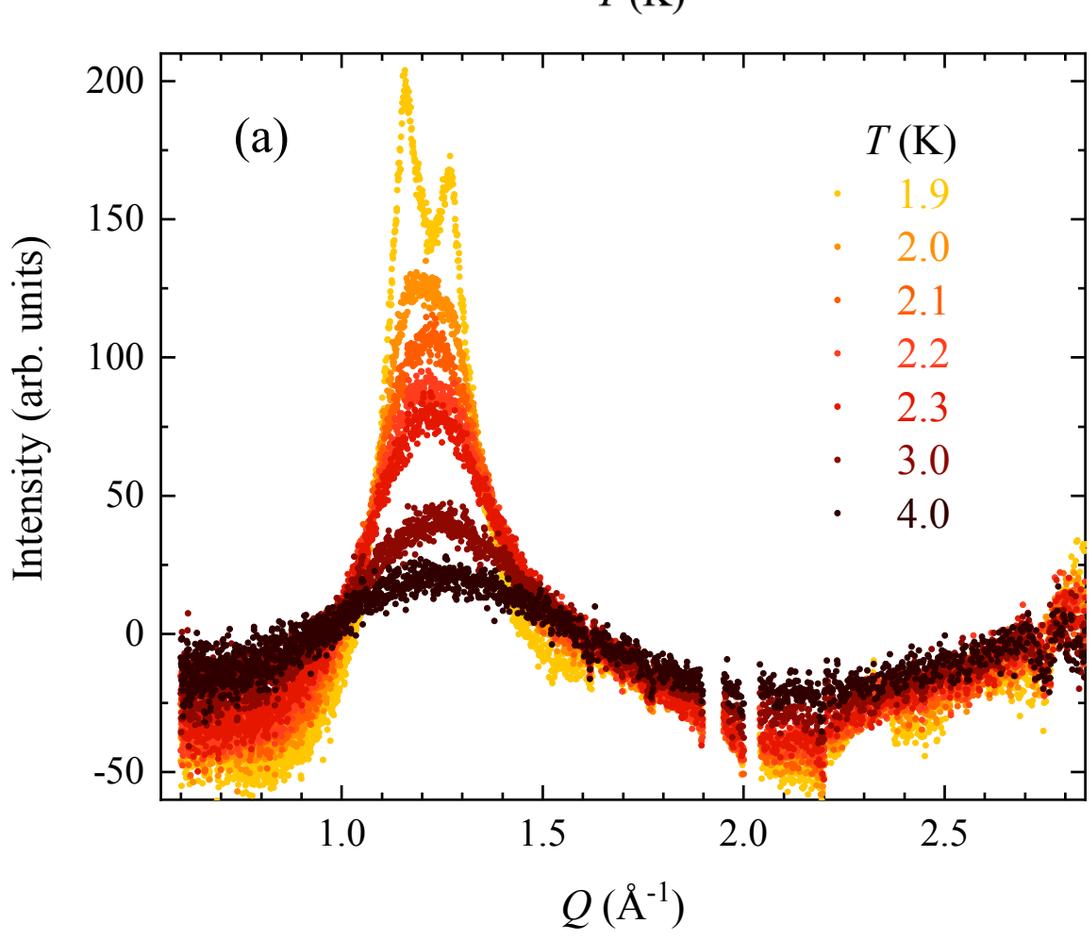

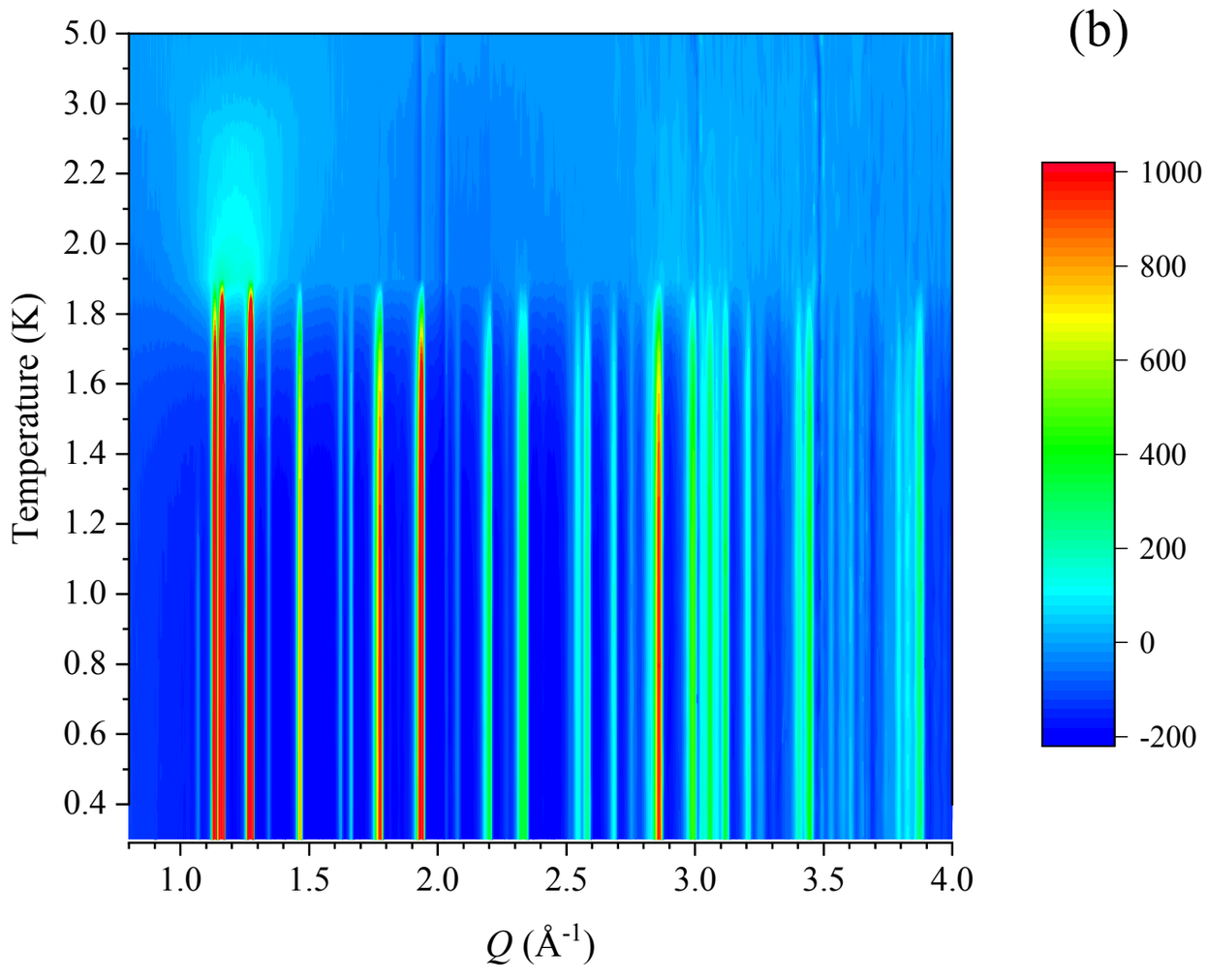

powder neutron diffraction

WISH, ISIS

$Er_2Si_2O_7$

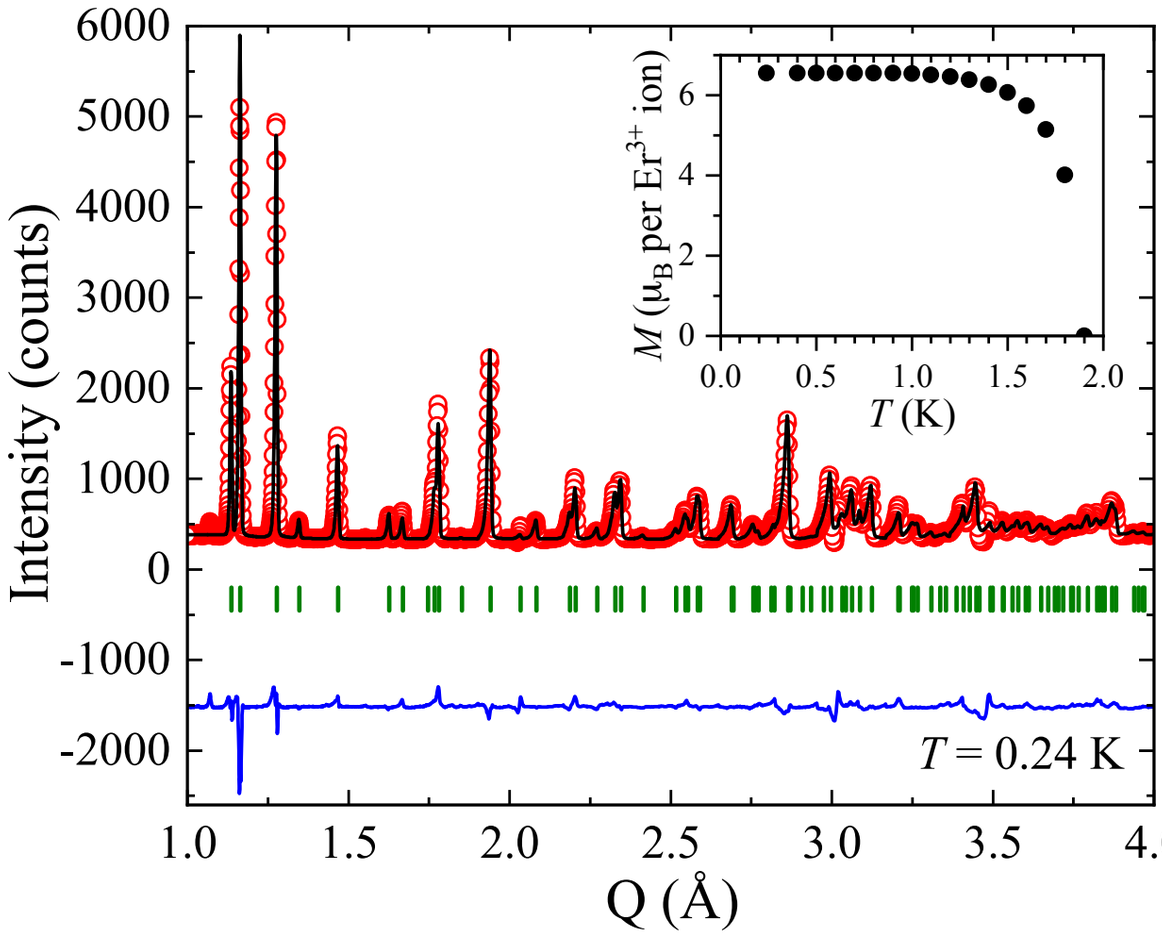
Intensity (counts)
6000
5000
4000
3000
2000
1000
0
-1000
-2000
1.0
1.5
2.0
2.5
3.0
3.5
4.0
Q (Å)
T = 0.24 K
M (μB per Er3+ ion)
0
2
4
6
0.0
0.5
1.0
1.5
2.0
T (K)

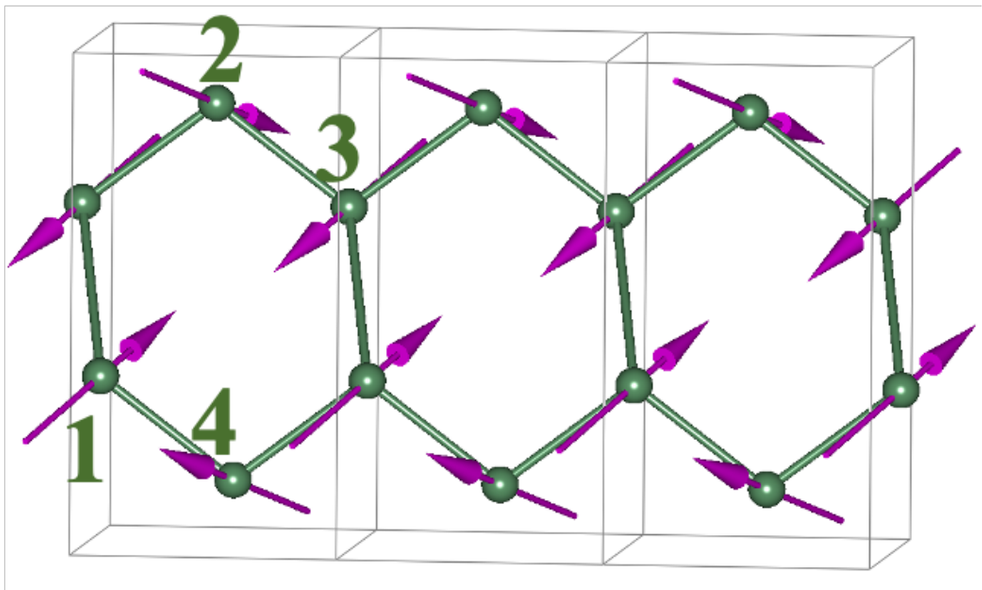
1
2
3
4

$Er_2Si_2O_7$

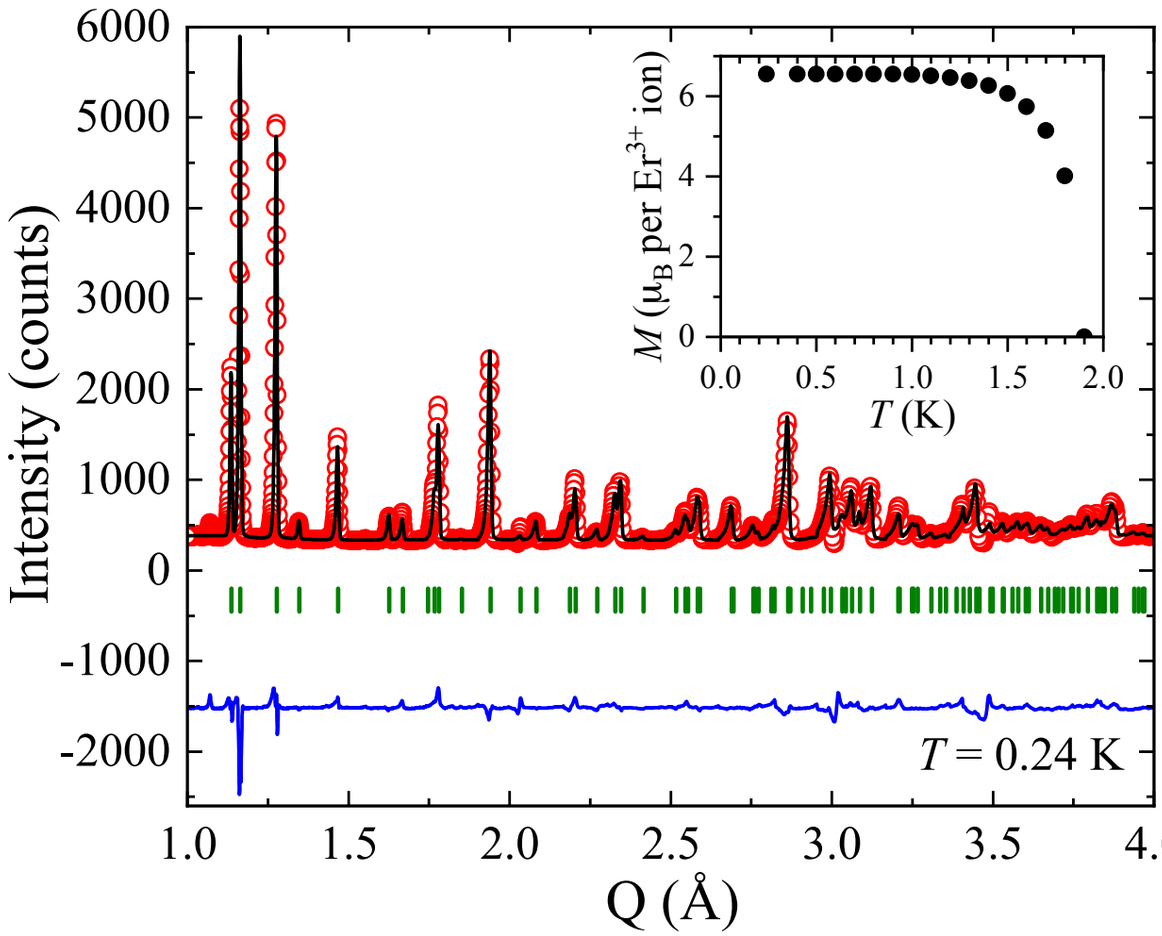

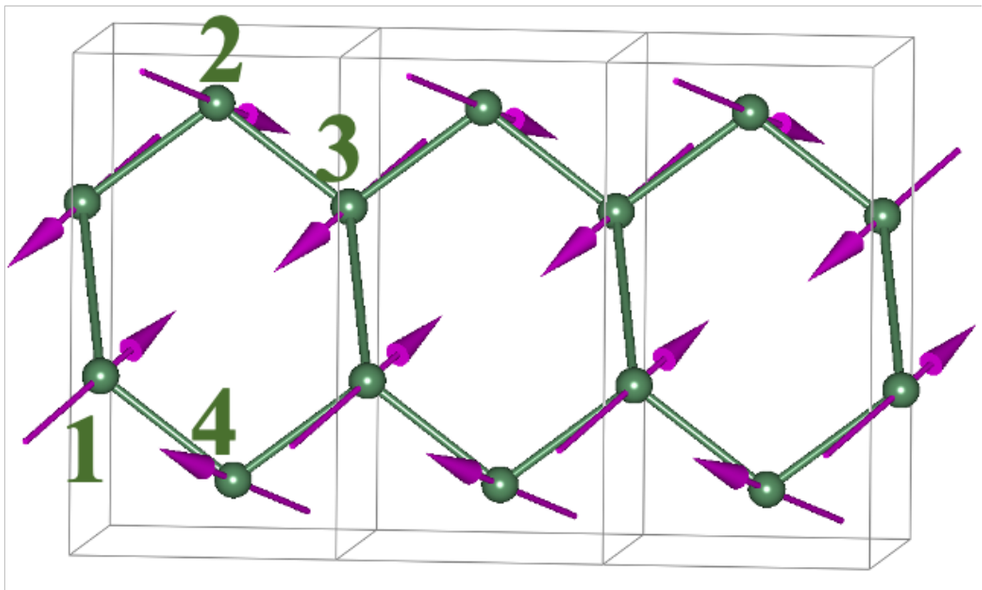

Magnetic structure, **k** = 0

Ion	Positions $(\boldsymbol{a}, \boldsymbol{b}, \boldsymbol{c})$ basis	μ_a	μ_b $[\mu_B]$	μ_c	Moment $[\mu_B]$
1	0.891 0.096 0.351	-5.621	2.105	2.082	6.546
2	0.109 0.404 0.851	-5.621	2.105	-2.082	6.546
3	0.109 0.904 0.649	5.621	-2.105	-2.082	6.546
4	0.891 0.596 0.149	5.621	-2.105	2.082	6.546

powder neutron diffraction

WISH, ISIS

$Er_2Si_2O_7$

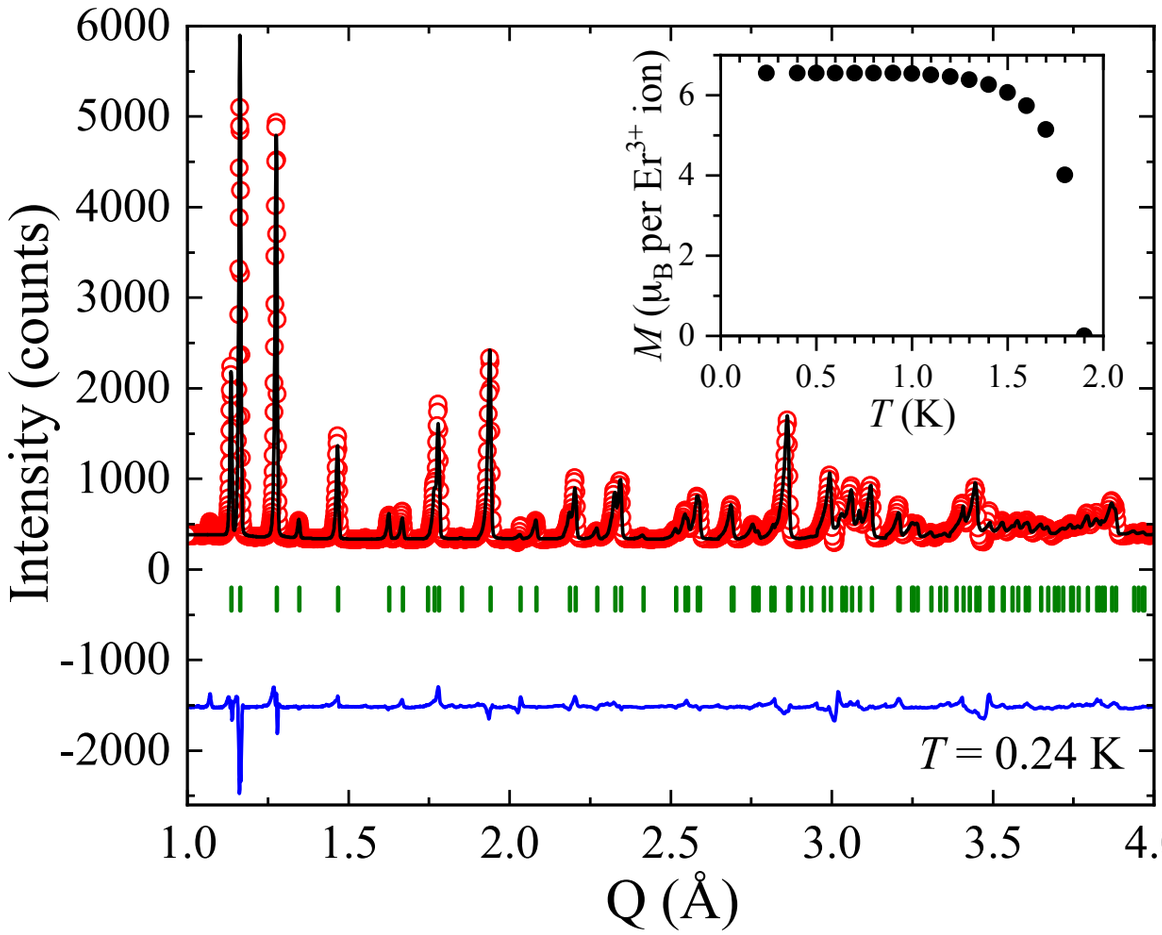

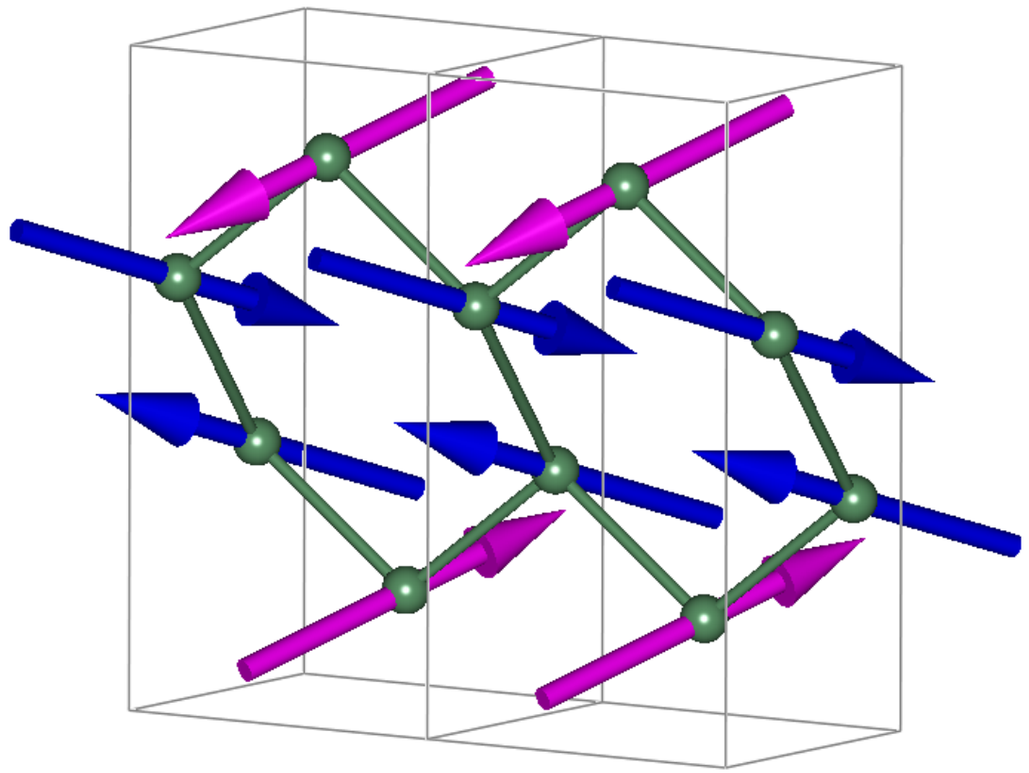

Magnetic structure, **k** = 0

Ion	Positions $(\boldsymbol{a}, \boldsymbol{b}, \boldsymbol{c})$ basis			μ_a	μ_b $[\mu_B]$	μ_c	Moment $[\mu_B]$
1	0.891	0.096	0.351	-5.621	2.105	2.082	6.546
2	0.109	0.404	0.851	-5.621	2.105	-2.082	6.546
3	0.109	0.904	0.649	5.621	-2.105	-2.082	6.546
4	0.891	0.596	0.149	5.621	-2.105	2.082	6.546

powder neutron diffraction

WISH, ISIS

$Er_2Si_2O_7$

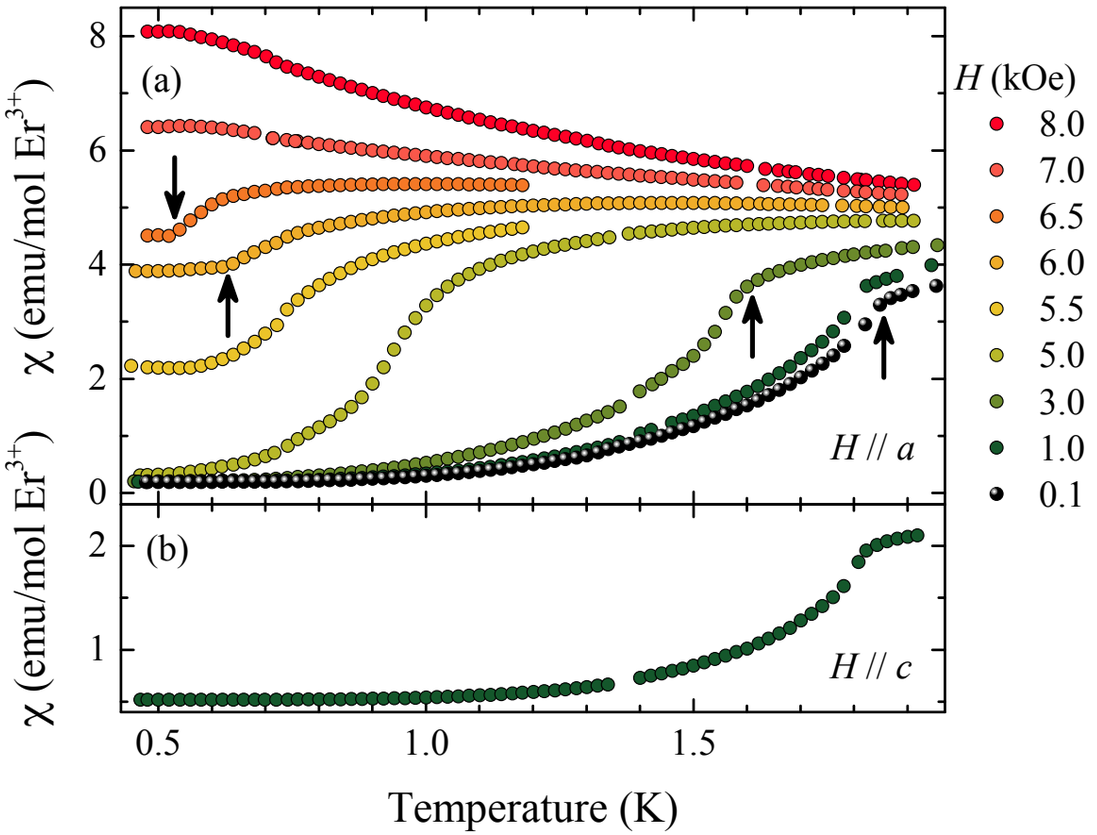
(a)
(b)
χ (emu/mol Er3+)
H // a
H // c
H (kOe)
8.0
7.0
6.5
6.0
5.5
5.0
3.0
1.0
0.1
Temperature (K)

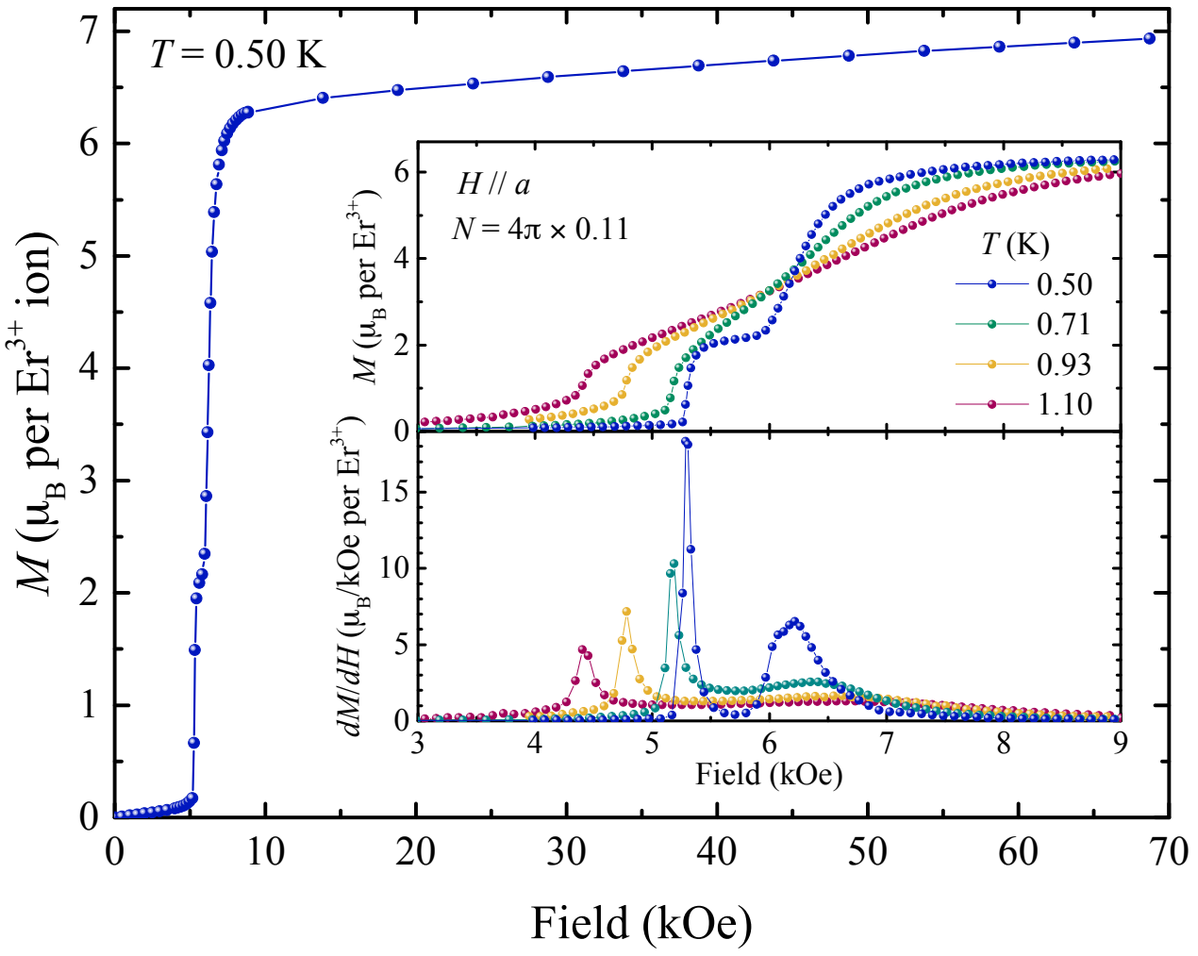
T = 0.50 K
M (μB per Er3+ ion)
Field (kOe)
H // a
N = 4π × 0.11
T (K)
0.50
0.71
0.93
1.10
dM/dH (μB/kOe per Er3+)

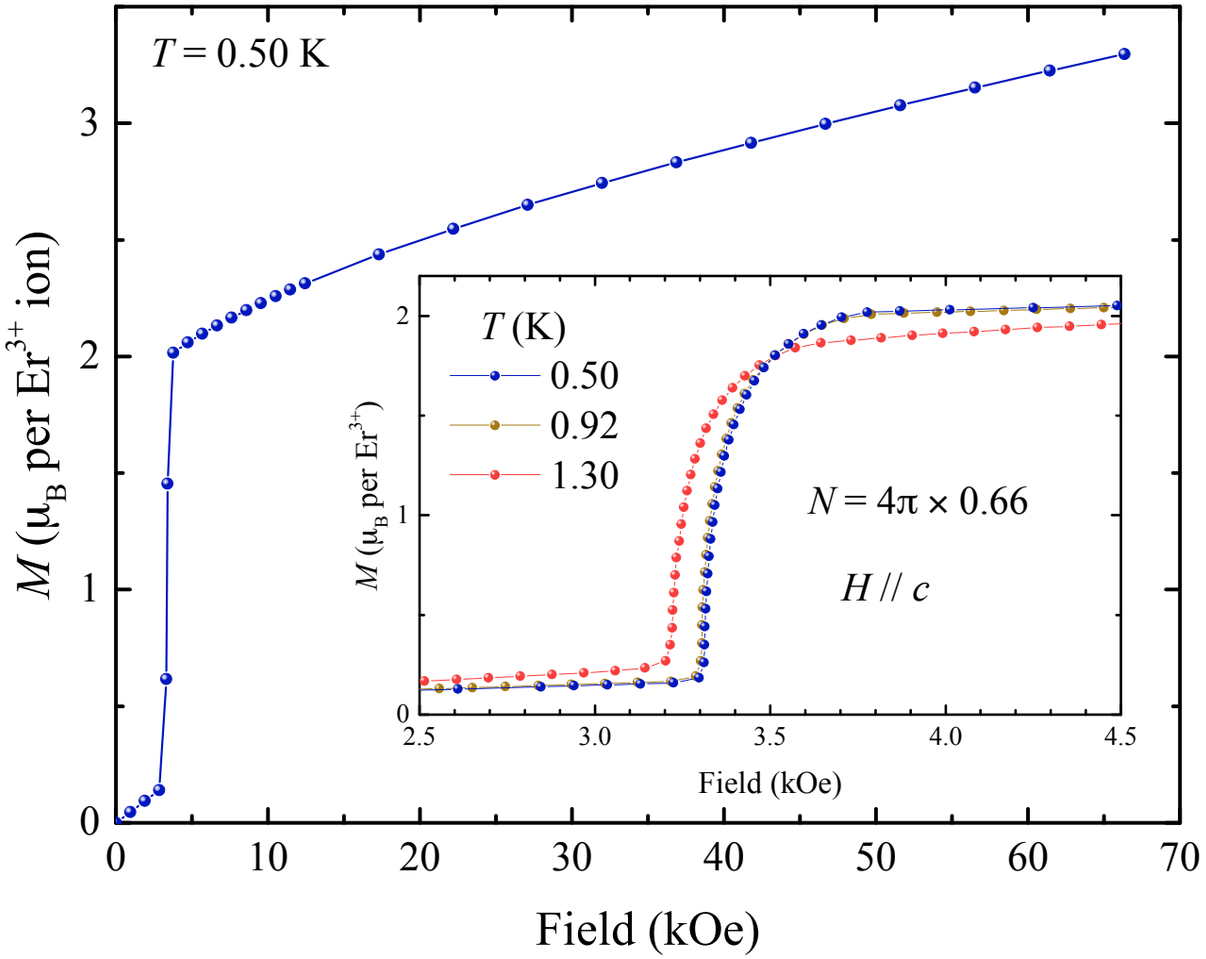
T = 0.50 K
M (μB per Er3+ ion)
Field (kOe)
T (K)
0.50
0.92
1.30
N = 4π × 0.66
H // c

$Er_2Si_2O_7$

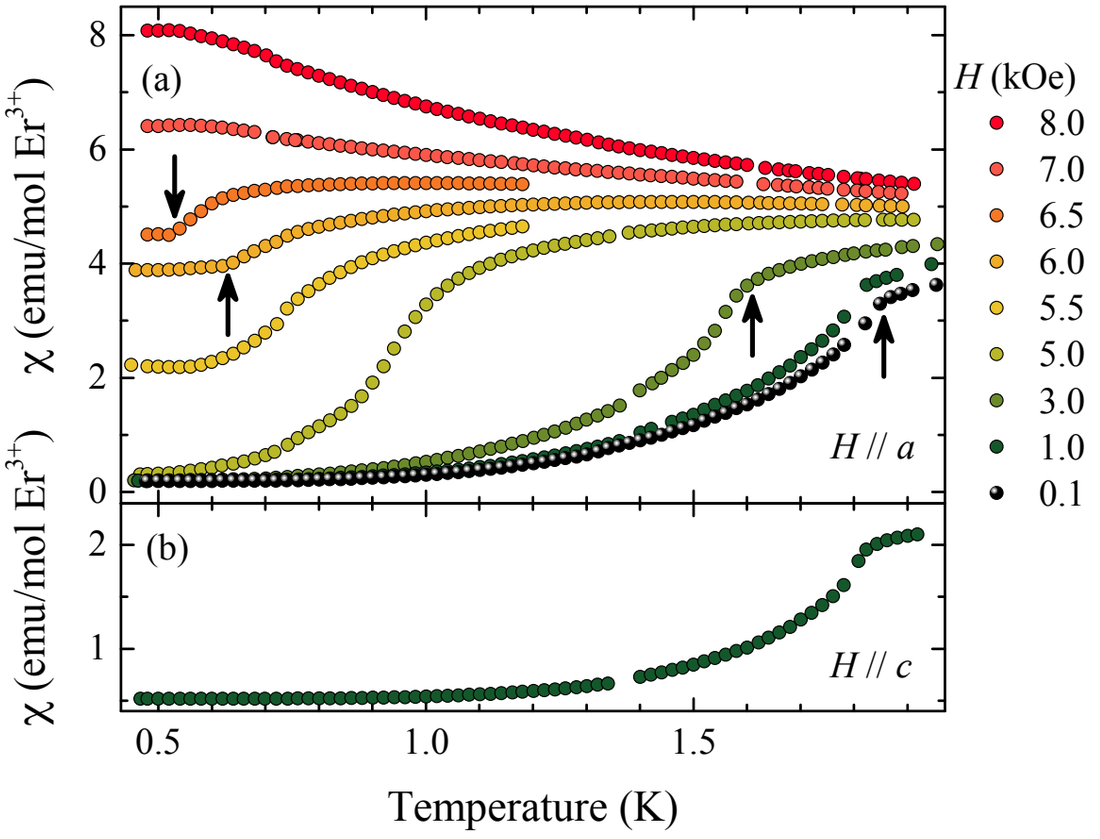

M.J.M. Leask *et al.*, J. Phys. C Solid State **19**, 1173 (1986)

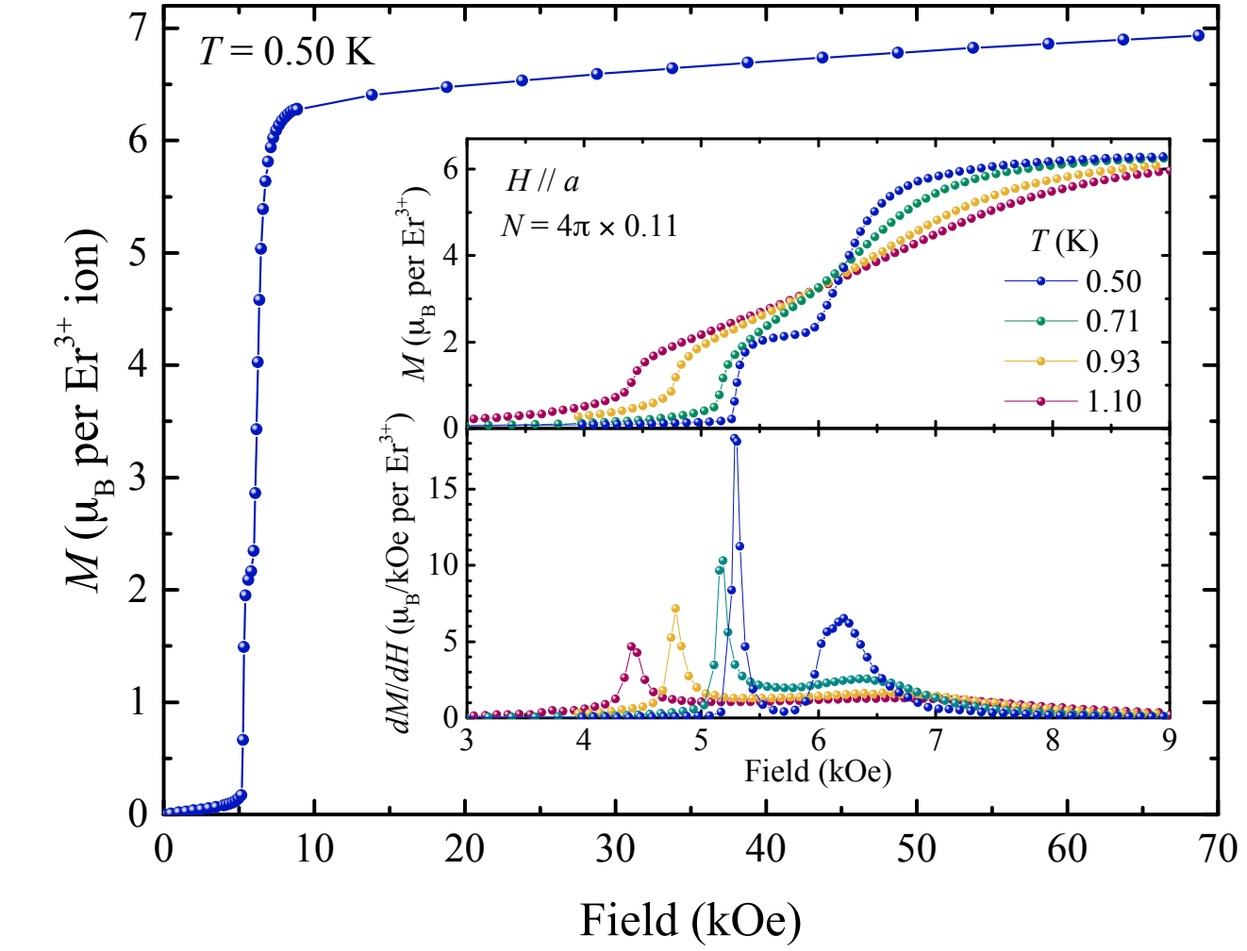

Magnetic properties of D-type $Er_2Si_2O_7$ 1177

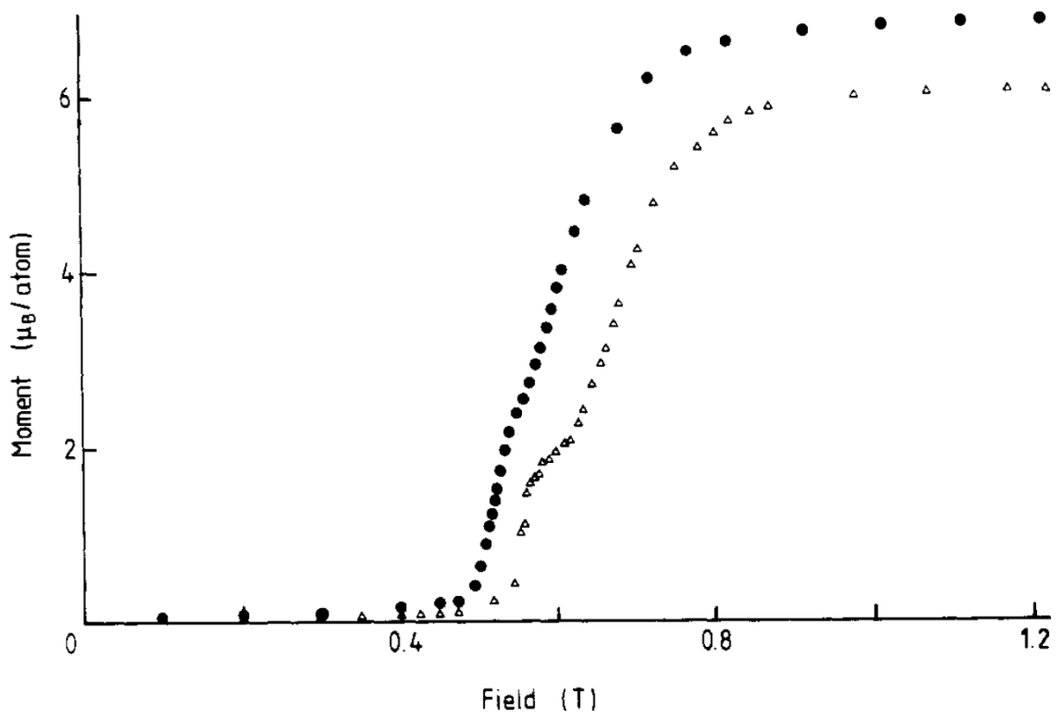

Figure 3. The magnetic moment of a single crystal of D-type $Er_2Si_2O_7$ in μ_B/atom as a function of the magnetic field (in T) applied parallel to the (△) *a* axis and (●) 'm' axis at 0.5 K.

$Er_2Si_2O_7$

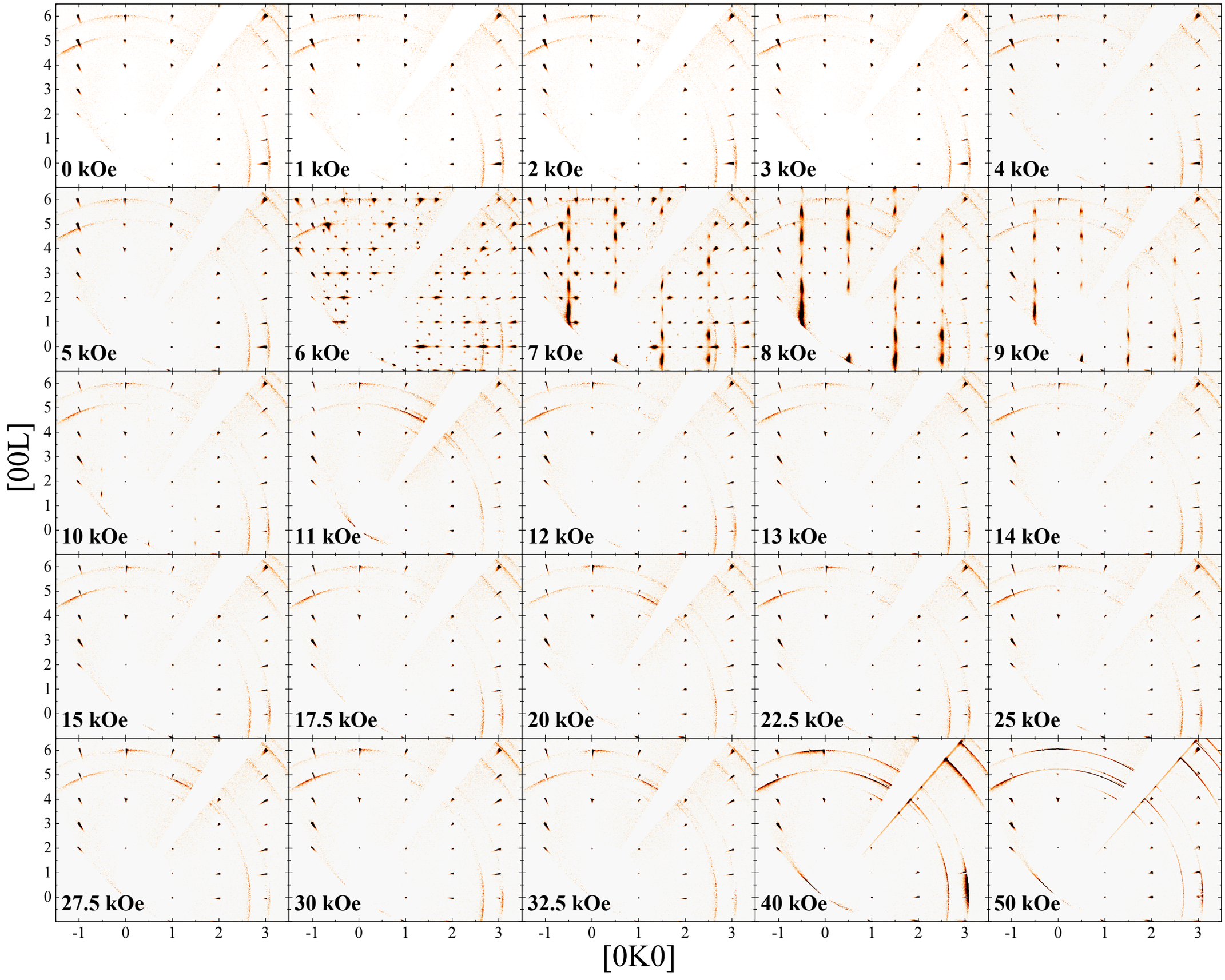

T = 0.24 K

H // *a* axis

single crystal neutron diffraction

WISH, ISIS

$Er_2Si_2O_7$

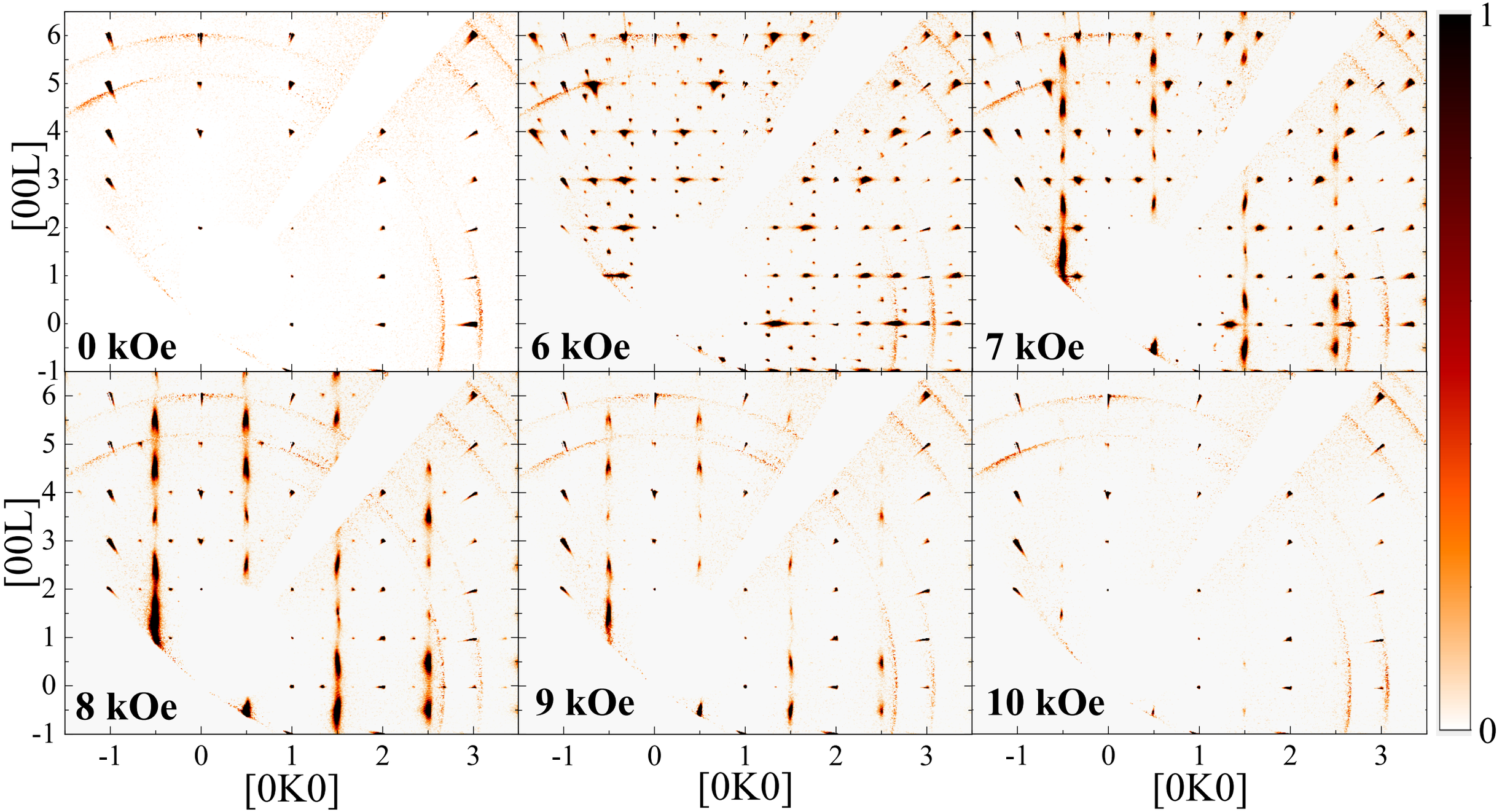

T = 0.24 K

H // a axis

$Er_2Si_2O_7$

q = (0 1/2 1/2)
q = (0 1/4 1/4)
q = (0 1/3 0)

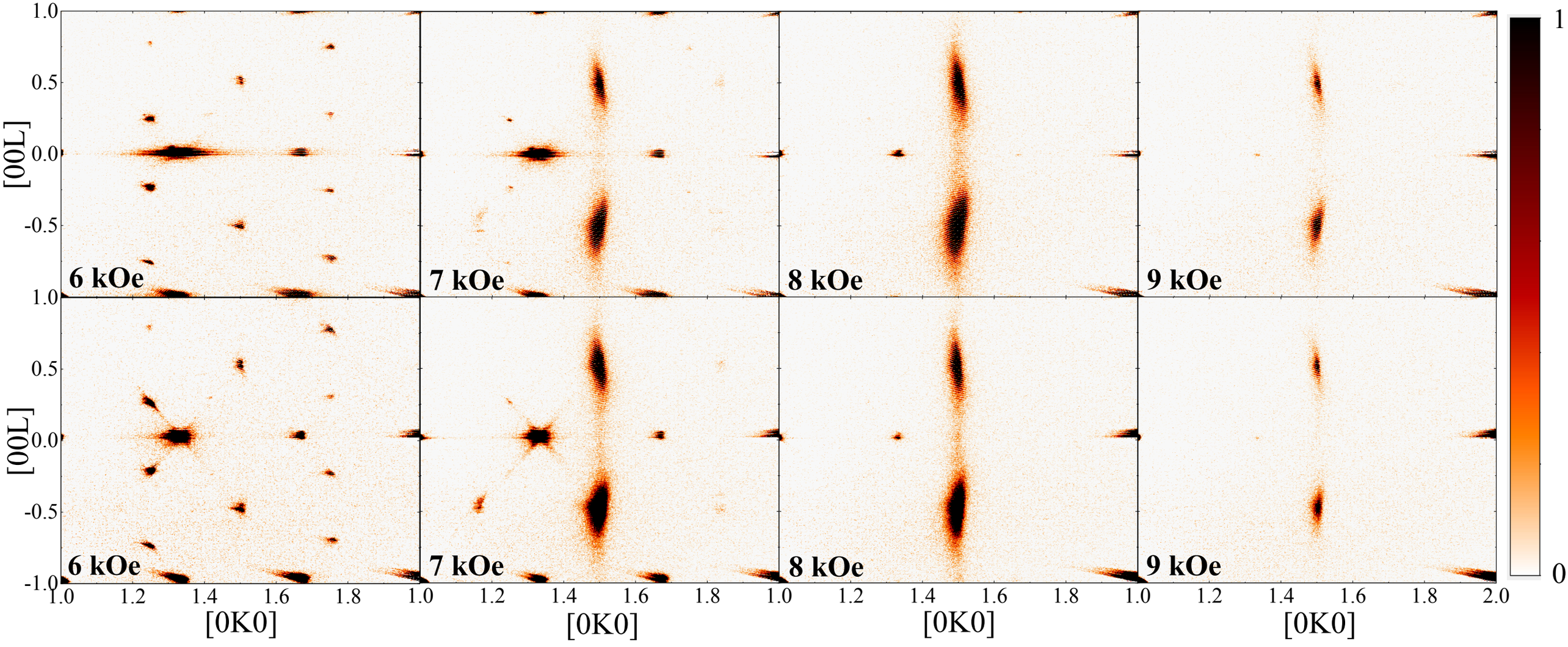

T = 0.24 K
H // *a* axis

$Er_2Si_2O_7$

T = 0.045 K

H // a axis

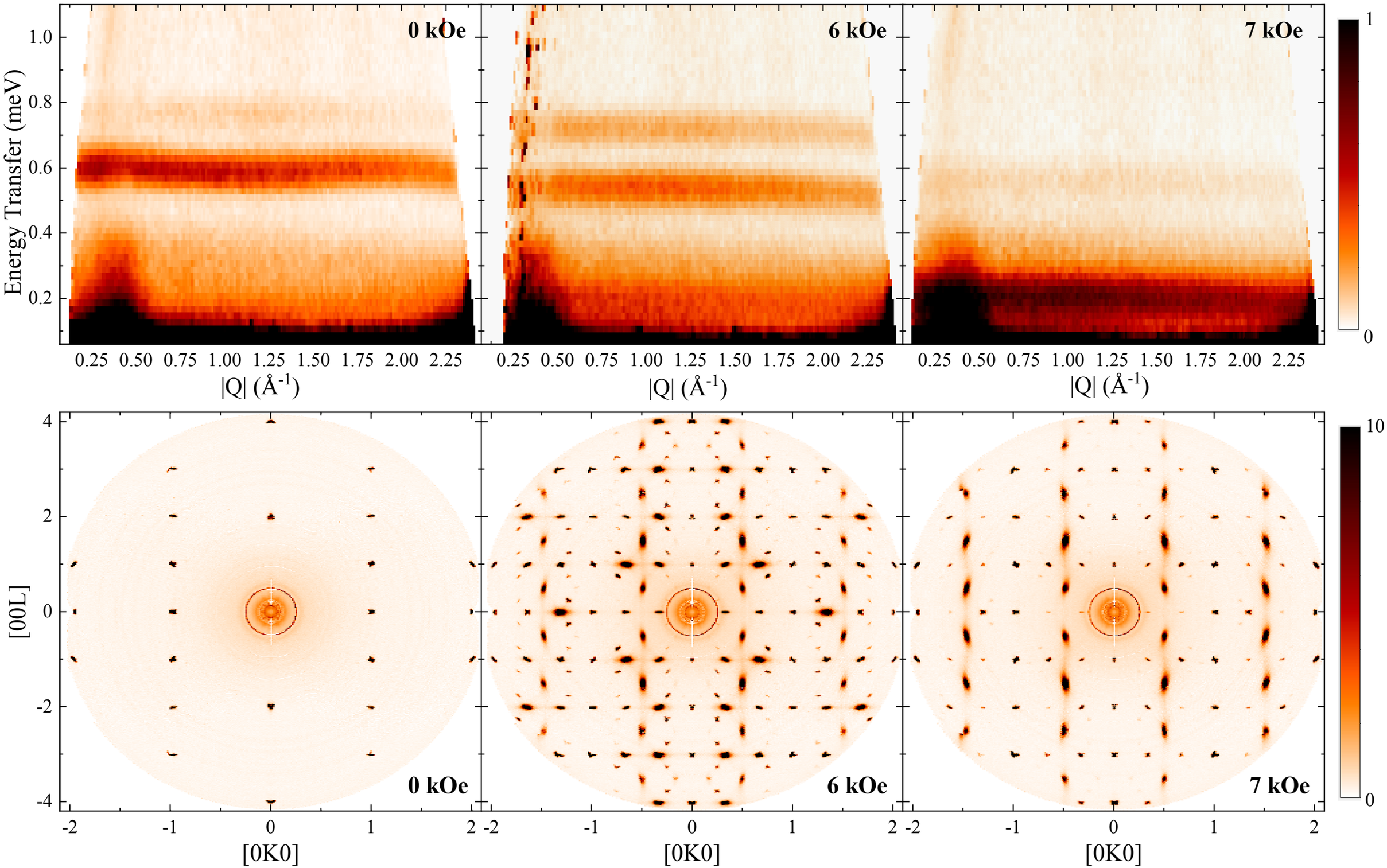

single crystal neutron spectroscopy

IN5, ILL

$Er_2Si_2O_7$

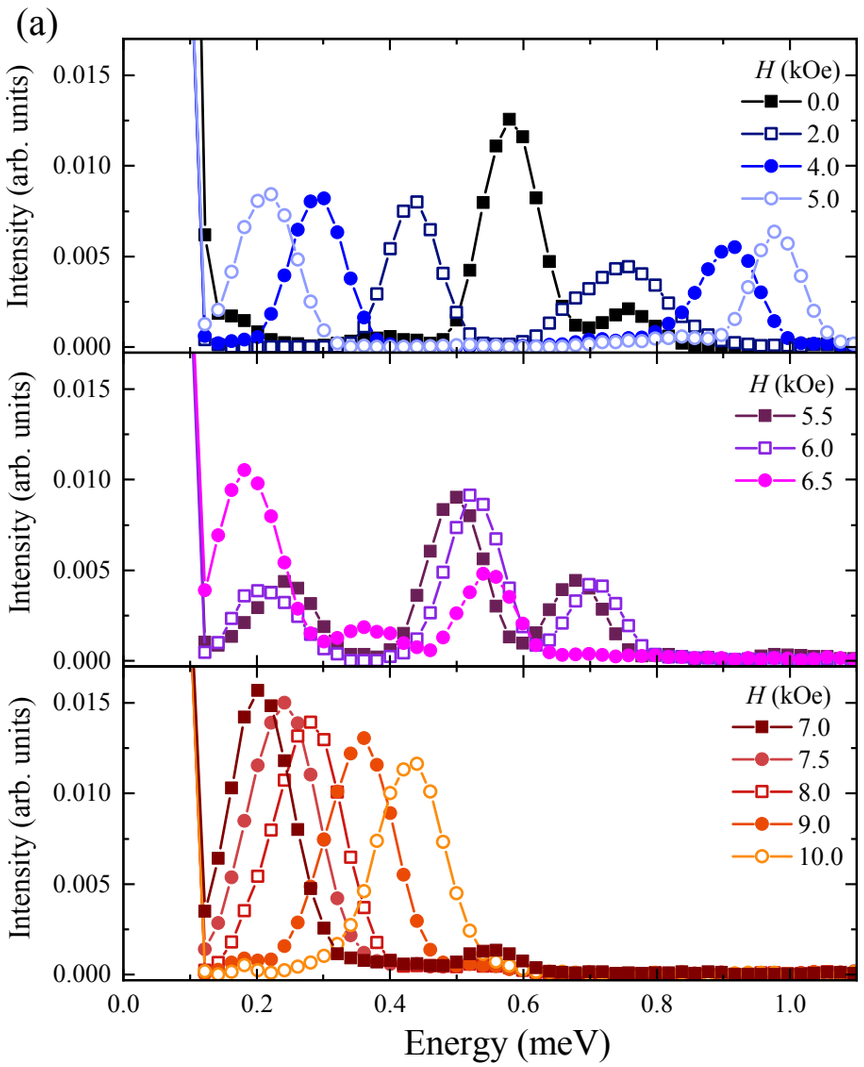
(a)
Intensity (arb. units)
H (kOe)
0.0
2.0
4.0
5.0
5.5
6.0
6.5
7.0
7.5
8.0
9.0
10.0
Energy (meV)

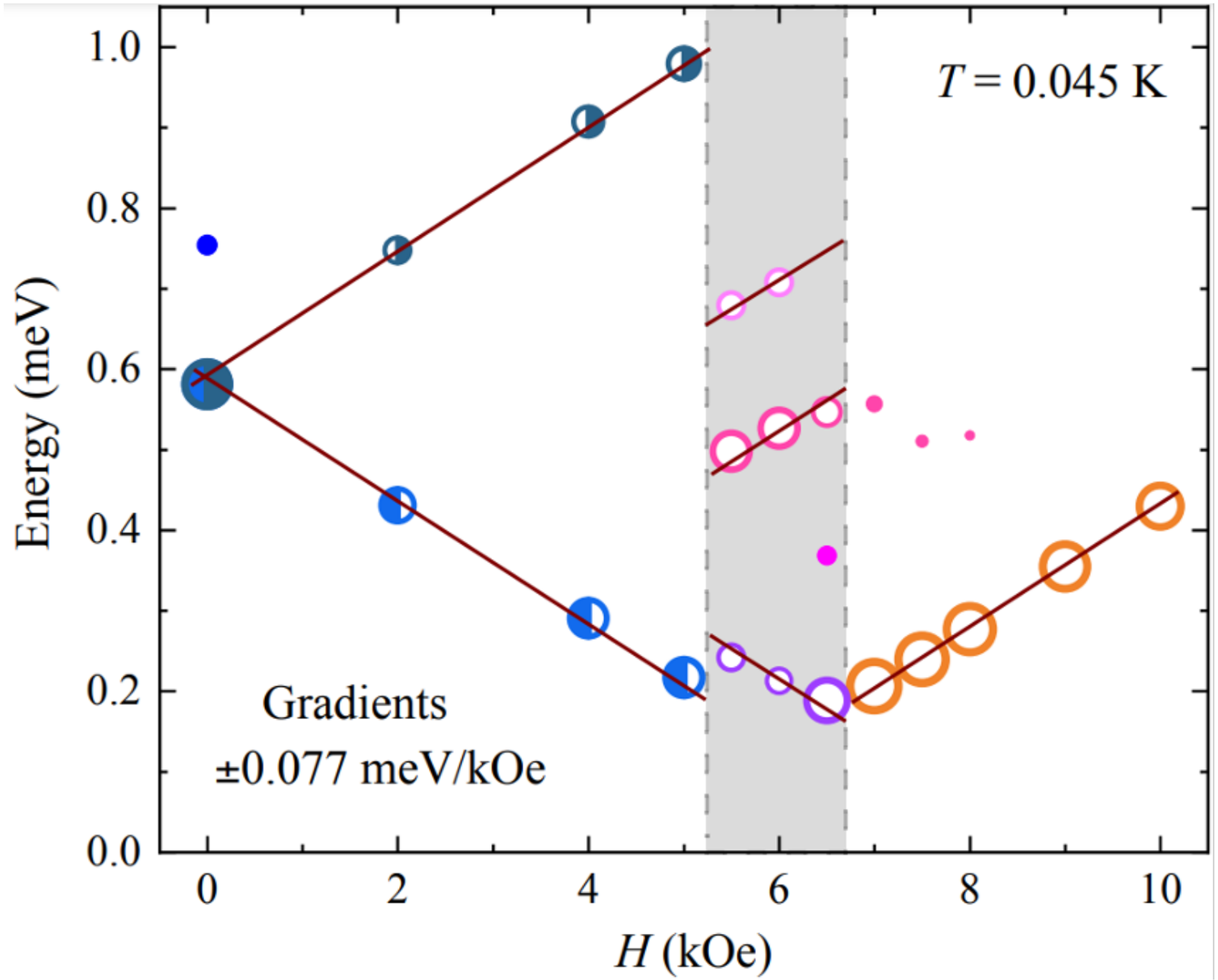
T = 0.045 K
Energy (meV)
Gradients
±0.077 meV/kOe
H (kOe)

$Er_2Si_2O_7$ Summary

D-type $Er_2Si_2O_7$ is an Ising-like antiferromagnet with 4-sublattice **k** = 0 structure below T_N =1.85 K with two pairs of collinear antiferromagnetic moments within the unit cell.

For H//*a*, a narrow and T-sensitive magnetisation plateau exists at 1/3 of saturation value.

The magnetic unit cell undergoes a significant increase within the plateau regime demonstrated by the appearance of a scattering signal at non-integer positions described by the propagation vectors (0 1/2 1/2), (0 1/4 1/4), (0 1/3 0).

The intensity, shape, and width of these field-induced features change rapidly with the applied magnetic field within the magnetisation plateau. The diffraction pattern then returns to integer peaks at higher fields, upon its entrance into the paramagnetic phase and out of the plateau.

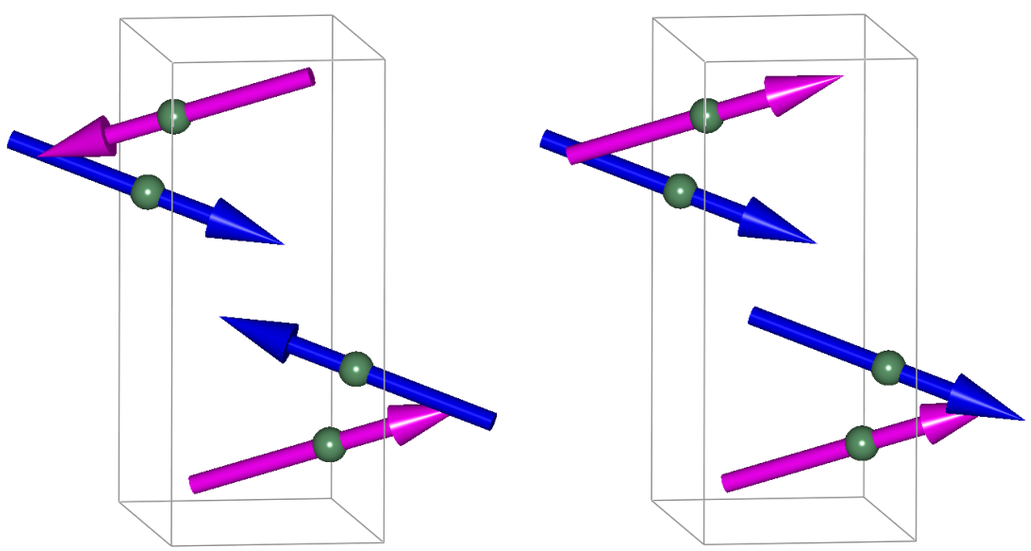

$Er_2Si_2O_7$ Summary

D-type $Er_2Si_2O_7$ is an Ising-like antiferromagnet with 4-sublattice **k** = 0 structure below T_N =1.85 K with two pairs of collinear antiferromagnetic moments within the unit cell.

For H//*a*, a narrow and T-sensitive magnetisation plateau exists at 1/3 of saturation value.

The magnetic unit cell undergoes a significant increase within the plateau regime demonstrated by the appearance of a scattering signal at non-integer positions described by the propagation vectors (0 1/2 1/2), (0 1/4 1/4), (0 1/3 0).

The intensity, shape, and width of these field-induced features change rapidly with the applied magnetic field within the magnetisation plateau. The diffraction pattern then returns to integer peaks at higher fields, upon its entrance into the paramagnetic phase and out of the plateau.

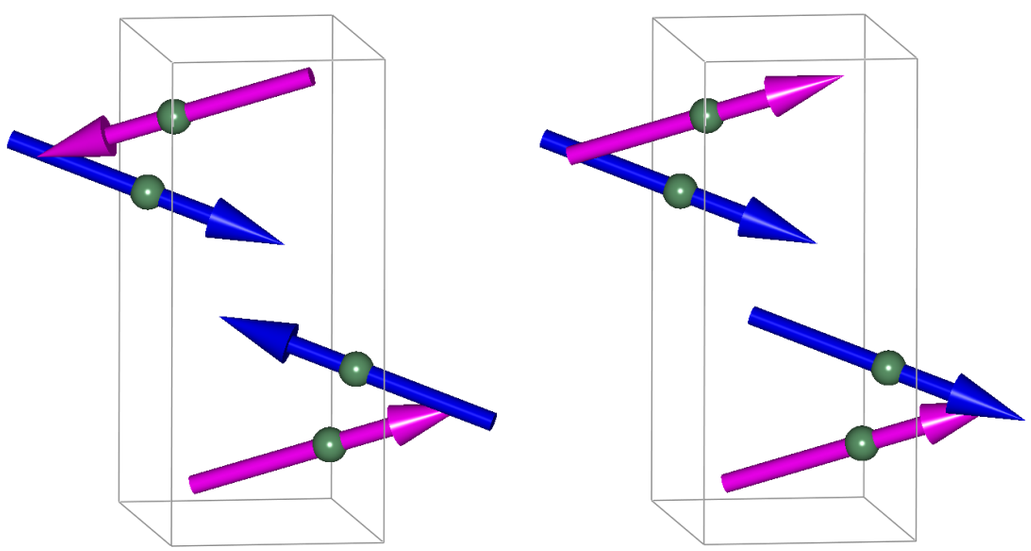

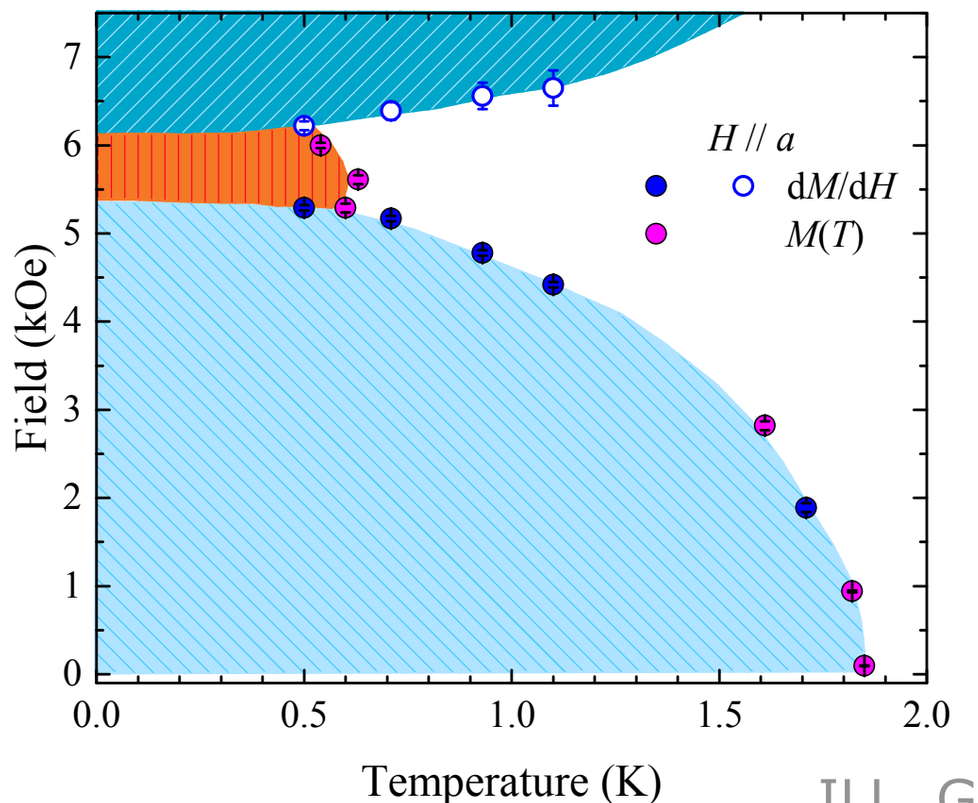

$SrRE_2O_4$ (RE= Gd, Ho, Er, Dy, Nd, Tb)

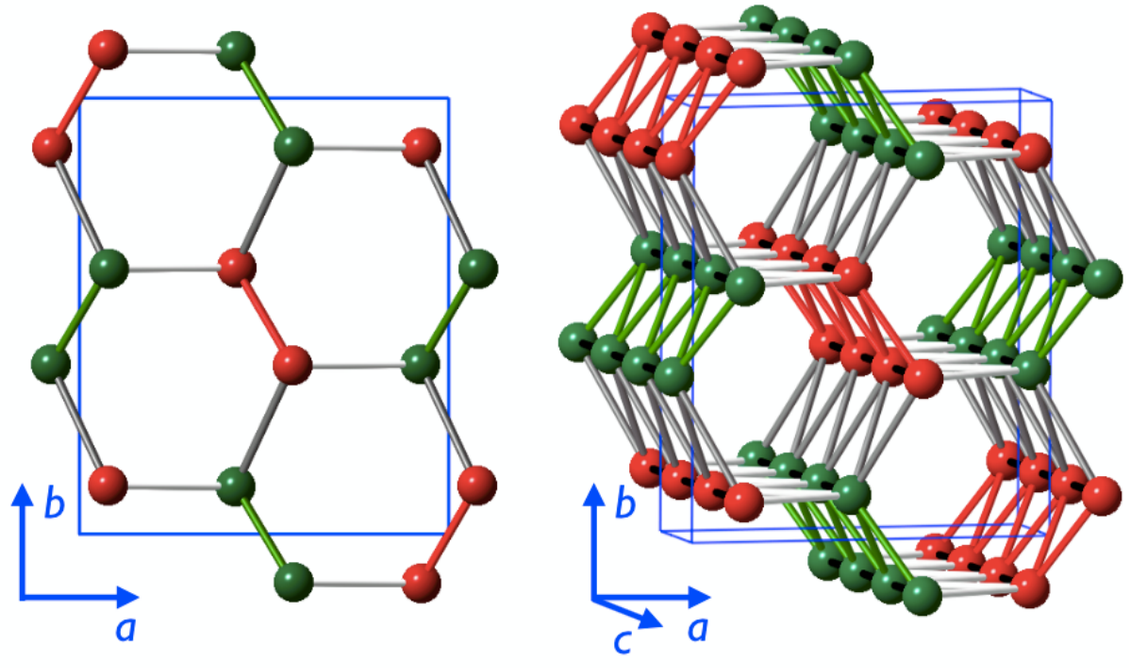

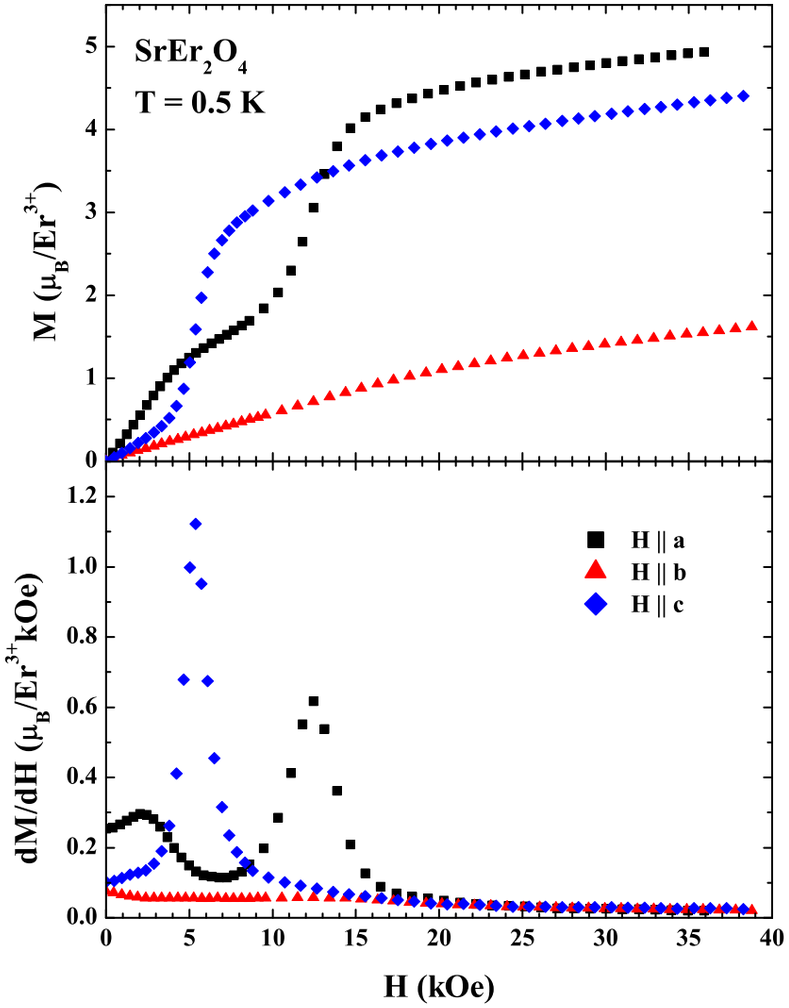

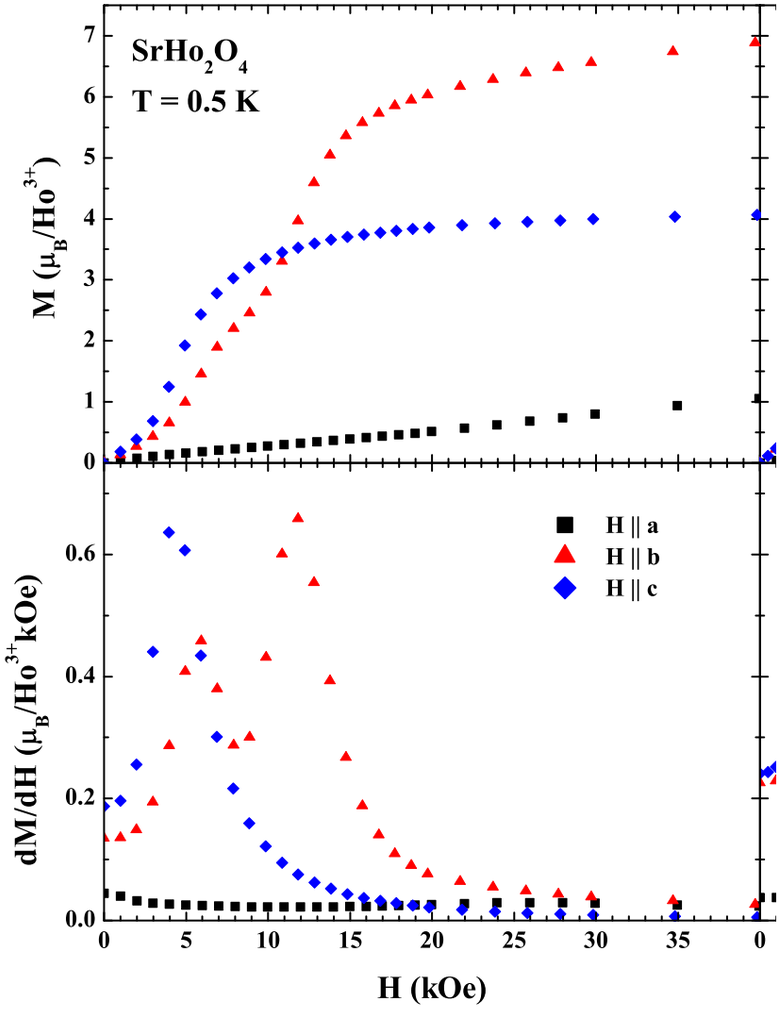

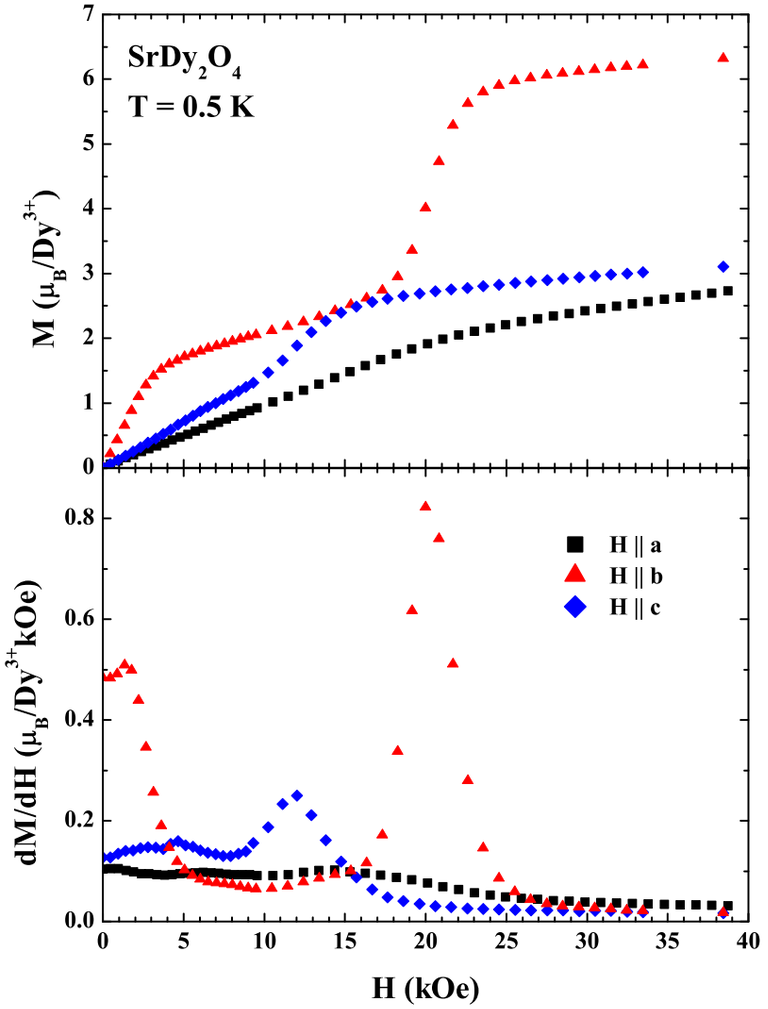

$SrEr_2O_4$

Coexistence of the two different magnetic components:

1/3 magnetisation plateaux for H//a.

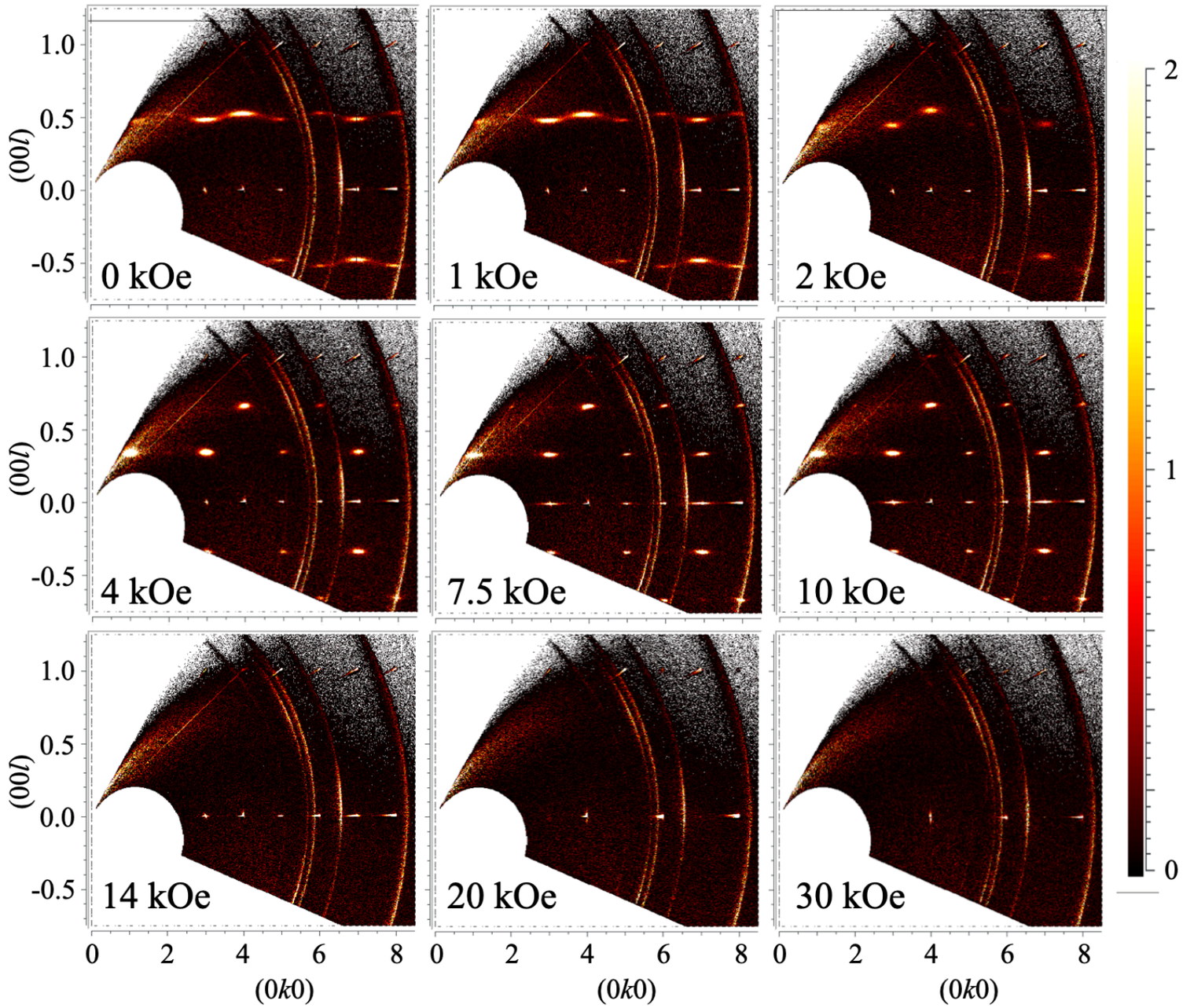

SciPost Phys. 11, 007 (2021)

single crystal neutron diffraction

WISH, ISIS

$SrEr_2O_4$

Coexistence of the two different magnetic components:

metamagnetic transition for H//c.

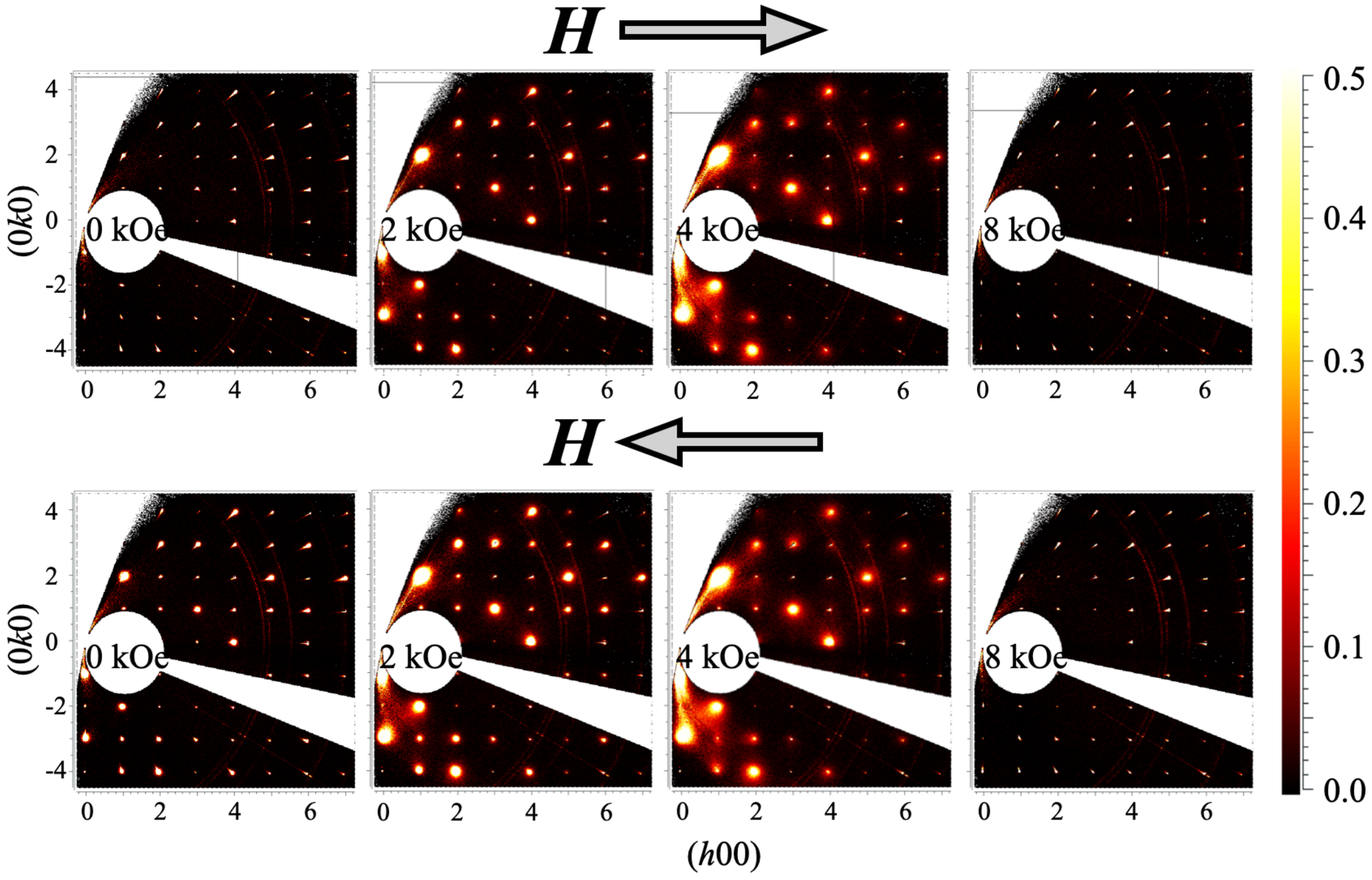

SciPost Phys. 11, 007 (2021)

single crystal neutron diffraction

WISH, ISIS

$SrEr_2O_4$

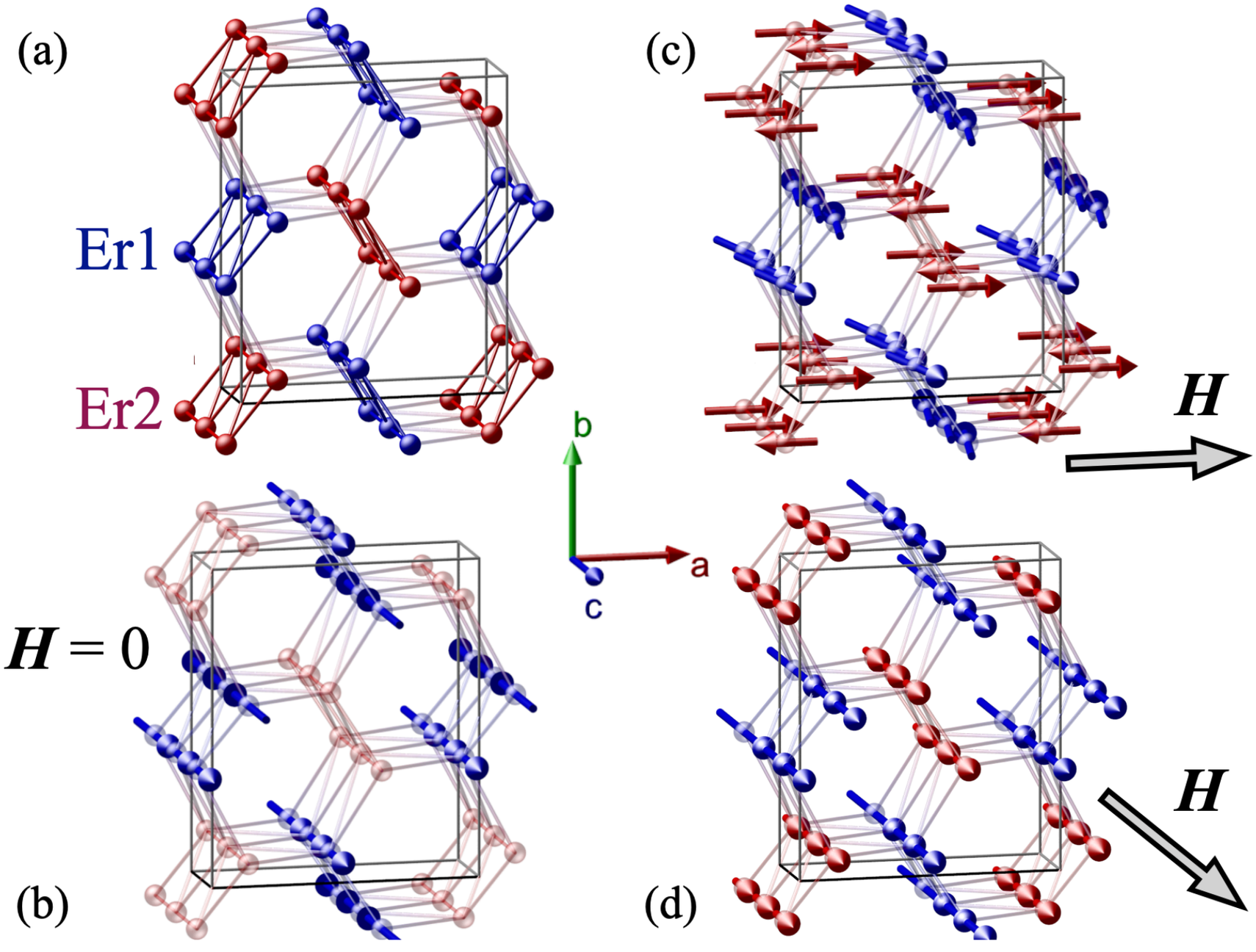

Summary

For $SrEr_2O_4$, single-crystal neutron diffraction reveals the nature of field-induced transitions.

For H//a, the applied field induces a transition to an extended, but still not fully long-range ordered UUD state of the Er2 sites.

For H//c, the applied field destroys the long-range antiferromagnetic order of the Er1 sites and induces a much shorter-range order during the metamagnetic transition prior to establishing a long-range ferromagnetic-like state of the Er1 moments.

REB_4 (RE = Ho, Tm, Er, Nd)

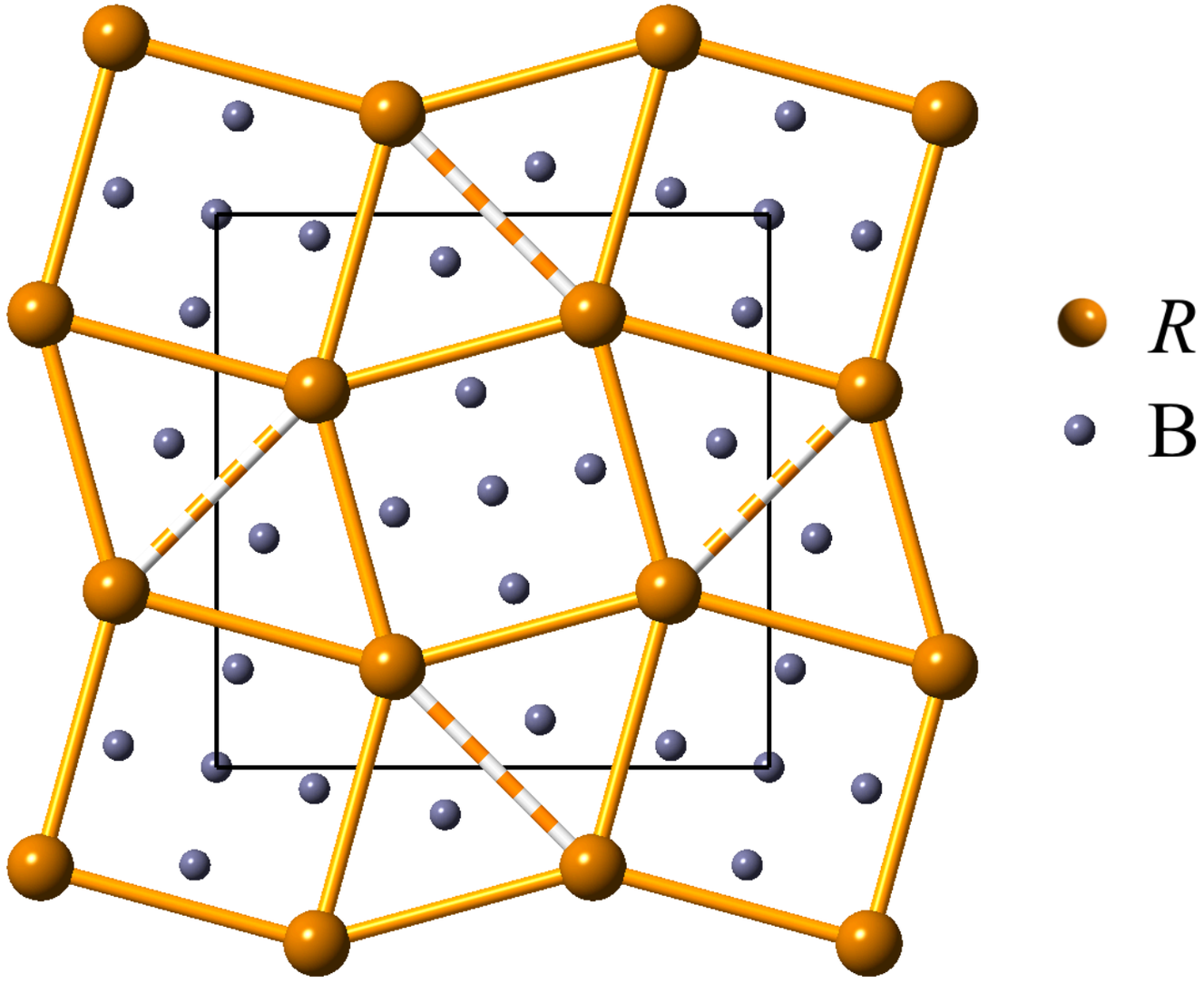

Shastry-Sutherland lattice REB_4 tetraborides

REB_4

LINDA YE, TAKEHITO SUZUKI, AND JOSEPH G. CHECKELSKY

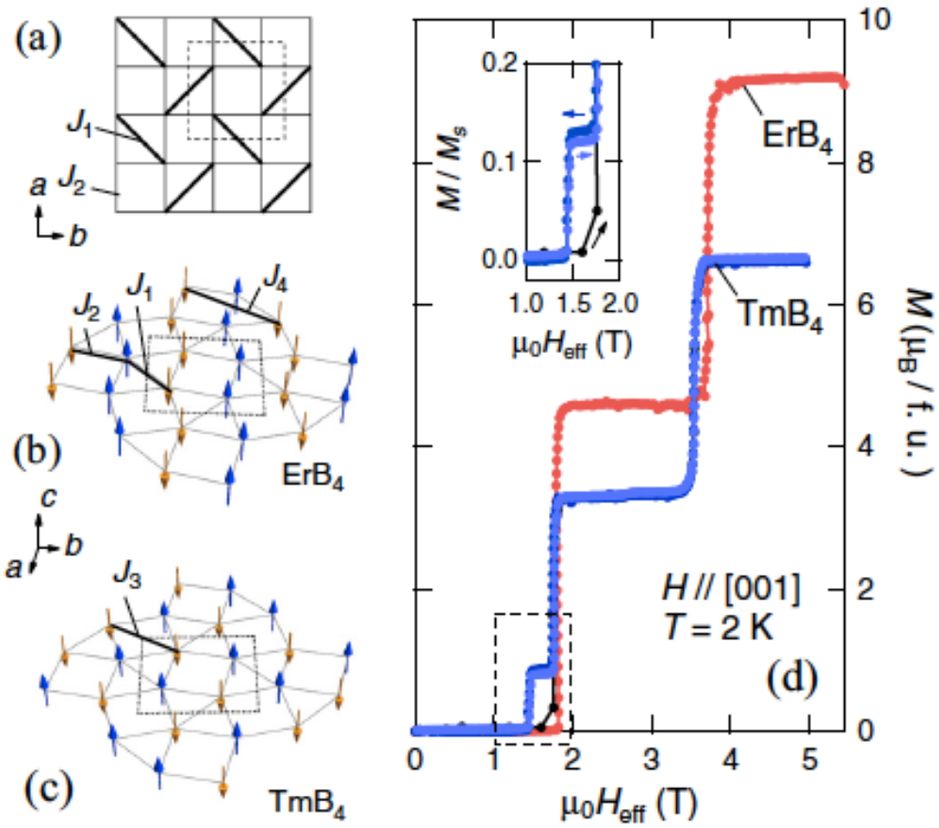

ErB_4 and TmB_4

PHYSICAL REVIEW B 95, 174405 (2017)

REB_4

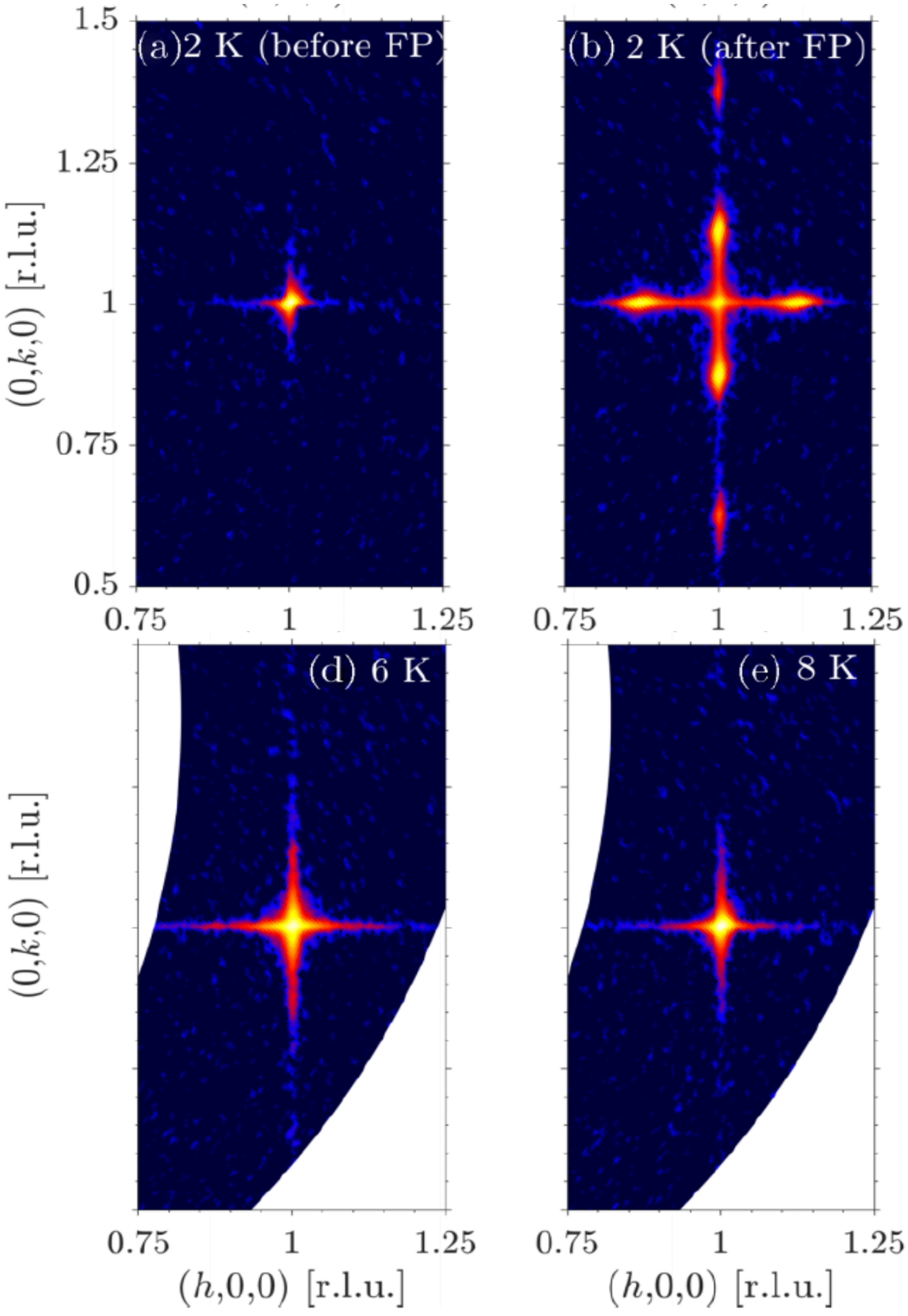

TmB_4

PRB **102**, 060407(R) (2020)

REB_4

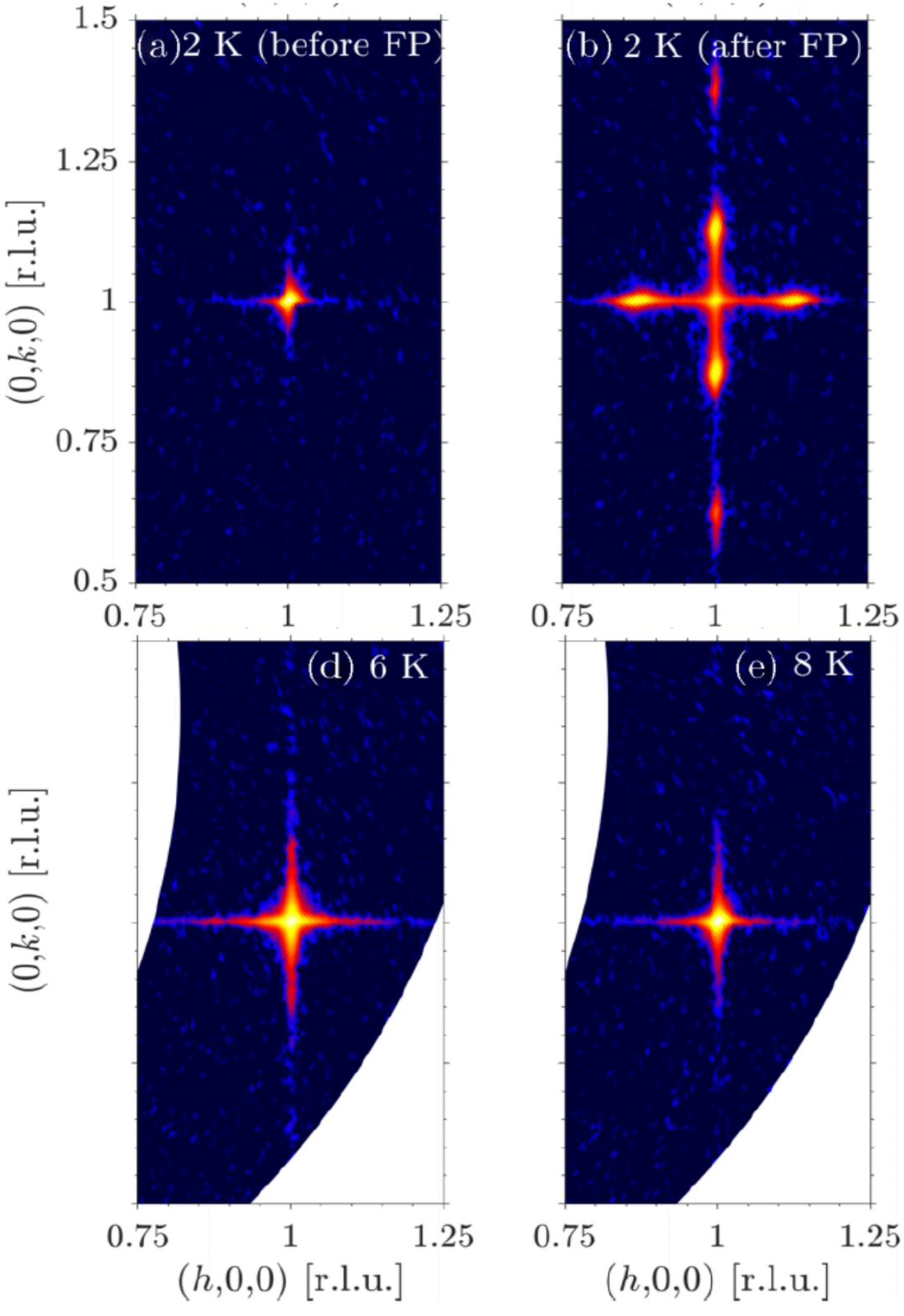

TmB_4

PRB **102**, 060407(R) (2020)

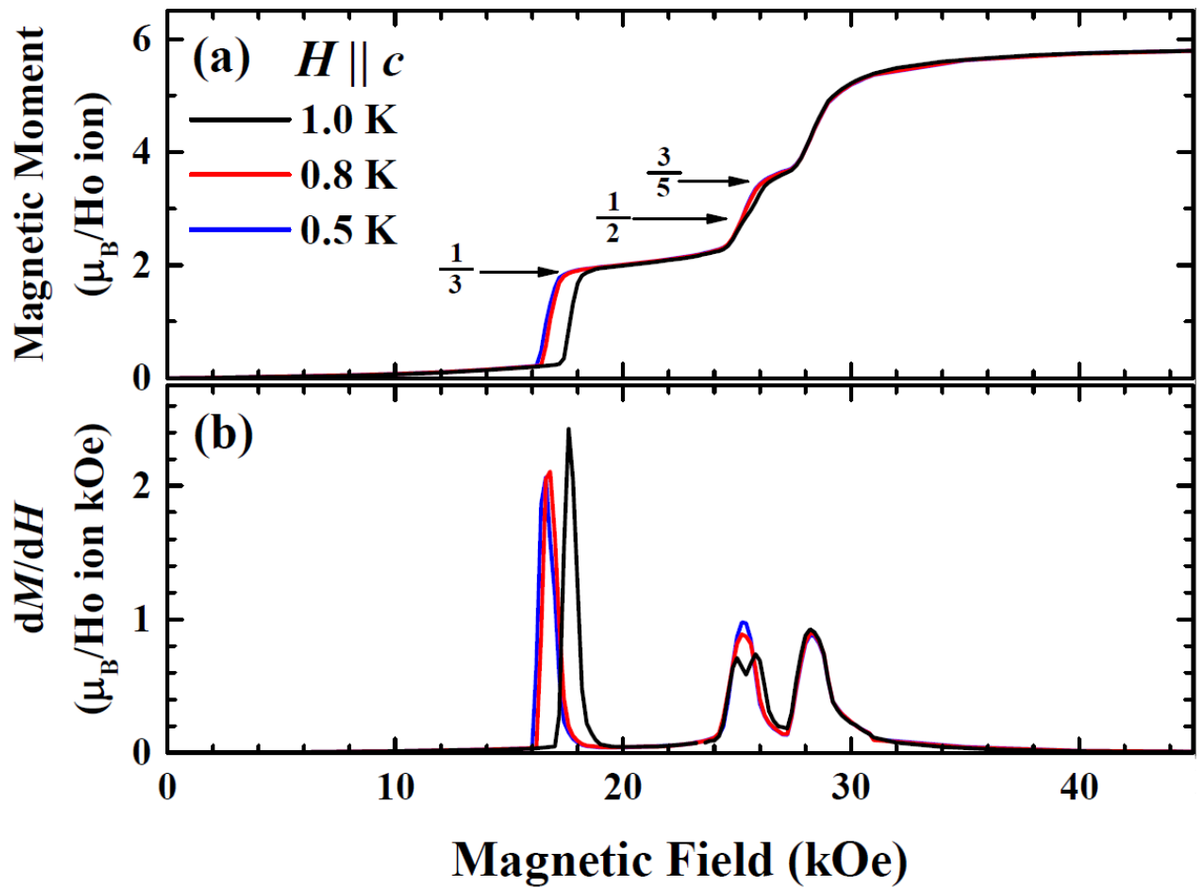

HoB_4

PRB **95**, 024410 (2017)

Scientific Reports 8, 232 (2018)

REB_4

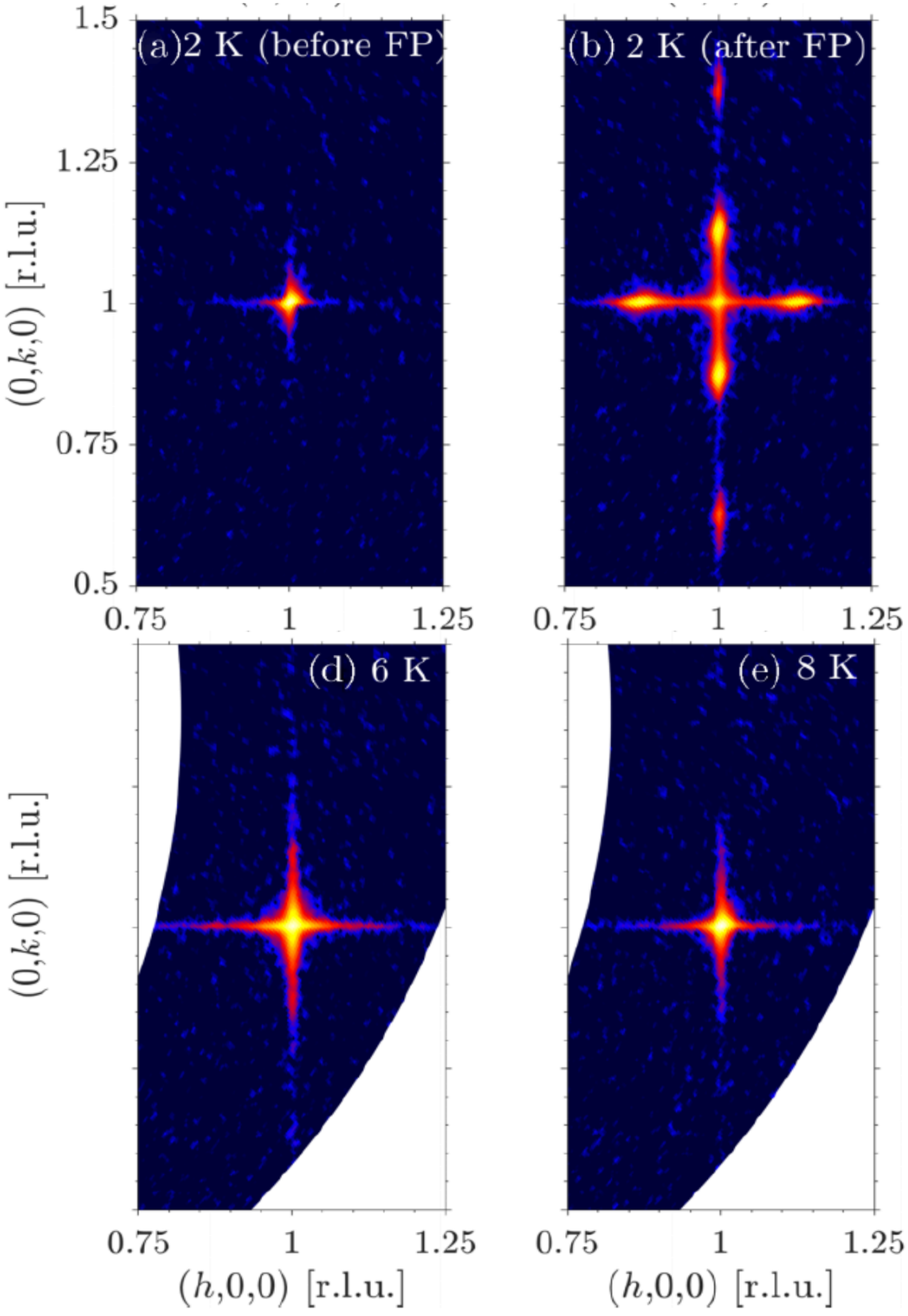

TmB_4

PRB **102**, 060407(R) (2020)

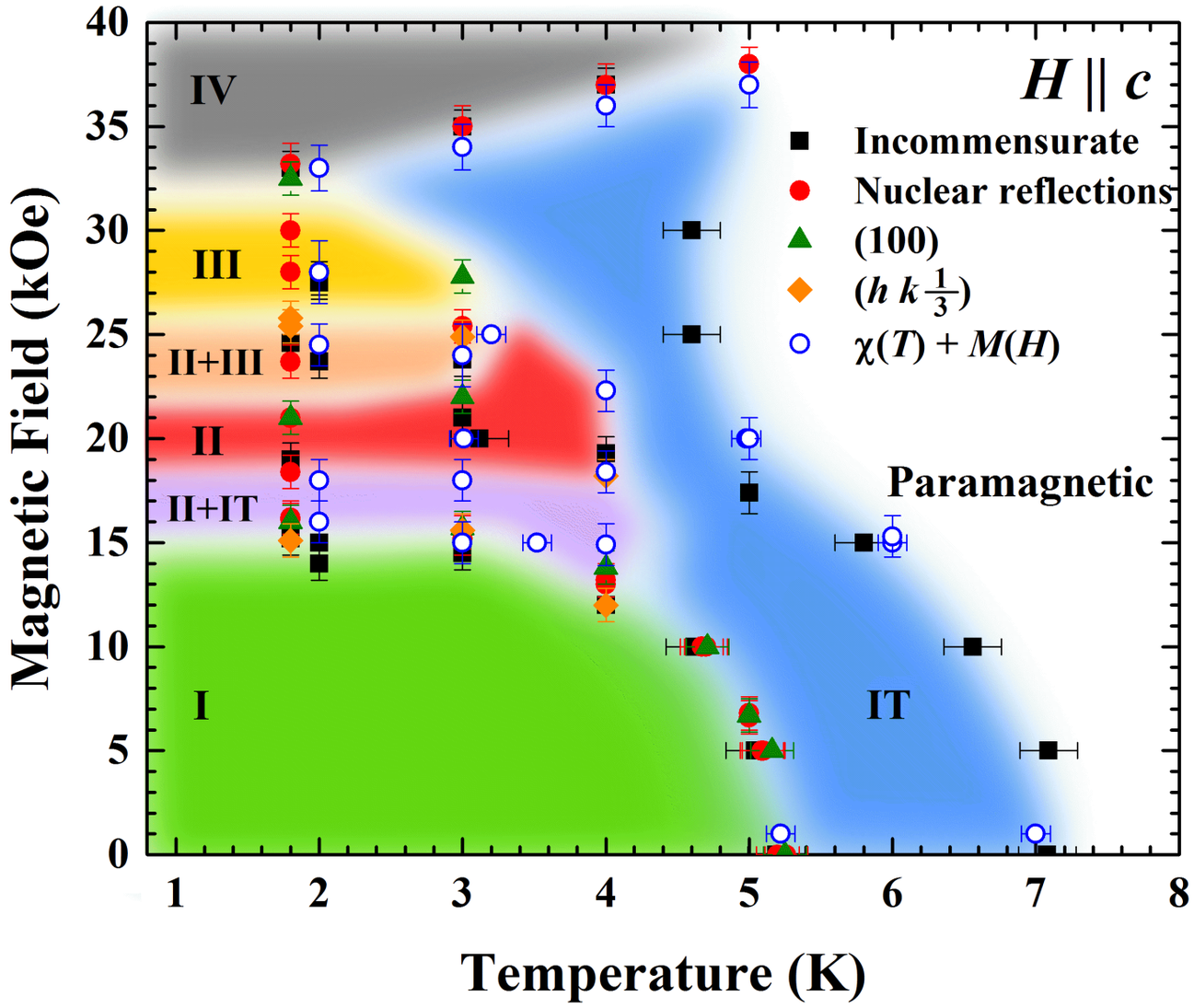

HoB_4

PRB **95**, 024410 (2017)

Scientific Reports 8, 232 (2018)

NdB_4 Magnetic properties

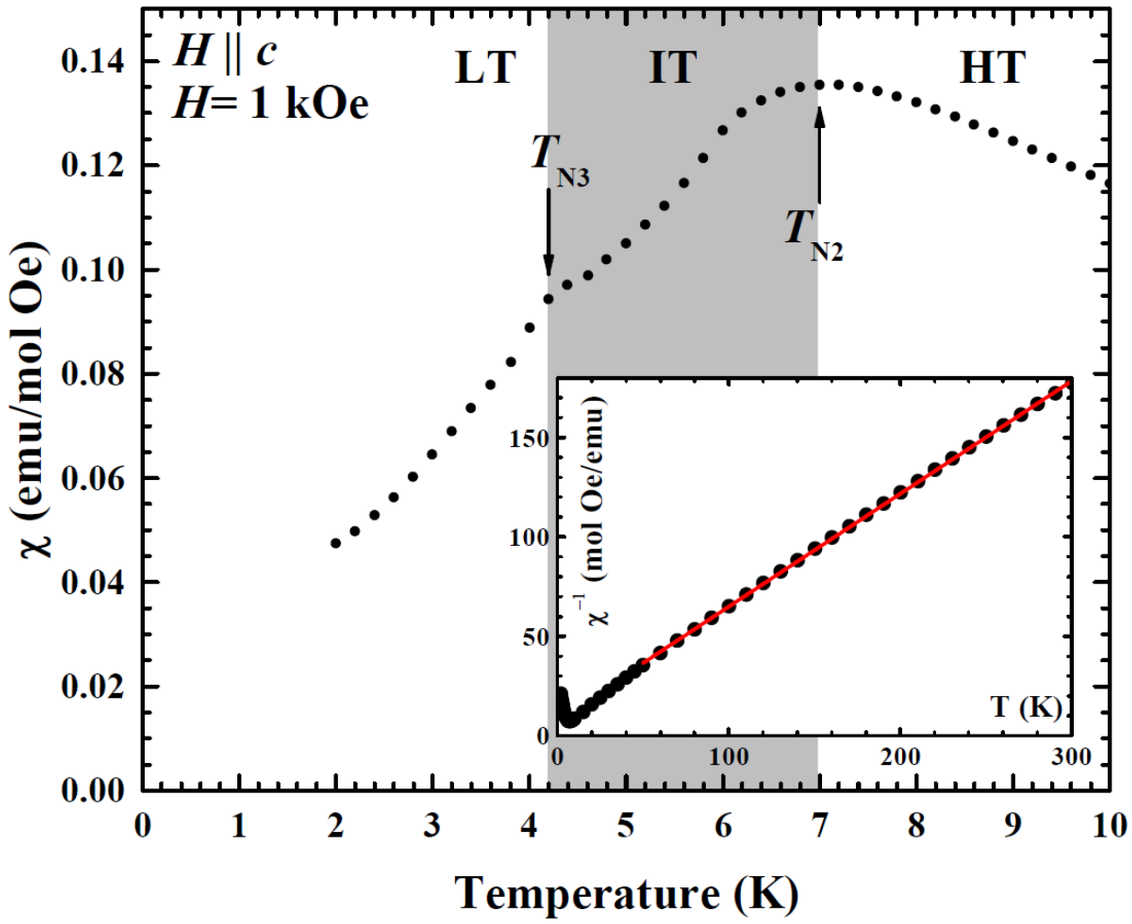

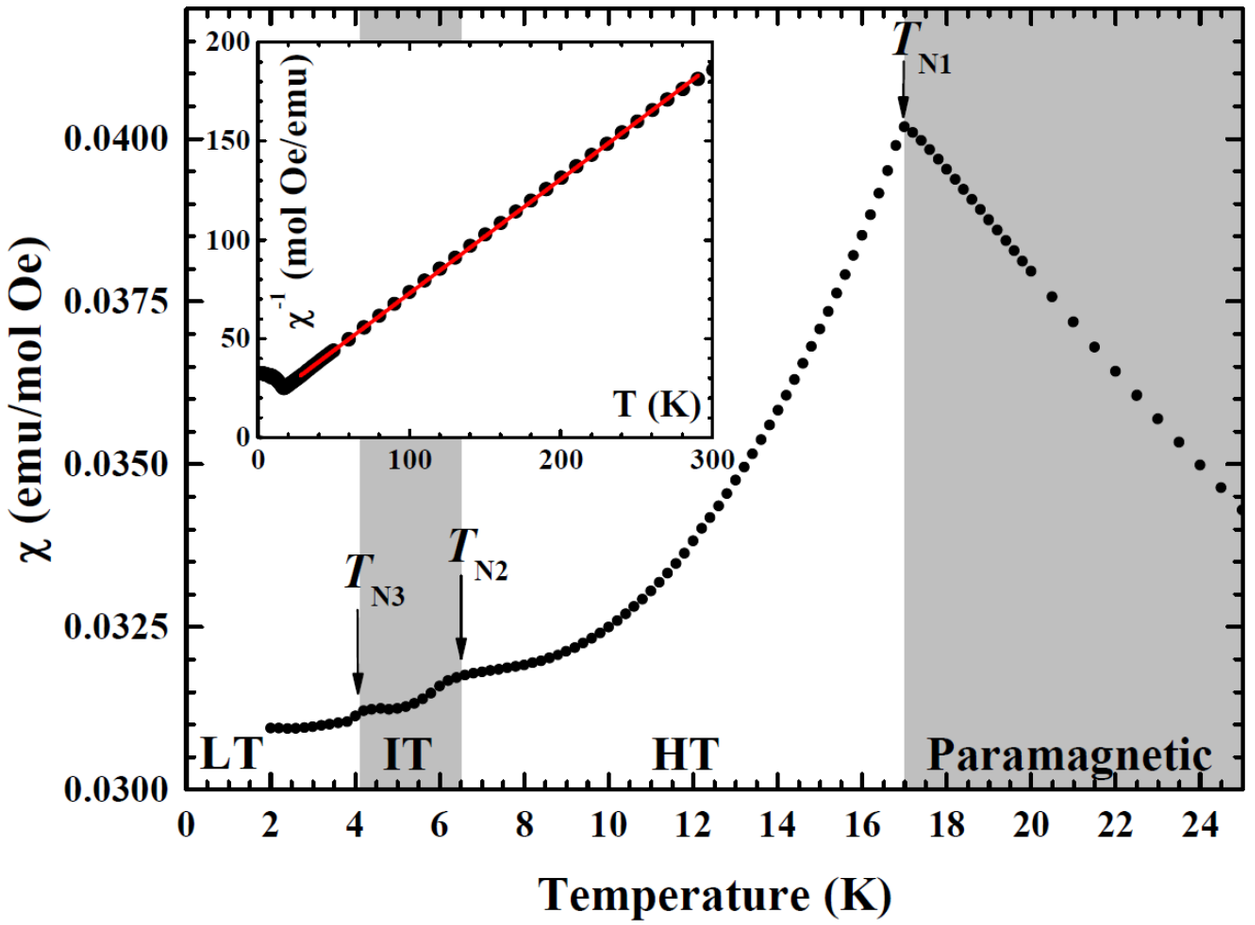

Magnetic susceptibility of NdB_4 in fields applied along and normal to the *c* axis. The insets show the inverse susceptibility.

T_{N1} = 17 K, T_{N2} = 6.8 K, T_{N3} = 4.9 K

Scientific Reports **8**, 232 (2018)

NdB_4 In-field behaviour

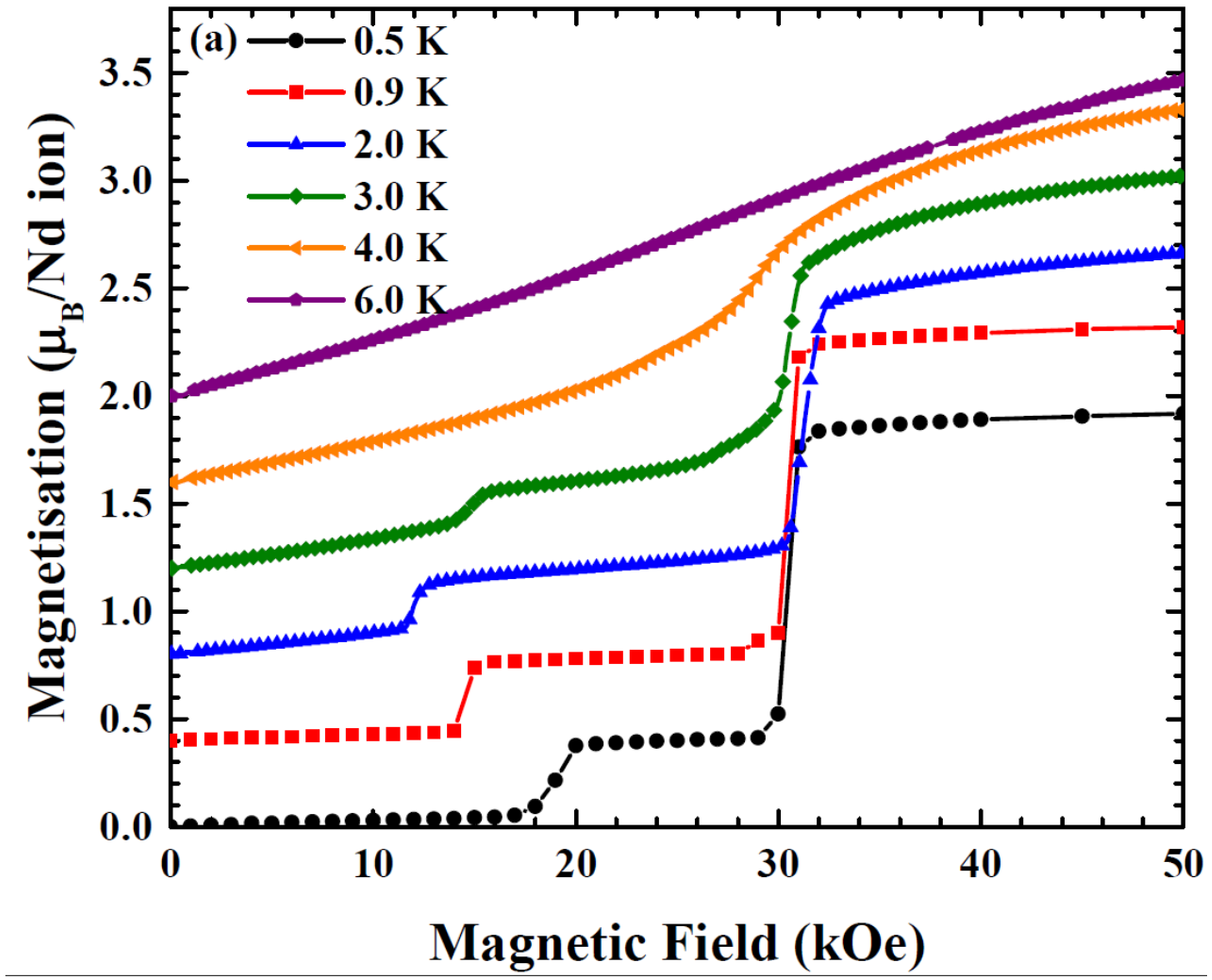

Field dependent magnetisation curves of NdB_4 for H//c.

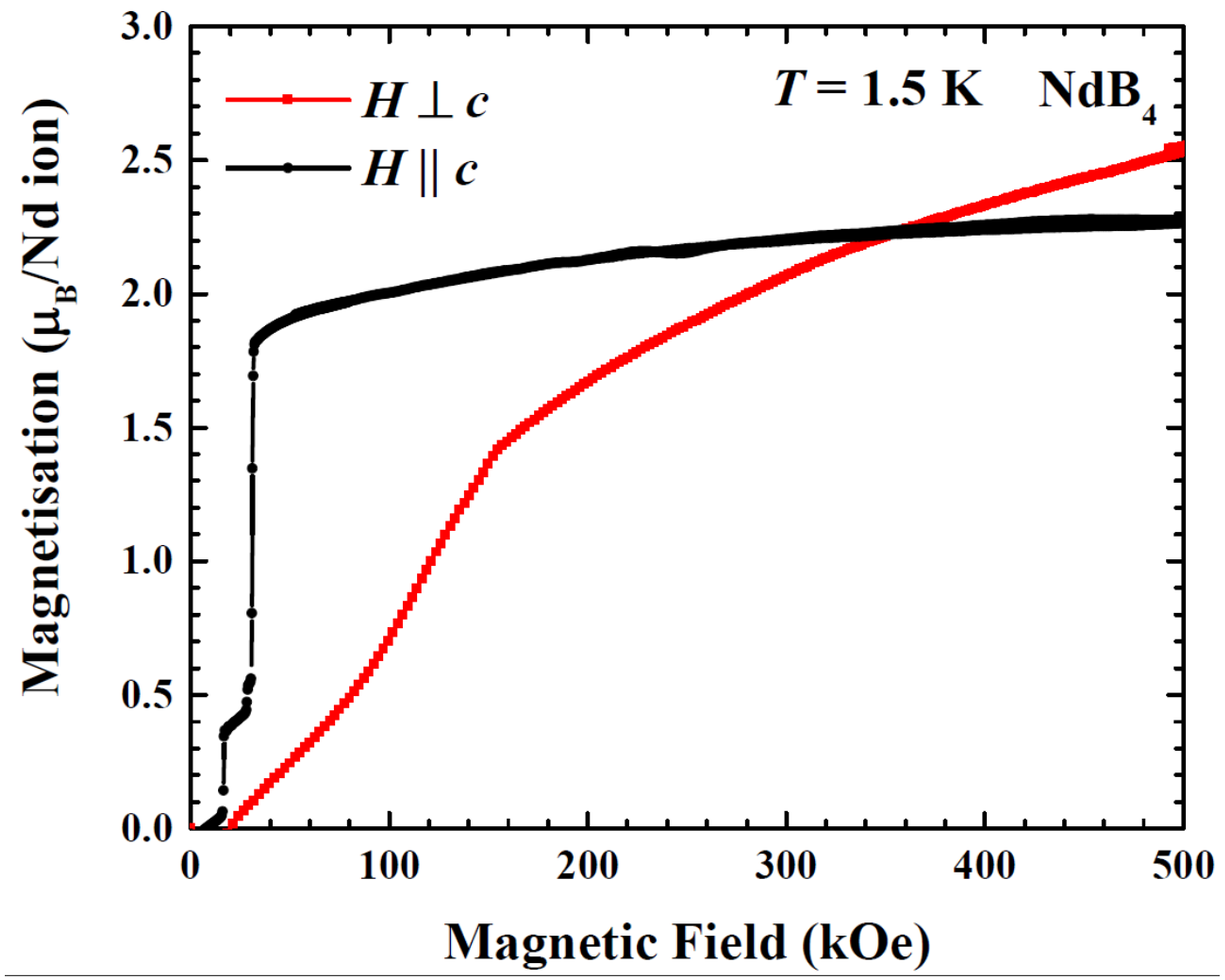

Magnetisation curves for NdB_4 in a pulsed magnetic field up to 500 kOe.

Scientific Reports **8**, 232 (2018)

NdB_4 Magnetic phase diagrams

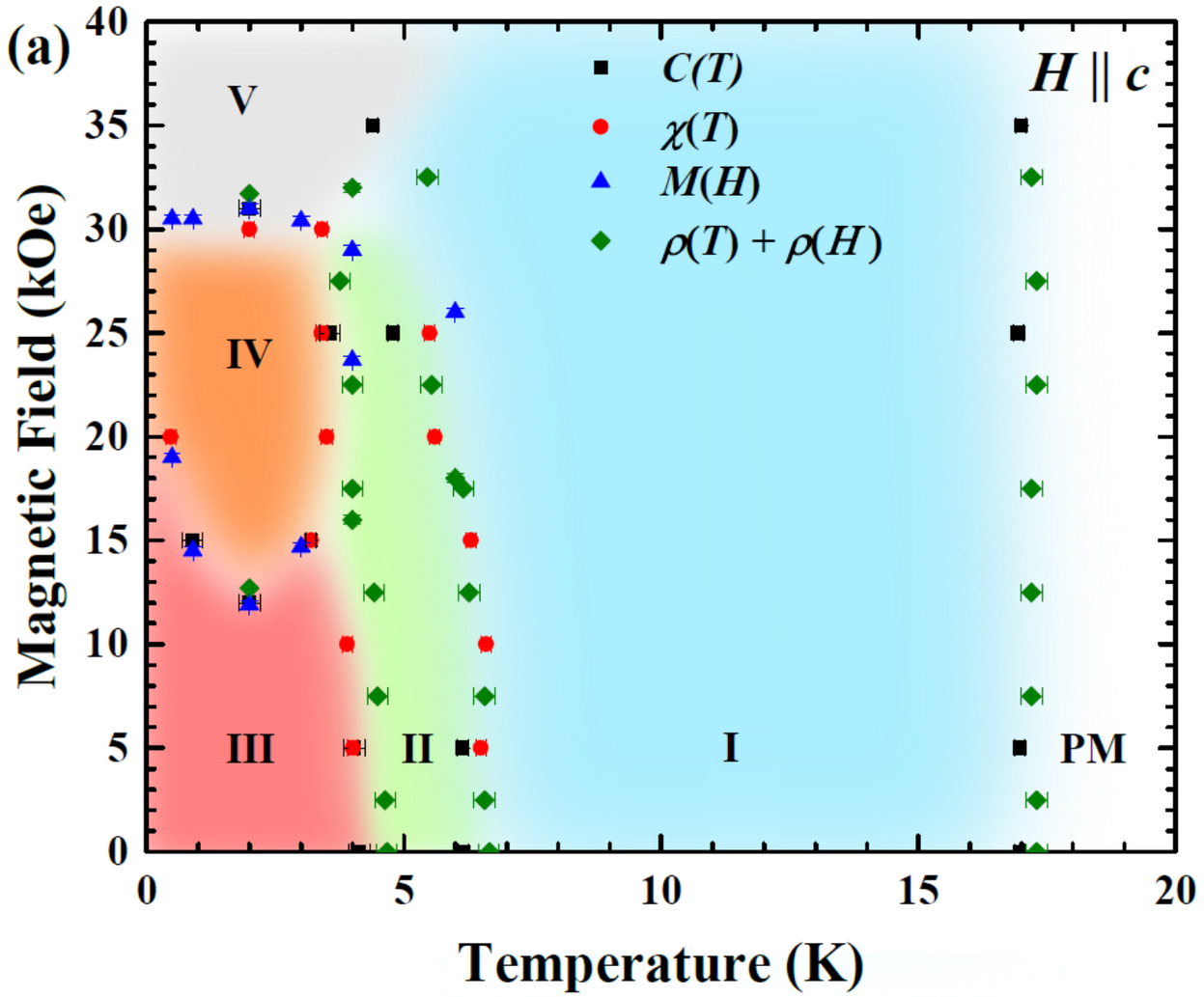

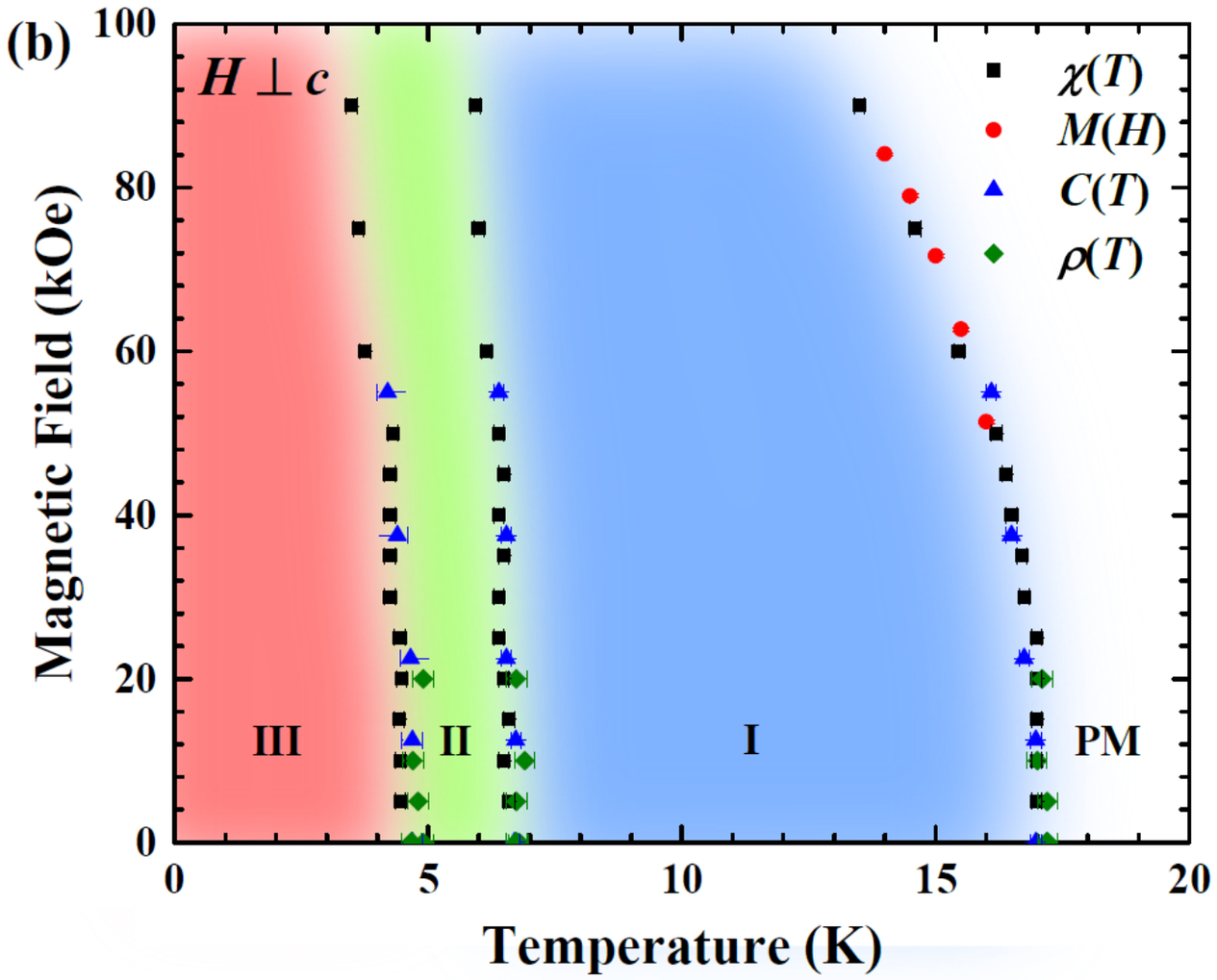

Magnetic phase diagrams of NdB_4 for different field directions.

Scientific Reports **8**, 232 (2018)

NdB_4

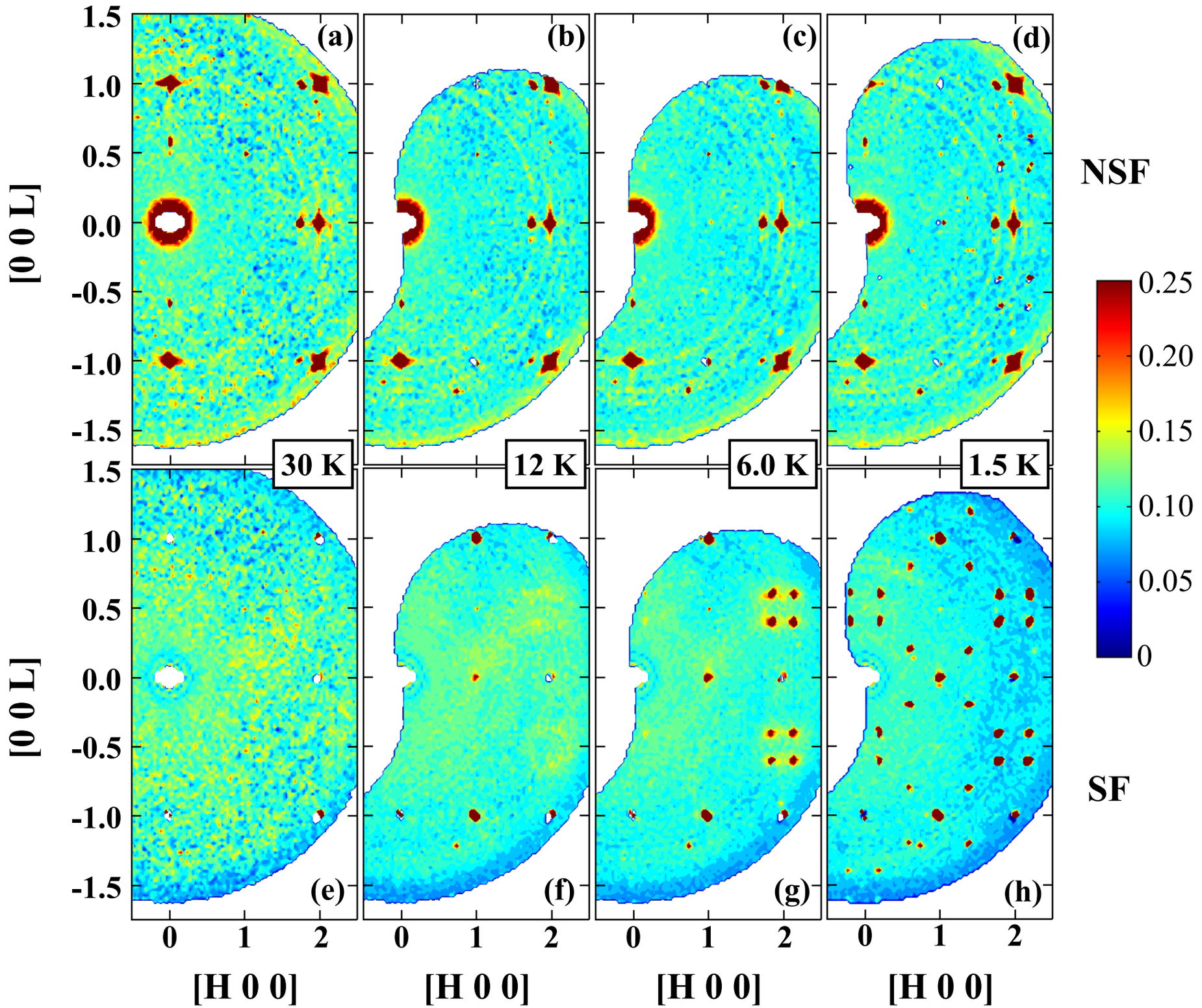

polarised neutron diffraction

D7, ILL

NdB_4 Zero-field unpolarised neutron diffraction

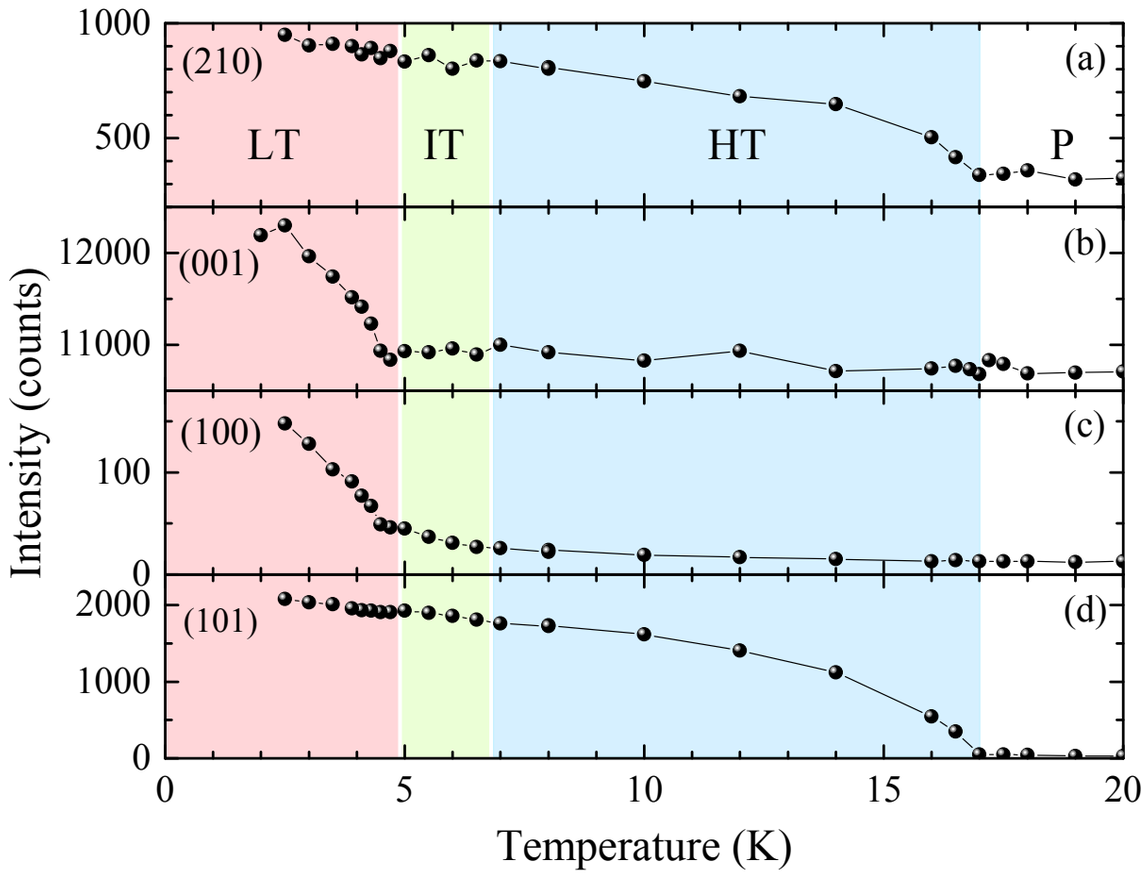

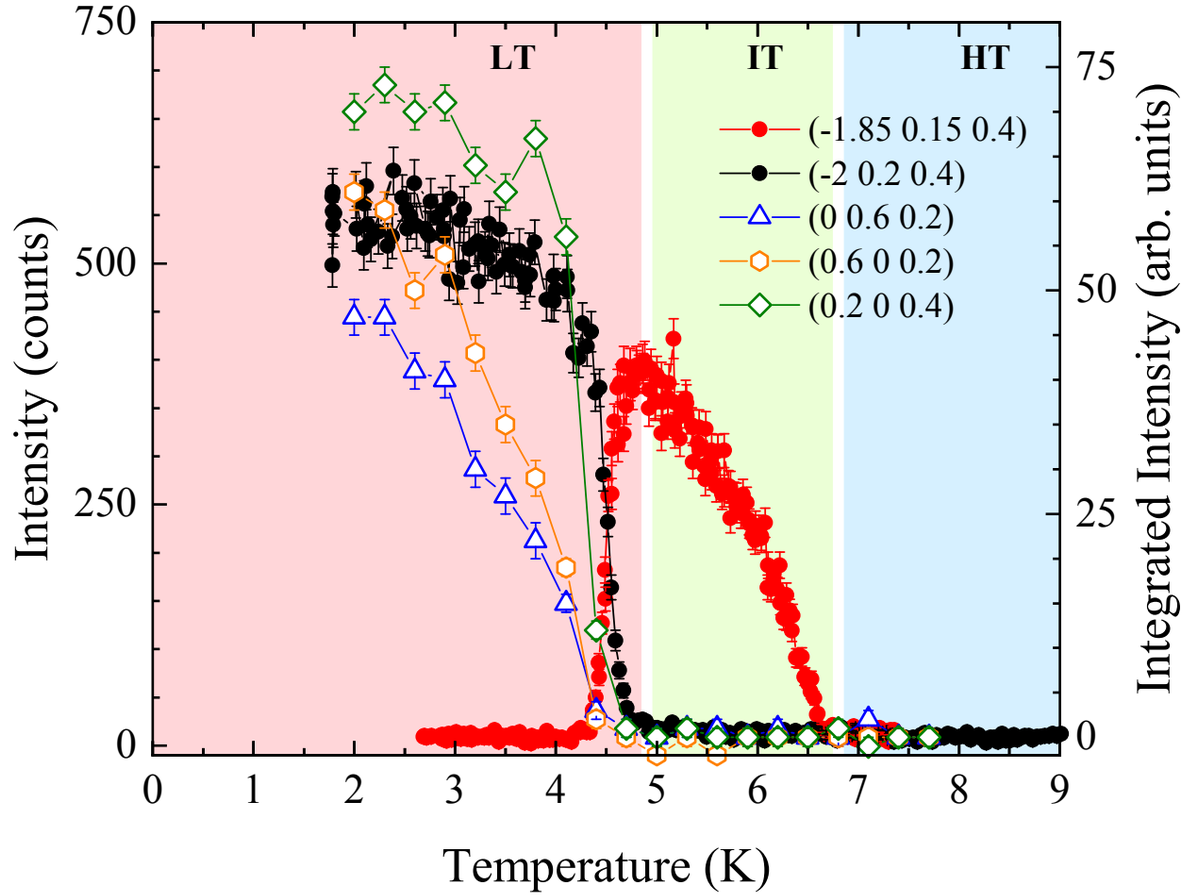

LT
$\mathbf{k_1} = 0$
$\mathbf{k_2} = (1/5\ \ 0\ \ -2/5)$
$\mathbf{k_3} = 2\mathbf{k_2} = (2/5\ \ 0\ \ -4/5)$

IT
$\mathbf{k_1} = 0$
$\mathbf{k'_2} = (0.142\ \ 0.142\ \ -2/5)$

HT
$\mathbf{k_1} = 0$

NdB_4 Zero-field polarised neutron diffraction

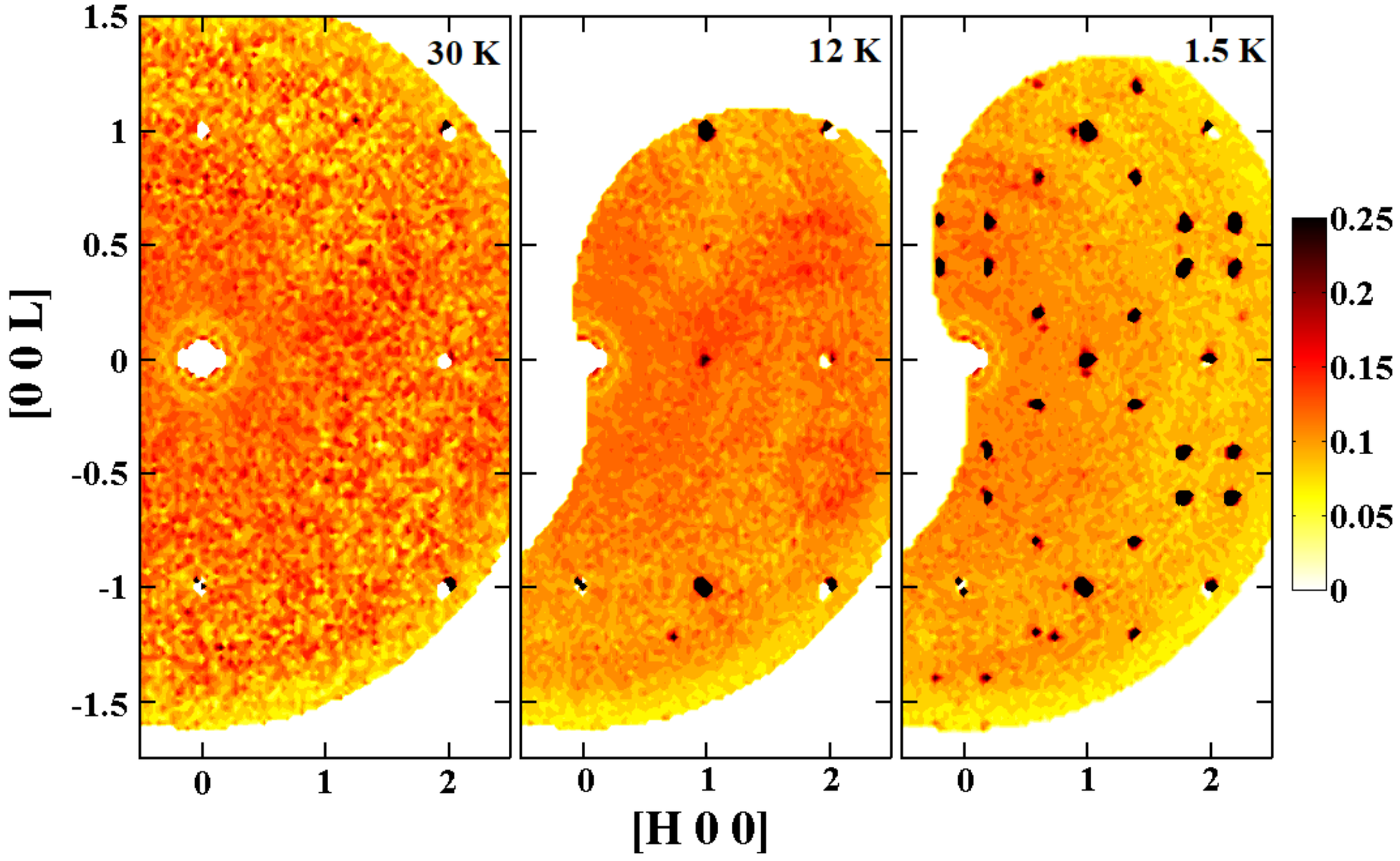

PRB **109**, L220411 (2024)

polarised neutron diffraction

D7, ILL

NdB_4

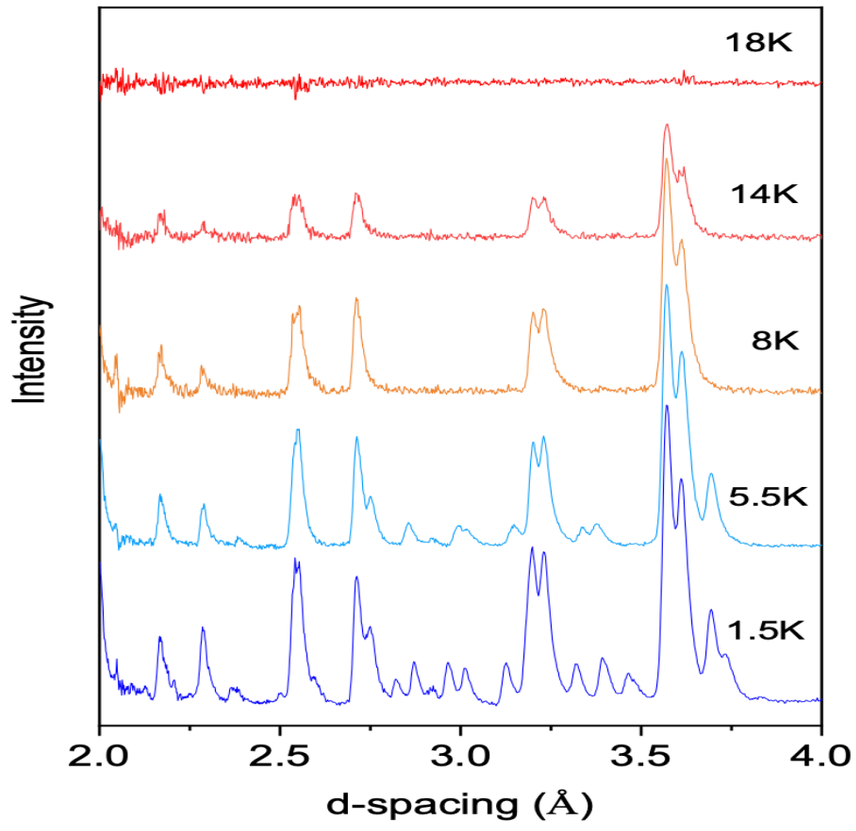

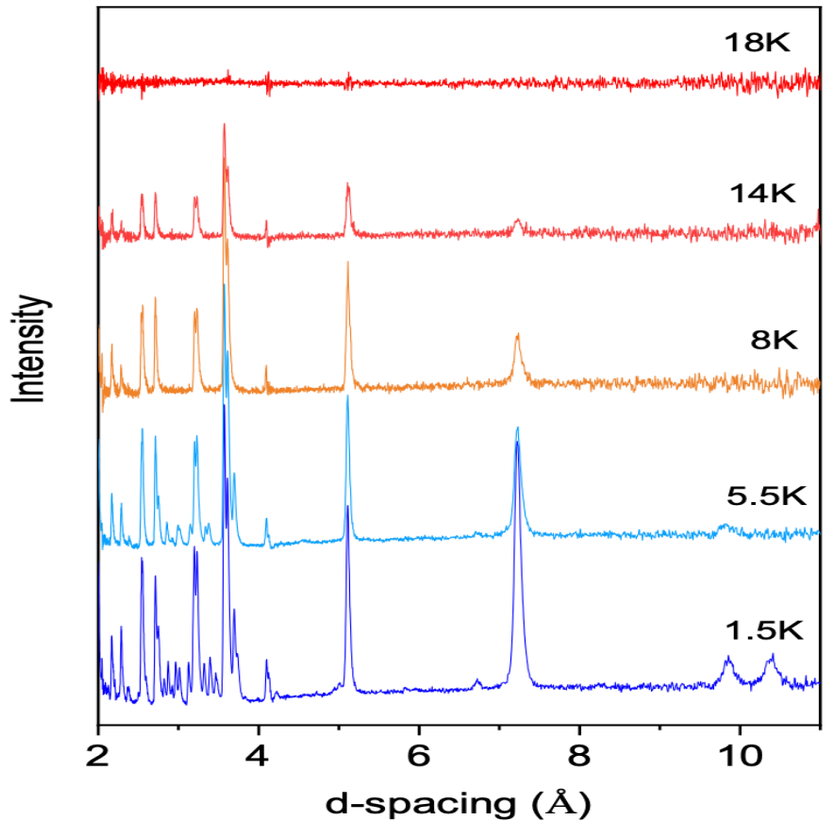

$\mathbf{k_1} = 0$

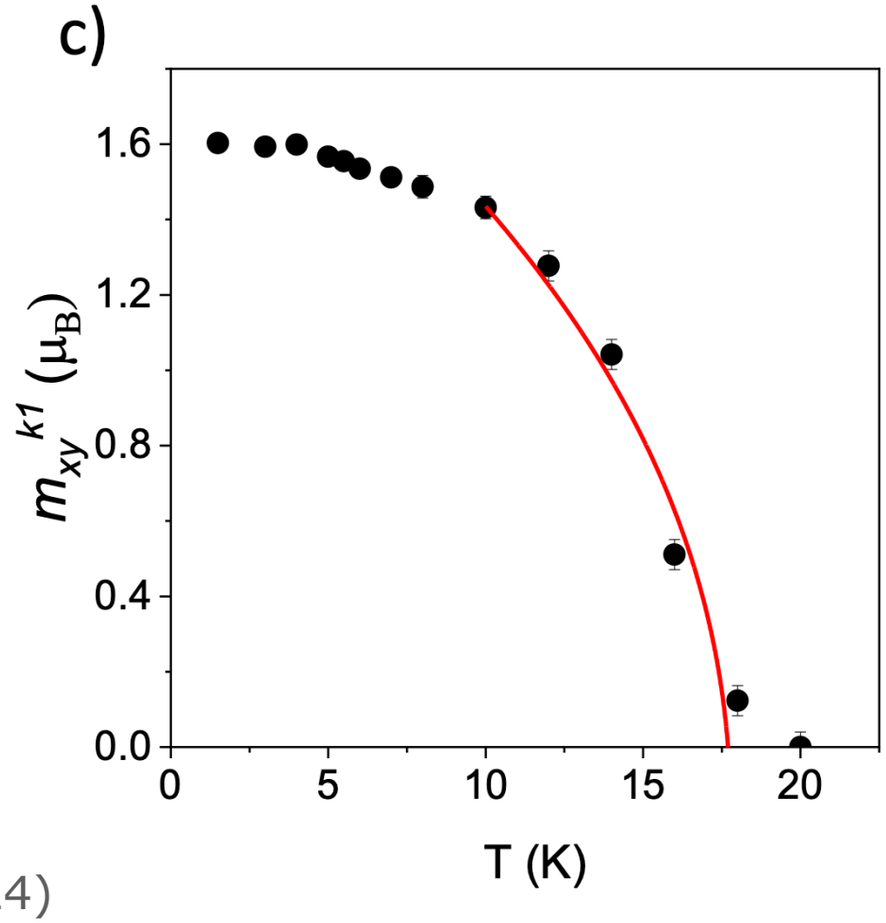

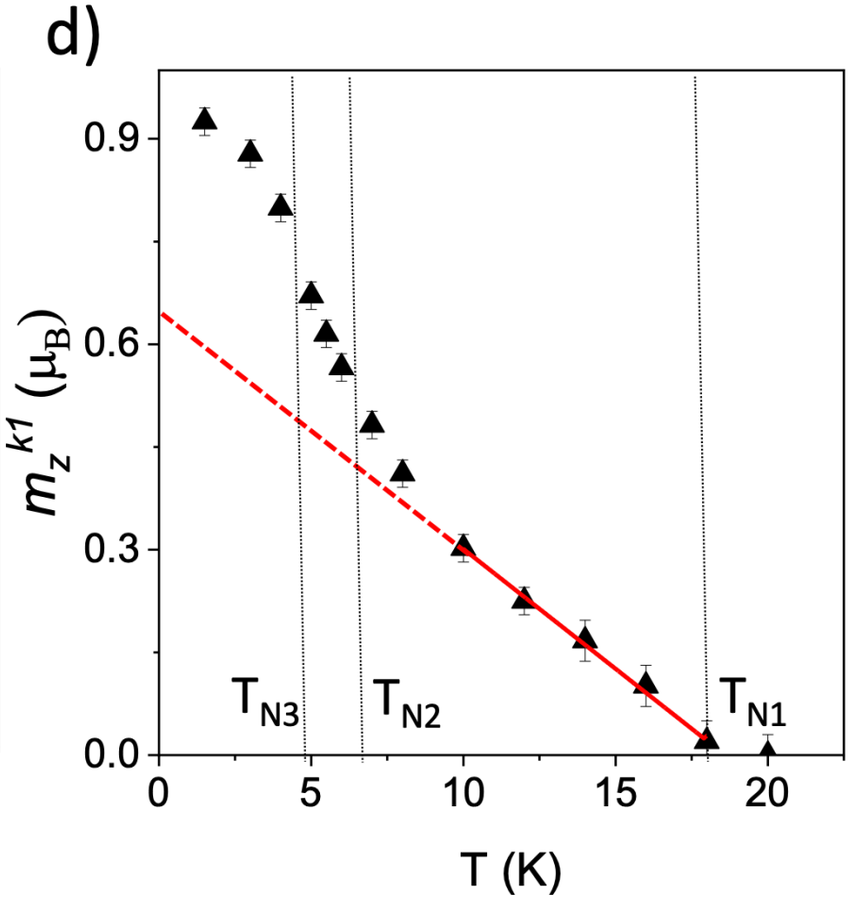

PRB **109**, L220411 (2024)

powder neutron diffraction

WISH, ISIS

NdB_4

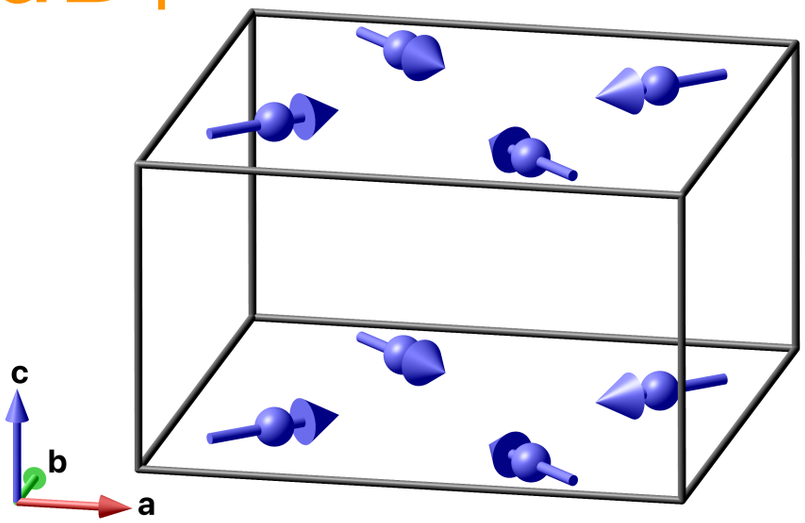

In-plane (all-in-all-out)
Fourier component, $m^{\mathbf{k1}}{}_{xy}$

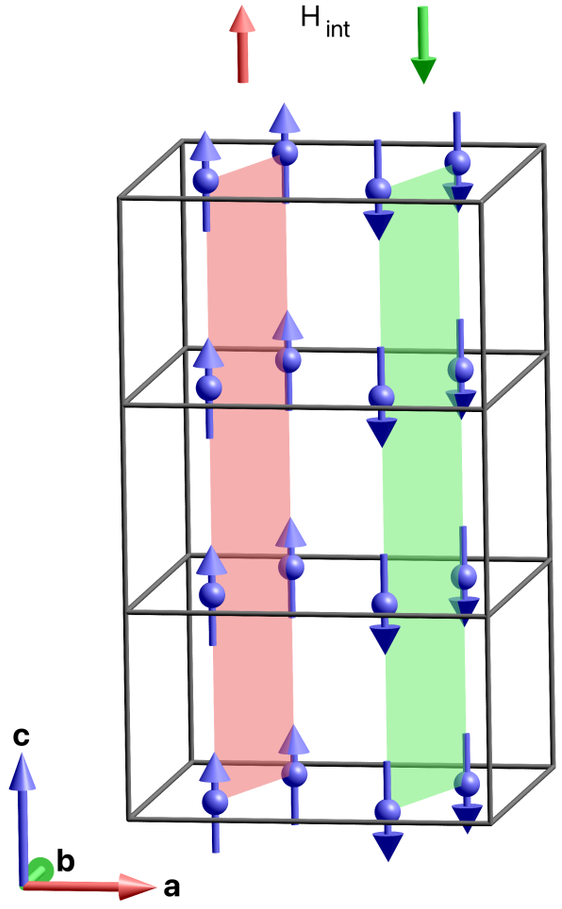

Out-of-plane Fourier component, $m^{\mathbf{k1}}{}_{z}$, defining the alternating nominally up direction of the internal staggered field, H_{int}

$\mathbf{k_1} = 0$
$\mathbf{k_2} = (1/5\ \ 0\ \ -2/5)$
$\mathbf{k_3} = 2\mathbf{k_2} = (2/5\ \ 0\ \ -4/5)$

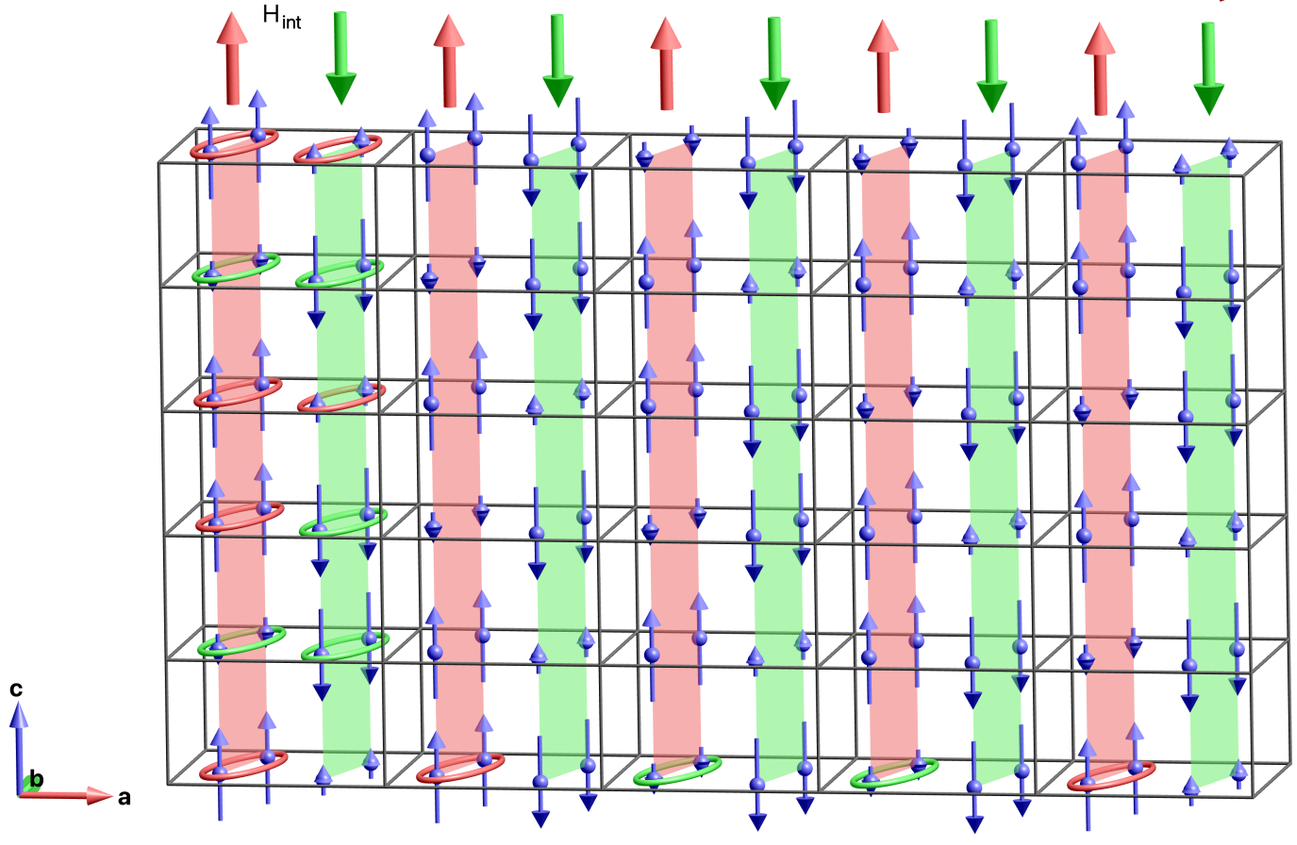

@ 1.5 K
$m^{\mathbf{k1}}{}_{xy} = 1.60\ \mu_B$
$m^{\mathbf{k1}}{}_{z} = 0.93\ \mu_B$
$m^{\mathbf{k2}}{}_{z} = 1.72\ \mu_B$
$m^{\mathbf{k3}}{}_{z} = 0.66\ \mu_B$

An anharmonic spin density wave consisting of three Fourier components, $m^{\mathbf{k1}}{}_{z}$, $m^{\mathbf{k2}}{}_{z}$, and $m^{\mathbf{k3}}{}_{z}$.

PRB **109**, L220411 (2024)

powder neutron diffraction

WISH, ISIS

NdB_4

$$J_1^x = J_1^y = 0$$

$$J_1^z \neq 0$$

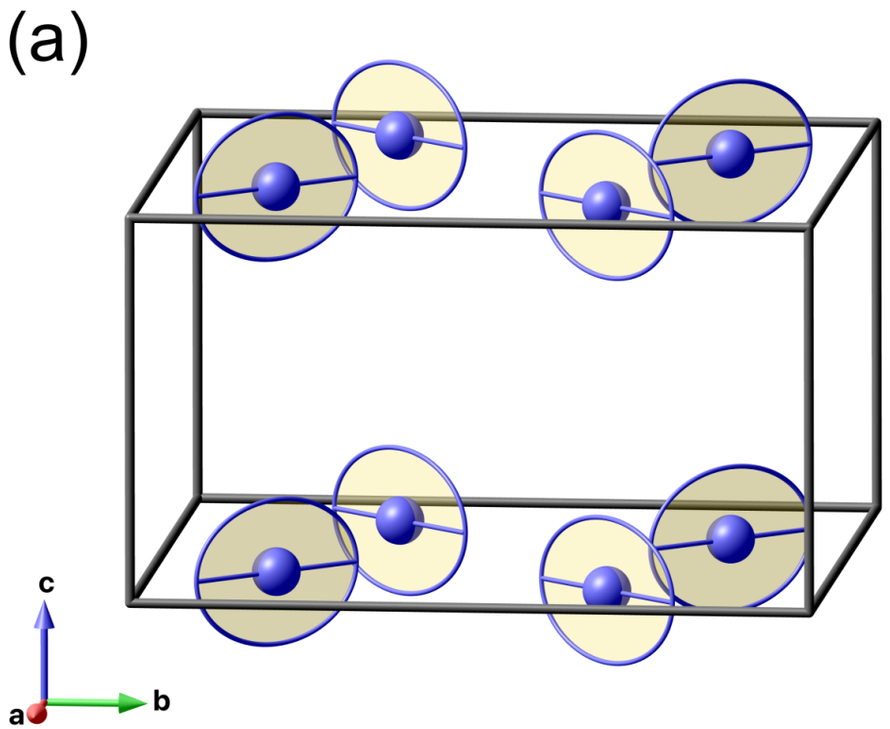

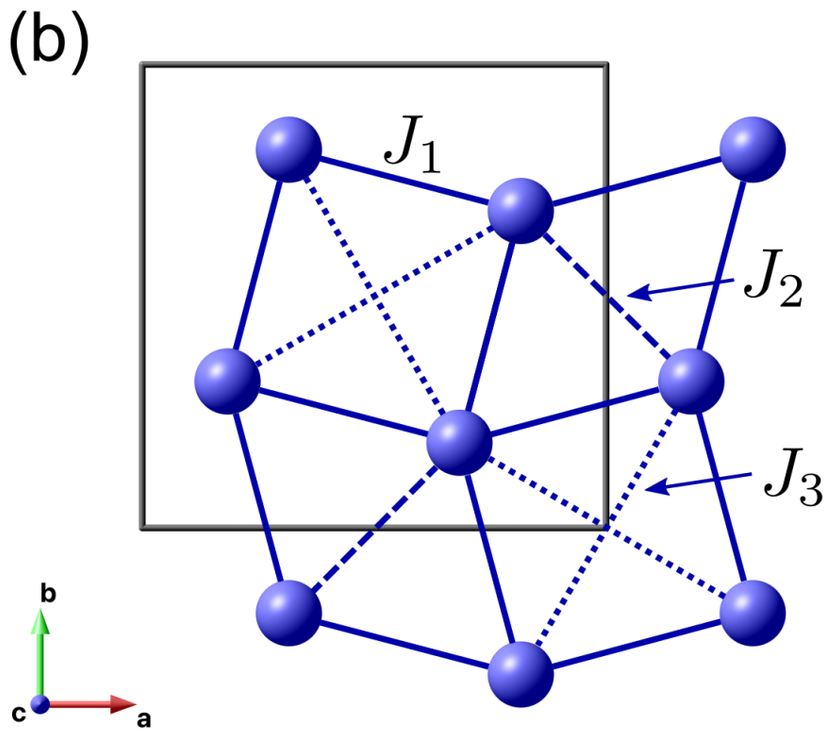

δ^{k1}

$\delta^{k1} m_{xy}^{k1} m_z^{k1}$

$\delta^{k1} m_{xy}^{k1} = H_{int}$

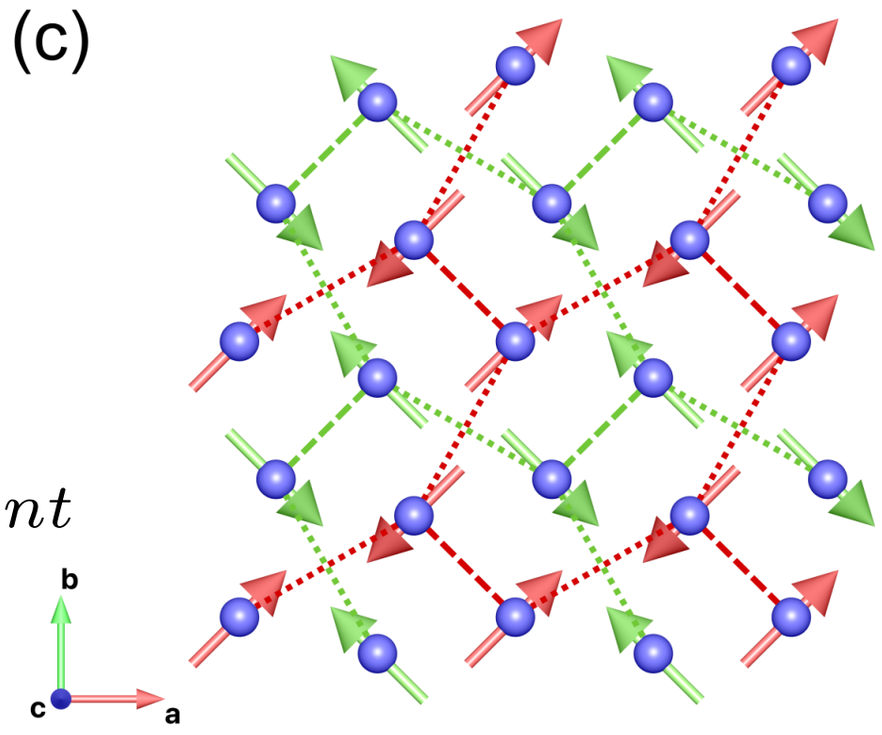

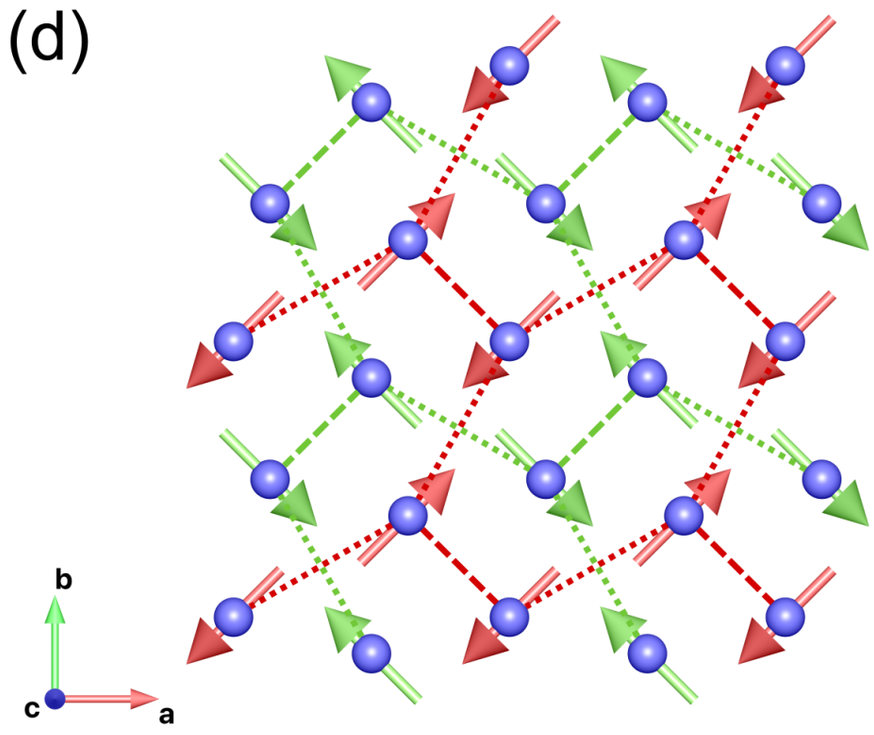

PRB **109**, L220411 (2024)

powder neutron diffraction

WISH, ISIS

NdB_4

In-field behaviour

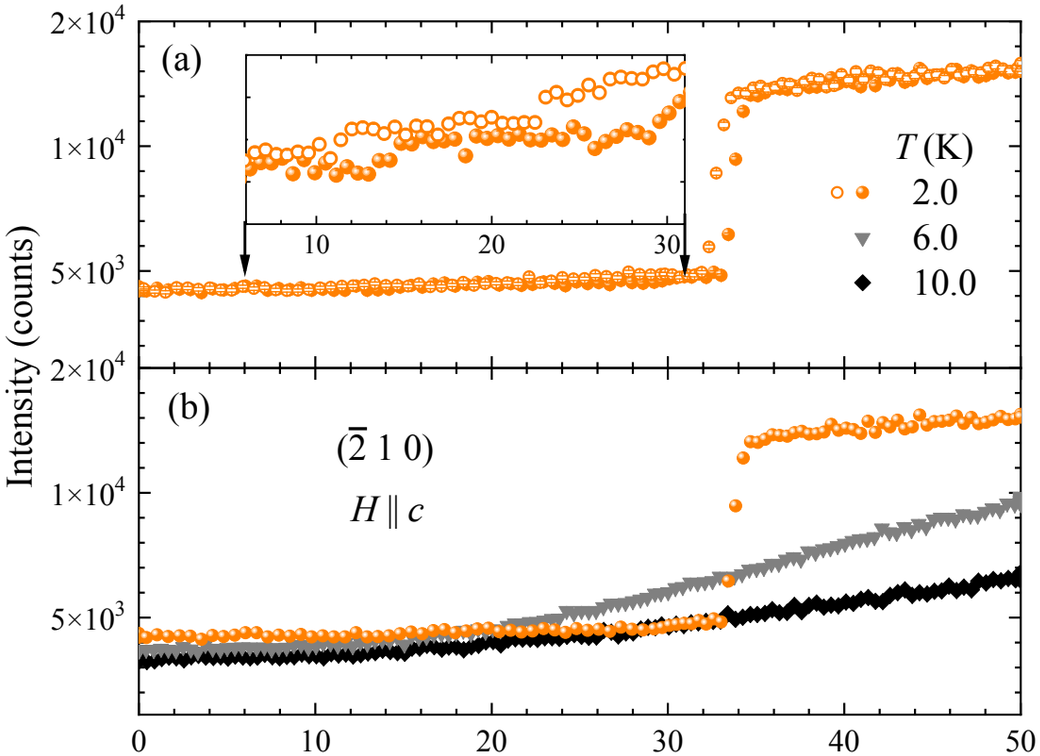

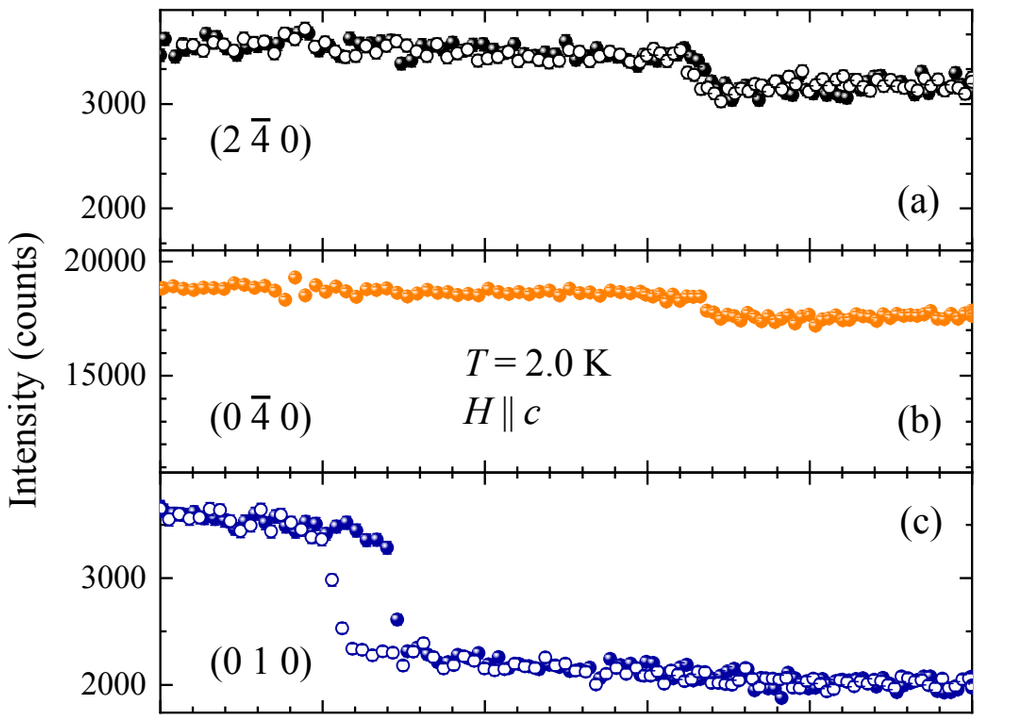

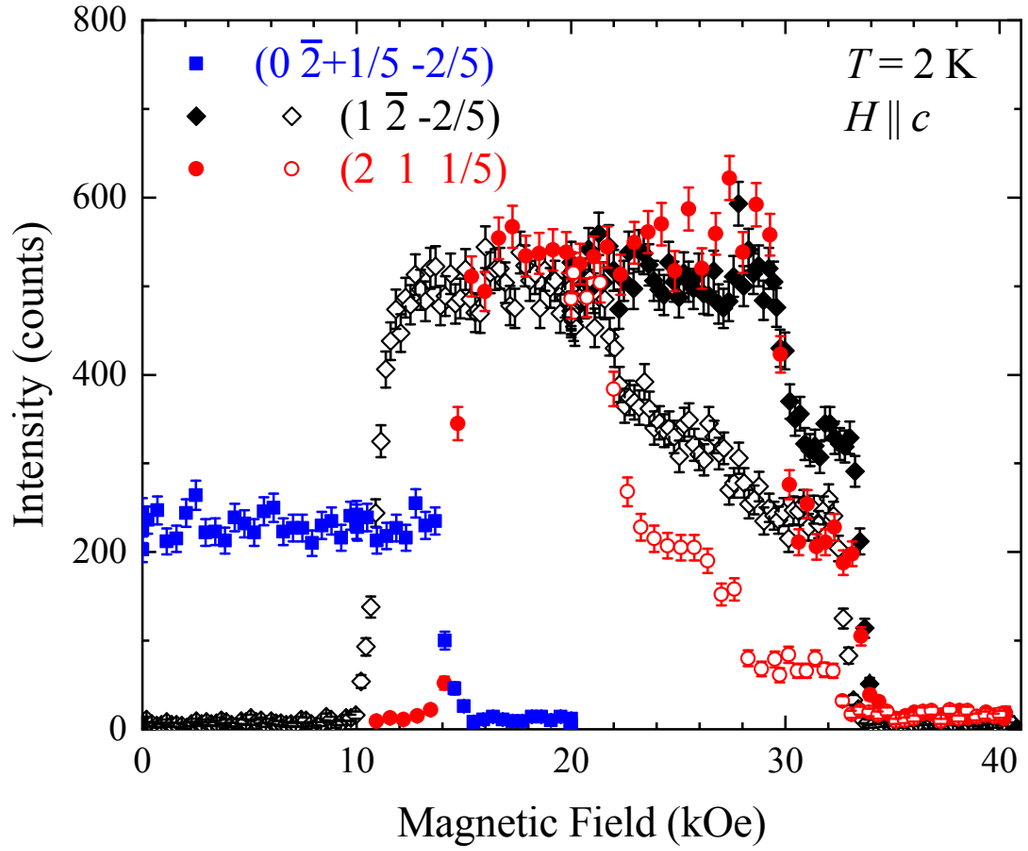

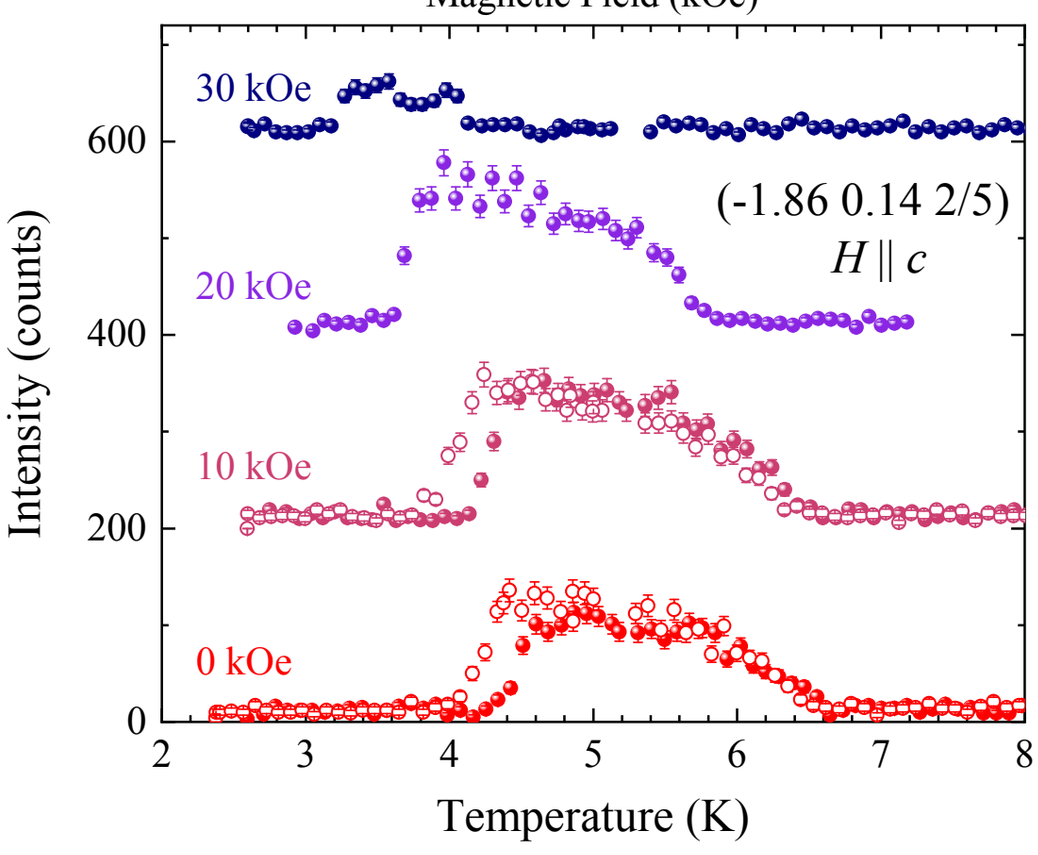

single crystal neutron diffraction

D10, ILL

Summary

- Ground state of NdB_4 represents a unique interplay between strongly anisotropic spins in a frustrated exchange topology and non-magnetic order parameter

- It involves coexisting instabilities coupled via an internal field created by the non-magnetic distortion, undetectable in the present diffraction data

- One instability is the orthogonal all-in all-out order of the *xy*-components of the moments. Another is SDW of the out-of-plane moments, locked to 5-fold periodicity of the lattice to form 3U2D structure

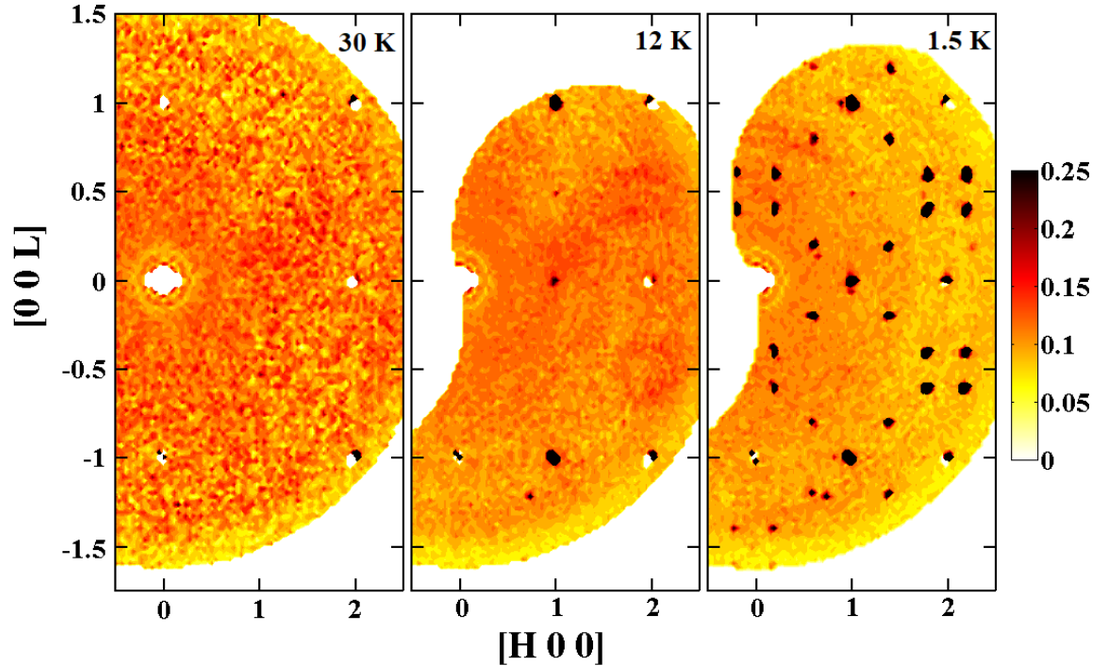

ErB_4

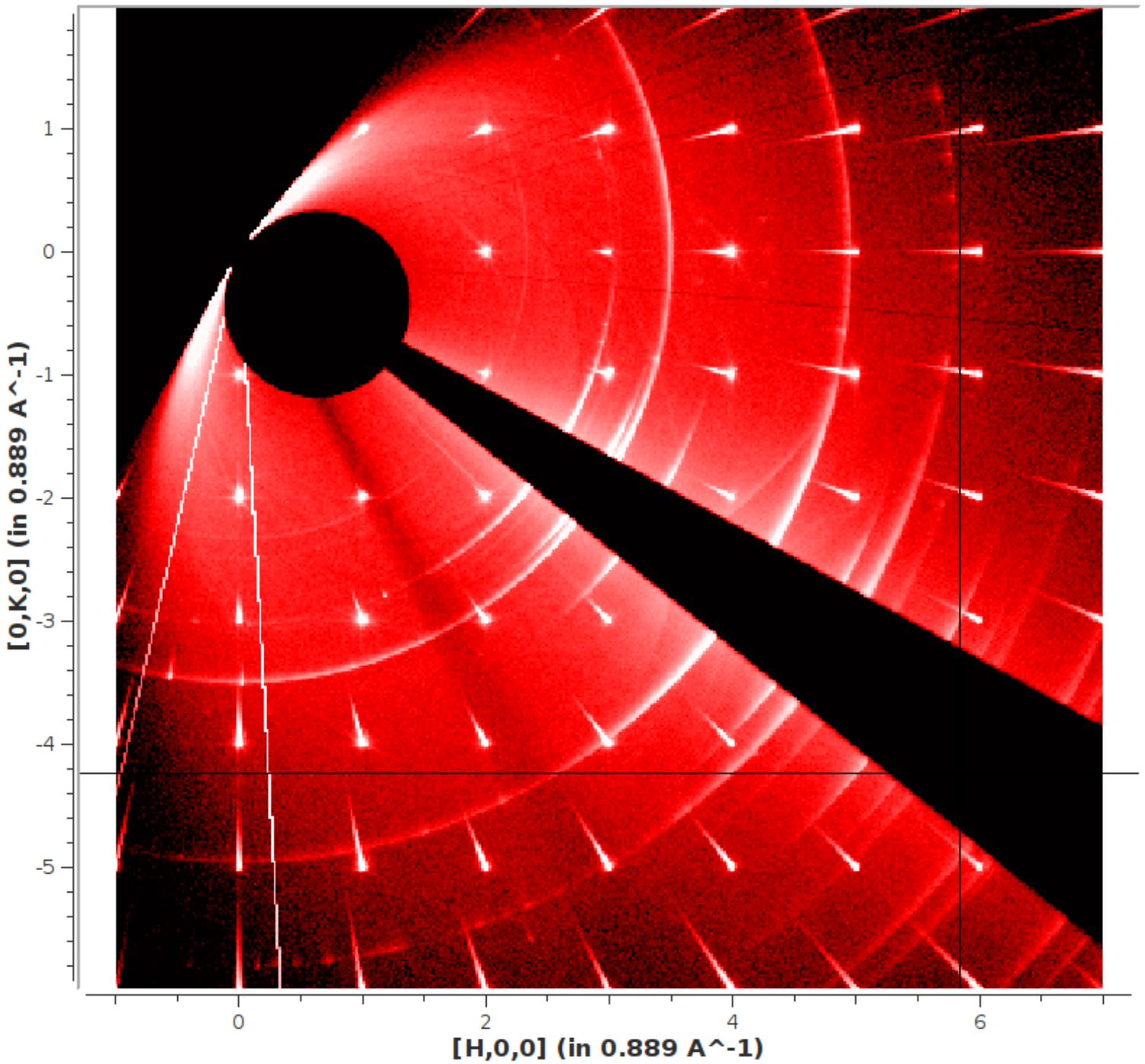

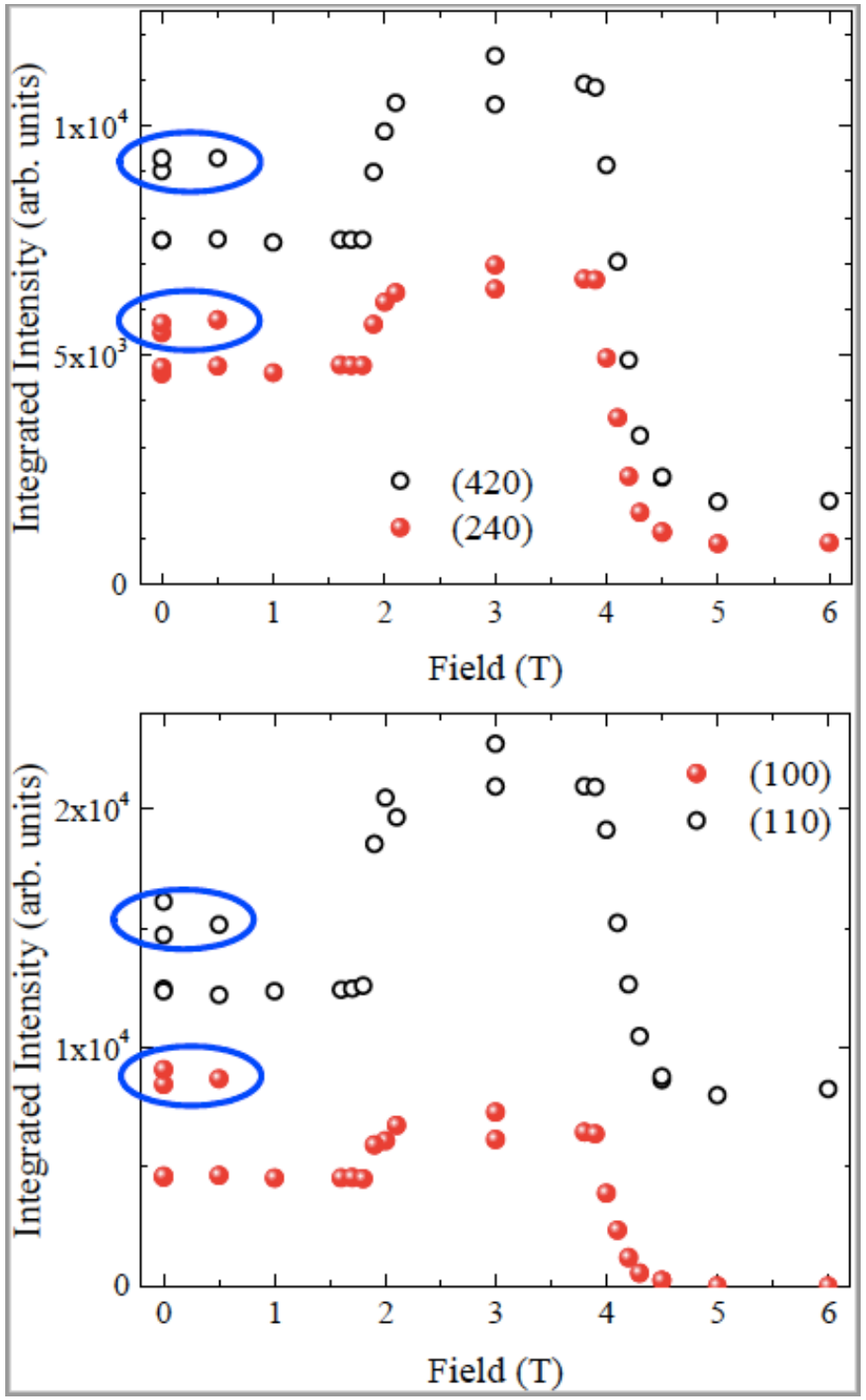

single crystal neutron diffraction

WISH, ISIS

ErB_4

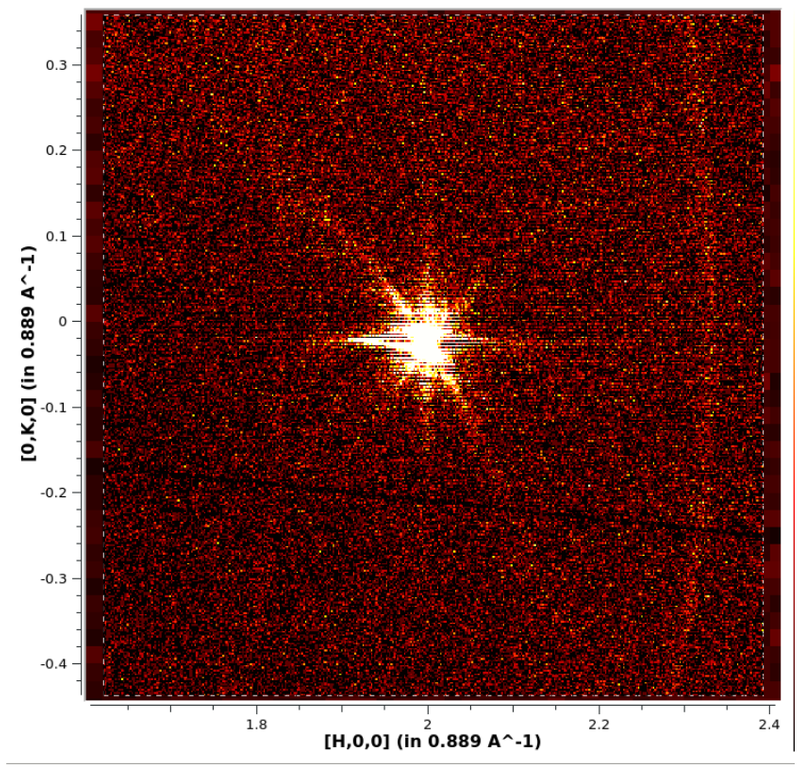
0.3
0.2
0.1
0
-0.1
-0.2
-0.3
-0.4
[0,K,0] (in 0.889 A^-1)
1.8
2
2.2
2.4
[H,0,0] (in 0.889 A^-1)

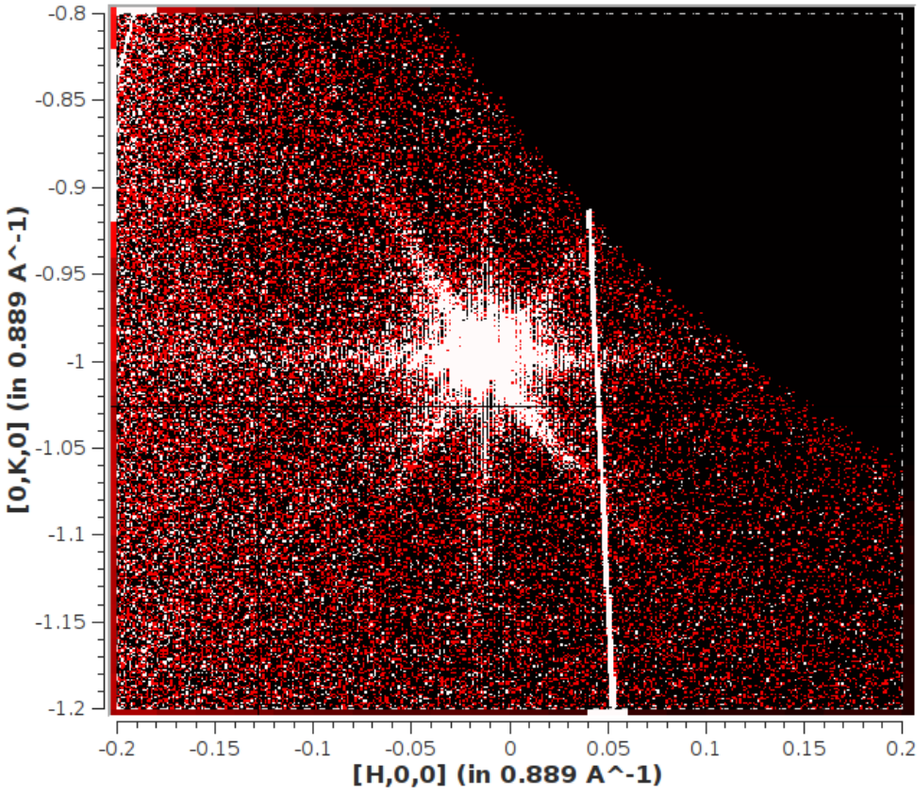
-0.8
-0.85
-0.9
-0.95
-1
-1.05
-1.1
-1.15
-1.2
[0,K,0] (in 0.889 A^-1)
-0.2
-0.15
-0.1
-0.05
0
0.05
0.1
0.15
0.2
[H,0,0] (in 0.889 A^-1)

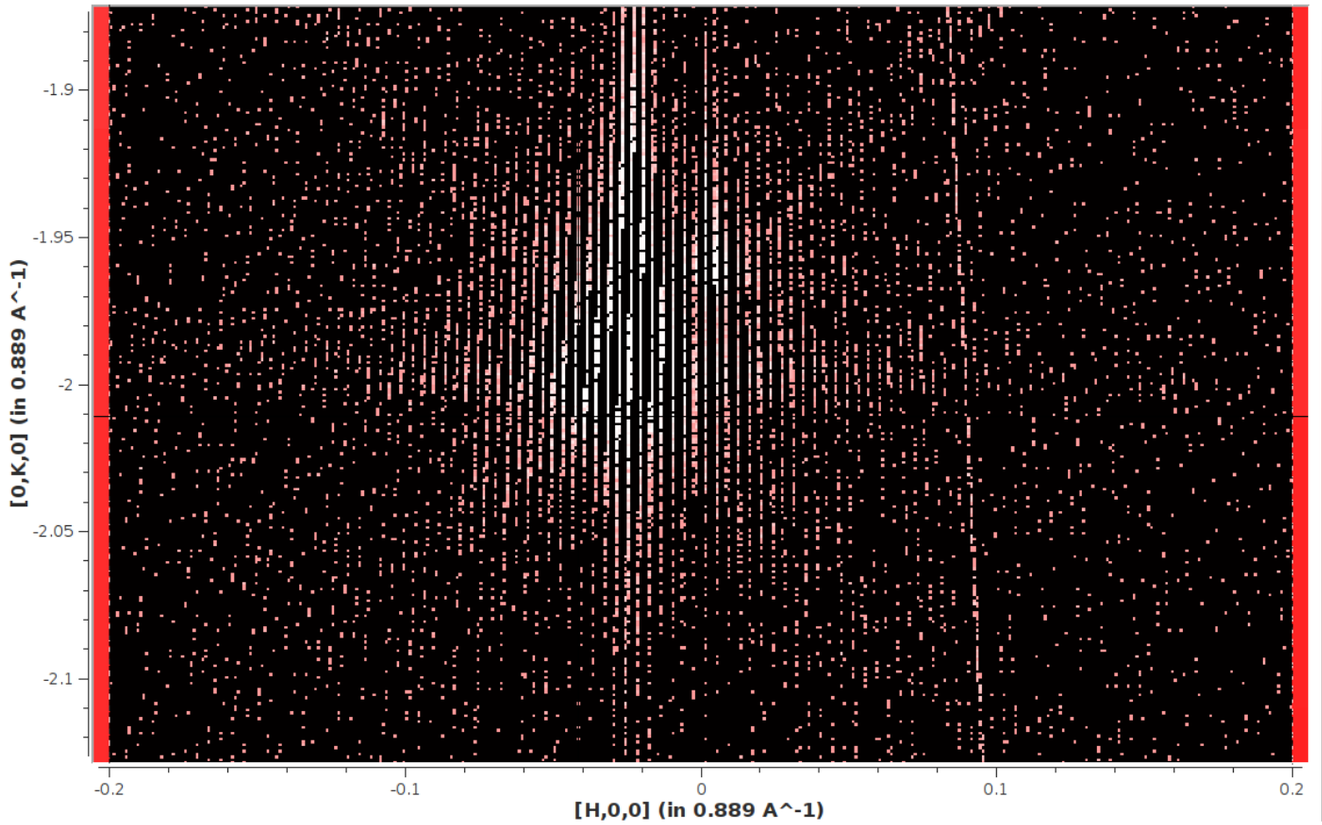
-1.9
-1.95
-2
-2.05
-2.1
[0,K,0] (in 0.889 A^-1)
-0.2
-0.1
0
0.1
0.2
[H,0,0] (in 0.889 A^-1)